A Theoretical and Experimental Study of The Evolution of Surface Ice

by

Fisaha Solomon Unduche

A thesis submitted to the Faculty of Graduate Studies in Partial fulfillment of the requirements of the degree of

Doctor of Philosophy

Department of Civil Engineering

University of Manitoba

Winnipeg, MB, Canada

THE UNIVERSITY OF MANITOBA

FACULTY OF GRADUATE STUDIES

*****

COPYRIGHT PERMISSION

"A Theoretical and Experimental Study of The Evolution of Surface Ice."

BY

Fisaha Solomon Unduche

A Thesis/Practicum submitted to the Faculty of Graduate Studies of The University of Manitoba in partial fulfillment of the requirement of the degree

Of

Doctor of Philosophy

Abstract

The theory of the formation of surface ice is not fully understood, yet its presence on water surface affects the operation of many different kinds of hydraulic structures. It is known that when the water surface temperature reaches supercooling ice particles are formed at the water surface. If the intensity of turbulence is low these ice particles will be suspended on the surface forming a surface ice. Herein, an experimental study that incorporates the effect of depth, velocity, roughness and air temperature is carried out in a counter-rotating flume to investigate the formation of surface ice in relation to these parameters. The experimental result is supported by a mathematical model based on the theory of formation of surface ice.

A mathematical model is developed based on a comprehensive theory and is solved using Matlab. The mathematical model integrates the effect of the heat balance on the water surface with the degree of turbulent mixing and the rate of growth of surface ice. The two calibrating parameters for the model are the magnitude of the initial seeding and the surface heat loss coefficient. The developed mathematical model is calibrated for the different types of surface ice formations for the data obtained from the experiment.

The experimental analysis shows that there are four main types of surface ice formations and their formation is mainly dependent on the degree of turbulence. It is also found that the types of these ice formations are dependent on the minimum supercooling temperature at an average depth. Moreover, it is demonstrated that skim ice particles are those ice particles that nucleate on the water surface during low to medium turbulent intensities and can have four

different types of shapes, namely needle shapes, finger shapes, hexagonal shapes and irregular shapes. The sizes and relative quantities of these ice particles on the water surface are also dependent on the degree of turbulence.

Acknowledgments

First of all I would like to praise the Lord, Jesus, for his faithfulness and care for me in every thing I have been through. "Those who wait for the Lord shall renew their strength, they shall mount up with wings like eagles."

I would like to thank Dr. J. C. Doering, my advisor, for his valuable and priceless advice, guidance and encouragement during the last four years. Dr. J. C. Doering's leadership, help and assistance, in any matter I may require, was always memorable. It is always a great privilege to be Dr. J. C. Doering's graduate student.

I would like to thank my advisory committee members, Dr. P. Rasmussen, Dr. R. W. Carson and Dr Tache for their comments and contribution to this thesis.

My gratitude also goes to Dr. S. Clark who has provided an unprecedented technical support during the experimental analysis period. With the help of Dr. S. Clark the ice room and the counter rotating flume which looked so complicated (at the first glance) was found to be a place to work safely and pleasantly.

This research was funded by the Natural Science and Engineering Research Council (NSERC) Canada. Many thanks goes to The University of Manitoba for honoring me with a graduate fellowship that financially helped me to carry out my studies on the last three years.

Dr. S. Wang, Dr. K. Qu, C. Magura, J. Malenchak, Dr. S. Ye and P. Channel all have been giving generous and uncountable support. It is a privilege to become a friend and to work with them.

Finally my wife, Hiwot, is a blessing to me and has been acting as a driving force on my studies. With out her endless support, it would have been impossible to accomplish this great task. I also want to thank all my families and friends for their encouragement and support.

Table of Contents

List of Tables

List of Figures

List of Symbols

Symbol	Definition
A	Velocity damping constant at the surface
A_s	Surface area of ice
A_e	Edge area of ice
a , b	Empirical constants
B	Water surface width
B_1 , B_*	Constants
b	Thickness of ice discs
c	Bowen's constant
C	Chezy coefficient
C_i	Ice concentration
C_p	Specific heat of water
C_r	Refraction coefficient
C_s	Cloud density coefficient
C_u	A universal constant for high Reynolds number turbulent flow = 0.09
C_w	Air drag coefficient
d_f	Maximum diameter of ice particle to float on the surface against surface pressure fluctuation

D	Mean diameter of ice particles
D_m	Maximum diameter of ice particles
D_o	Limiting diameter of ice particles for rise velocity
D_w	Turbulent energy damping factor
D_{50sp}	Stable state of D
e_a	Vapour pressure
e_s	Saturation vapour pressure
e_z	Vapour pressure at elevation z
E	Turbulent energy spectra
f	Friction factor
f_r	Frequency
g	Gravitational acceleration
G	Turbulent energy generation
h	Water depth
h_i	Surface ice thickness
h'	Root mean square value of the pressure fluctuation of the depth
h_w	Heat transfer coefficient between ice and water
h_{wl}	Heat transfer coefficient between water and air
k	Turbulent kinetic energy
k_i	Thermal conductivity of ice

k_s	Nikurade's roughness coefficient
k	Wave number
k_f	Wave number for floating eddy size
K_w	Turbulent kinetic energy at Eulerian frequency
k_w	Turbulent kinetic energy at the water surface
k_{wi}	Thermal conductivity of water
l	Ice face radius
ℓ_v	Viscous layer thickness
L_i	Latent heat of ice
$L_x(w)$	Integral scale of turbulence
M_i	Volume concentration of frazil ice
M_{*T}	Flows entrained frazil generating capacity
m^*	Ratio between the face radius of ice crystals and Kolmogorov scale
n_c	Extent to which the sky is covered by cloudness
n_e	Bulk extinction coefficient
n_r	Bulk extinction coefficient for reflected energy
N_u	Nusselt number
p_a	Atmospheric pressure
p	Probability
p'	Pressure fluctuation

P_r	Turbulent Prandtl number
Q_{wi}	Heat loss due to formation of ice
R	Hydraulic radius
R_e	Reynolds number
R^*	Bowen's ratio
R_*	Shear stress Reynolds number
S	Slope of the energy gradient
T_a	Air temperature
T_e	Equilibrium temperature of water ice mixture
T_h	Water surface temperature
T_i	Surface temperature of ice
T_s	Top surface temperature of ice in contact with the atmosphere
T_v	Vertical average water temperature
t	Travel time
u_*	Bed shear stress velocity
n_c	Extent to which the sky is covered by cloudness
U	Average stream flow velocity
U_{max}	Maximum stream flow velocity
U^+	Dimensionless velocity
$\overline{U}$	Instantaneous velocity in x-direction

U_s	Current speed at the surface
u	X-component of the velocity (stream wise)
u_i	Buoyancy velocity (rise velocity) of ice particle
u_{im}	Rise velocity for the maximum ice particle size
u_{io}	Rise velocity of the limiting ice particle size for suspension
u'	Turbulent intensity in x-direction
v	The y-component of the velocity (vertical)
u', u_{rms}	Turbulent intensity in x-direction
$\overline{u}$	Average fluctuation component in x-direction
v', v_{rms}	Turbulent intensity in y-direction
$\overline{v}$	Average fluctuation component in y-direction
v_t	Kinematic eddy viscosity
w	Z-component of the velocity (spanwise)
w', w_{rms}	Turbulent intensity in z-direction
$\overline{w}$	Average fluctuation component in z-direction
$w(y/h)$	Wake function
W	Wind speed 2 m above the water surface
W_e	Wind speed in current direction
y^+	Dimensionless y-coordinate
z	Elevation (potential head)
Z^+	A non-dimensionalized length measured from the water surface to the

	depth
$\sigma_{u'}, \sigma_{v'}$	Standard deviation of the rms of the longitudinal and vertical fluctuating component of the velocity
μ_1, σ_1	Mean and standard deviation of the lognormal upward velocity fluctuation
μ_2, σ_2	Mean and standard deviation of the turbulent velocity fluctuation
η	Kolmogorov microscale
ϕ_B	Net radiation heat transfer
ϕ_E	Latent heat transfer due to evaporation
ϕ_h	Heat flux per unit area from the water to the water surface
ϕ_H	Sensible heat transfer due to convection and conduction
ϕ_i	Heat flux through the ice cover
ϕ_o	Rate of heat loss from the water surface
ϕ_r	Penetrative shortwave radiation
ϕ_{EH}	Heat loss due to evaporation, conduction and convection
$\phi_{sw}(B)$	Vertical heat energy distributed returned as refraction from bed
ϕ_{ia}	Heat flux from the ice surface to the air
ϕ_{wi}	Heat flux from the underside of the ice
θ	Latitude in degrees
θ'	Virtual temperature
α'	Coefficient of reflection, albedo

α_T	Turbulent intensity indication number
α_r	Thermal diffusivity
ε_w	Turbulent dissipation rate at the water surface
ρ	Density of water
ρ_a	Density of air
τ_s	Wind shear stress
δ	Water surface deflection
κ	Von Karman constant
α	Coefficient of heat transfer between the water and the water surface
ν	Kinematic viscosity of water
$\lvert\overline{v'_{zo}}\rvert$	Mean value of the vertical component of turbulent fluctuation
τ	Shear stress
τ_b	Bed shear stress
ε	Turbulent energy dissipation rate
μ	Dynamic viscosity of water
dt	Incremental time
T	Water temperature
σ_t	Turbulent Prandtl number
dM_i	Volume concentration of surface ice formed over time dt
H_w	Heat transfer coefficient for the total volume of ice formed
k	A constant determined by calibration

M_o	Initial surface ice concentration
ρ_i	Density of ice
y	Depth measured from the bed
β	Coefficient
d_{90}, d_{50}	Ninety and fifty percent grain size
ε	Dissipation rate of turbulent kinetic energy
E_1	Constant approximately equal to 9.8
R_*	Shear stress Reynolds number
F_r	Froude number
χ	An empirical constant = 0.18

CHAPTER 1 Introduction

1.1 Background

In cold regions, as the air temperature begins to drop during winter periods, surface water on rivers and lakes may cool below the freezing point, which initiates the formation of ice on the surface. Though the type of ice formed on a water surface may vary depending on hydrological, hydraulic and meteorological characteristics, all of these variables can have a profound effect on the development of water resources projects. Therefore, ice formation should be considered in the development of water resources such as design and operation of hydraulic structures, flood protection due to ice jams, hydropower operation, inland navigation, ecology, environment etc (Shen, 2003; Ye, 2002; Lia, 1998; Ashton, 1986). Considerable theoretical and experimental research has been carried out in an attempt to alleviate these problems, and to better understand the mechanism of formation, growth and transportation of frazil ice, anchor ice, border ice, and ice jams (Osterkemp, 1978; Daly, 1984; Svensson, *et al.*, 1989; Beltaoes, 1983; Lal and Shen, 1991; Andres, 1995; Shen,

2003; Ye and Doering, 2003). Despite this previous work, limited research has been done on the formation of skim ice and surface freeze ups. As a result, there is a little supporting theory and this theory is not well developed (Shen, 2003; Matousek, 1984). Therefore, a detailed and comprehensive theoretical and experimental analysis will be presented in this study, to cover susceptible scenarios that may affect the formation, evolution and transport of skim ice.

1.2 Literature Review on Surface Ice Formations

1.2.1 The Supercooling Process and Frazil Ice Formation

During winter periods when the air temperature consistently remains below 0°C the water temperature in rivers also cools below the freezing point (usually 0°C). If this air temperature is maintained, there will be a continuous removal of heat from the water surface to the air, which supercools the water. Once the water supercools, the primary ice particles, called frazil ice crystals, form on the water surface. The initial frazil ice formation in turbulent water begins when water is supercooled and seeded with ice crystals from the atmosphere (Svensson and Omstedt, 1994). Due to the formation of these frazil ice crystals the latent heat of fusion is released by the ice particle, which increases the water temperature. However, at the beginning of this process the small amount of heat of fusion released by the small number of frazil crystals is insufficient to balance the heat loss from the surface. The water temperature, therefore, will decrease at a constant rate, called the cooling rate, below the freezing point until it reaches the maximum supercooling temperature (minimum water

temperature) where the heat loss from the surface is balanced by the latent heat of fusion. The increased release of the latent heat of fusion leads to a slow increase of the water temperature, called the warming rate, until it reaches an equilibrium temperature at which point, the rate of heat loss balances the rate of heat released, *i.e.*, the latent heat of fusion.

The equilibrium temperature, the cooling rate, the warming rate and the maximum supercooling temperature are dependent on hydrometreological conditions such as the rate of heat loss from the surface and the turbulence intensity of the flow. Moreover, a very thin surface layer may get supercooled, but the depth averaged temperature of the water may remain slightly above 0^{o}C, in the case of weak turbulent flow (see Figure 1 for a typical supercooling curve).

1.2.2 Kinds of Surface Ice Formations

Even though frazil ice is thought to be the origin of almost all other kinds of river ice (*e.g.*, anchor, border), the ultimate type of surface ice can have different forms depending on hydraulic and metrological conditions. Frazil ice particles grow in size and number until they reach the surface as different forms of surface ice runs. These varieties of surface ice forms are discussed below.

1.2.2.1 Frazil ice particles

Since the rise velocity and buoyancy of frazil particles depend on their shape and size, it is important to understand the variation of frazil crystal shapes. Different shapes and sizes of

"new born" frazil ice are reported in the literature from laboratory data and field observations. By far the most prevalent form of frazil ice particles observed both in the laboratory and in the field, which are formed at low supercooling characteristics of turbulent flow, are the thin circular disks whose diameter may vary between 30 μm and several millimeters (Daly and Colbeck, 1986). The time varying size distribution of these crystals follows a log normal distribution, which will be discussed in detail later (Daly and Colbeck, 1986; Clark and Doering, 2004; Ye and Doering, 2004). The diameter to thickness ratio of these particles has been observed to vary between 6 to 10 according to Daly and Colbeck (1986), and recent studies have shown a diameter to thickness ratio up to 15 or 16 (Clark and Doering, 2004). Hexagonal particles have also been observed both in the laboratory (Clark and Doering, 2002) and the field (Osterkamp, 1982). Needle-shaped particles have been observed in nature (Osterkamp and Gosink, 1983). Hanley and Rao (1982) indicated that needle frazil forms only when the turbulence level of the water is low. Clark and Doering (2002) also observed needle ice formation in a counter-rotating flume. Moreover, they reported that typically such particles form near the surface but quickly become entrained in the flow through turbulence.

Irregular shapes of ice particles were also observed by Clark and Doering (2002), which suggests that frazil ice particles have different shapes and sizes (thickness and diameter) that is dependent on the degree of supercooling and turbulence intensity. Ramseir (1970) showed that with a supercooling of -0.2°C the initial crystals are of disk shape with a diameter of 0.2 cm whereas thickness of 0.01 cm and with a supercooling of -1.0°C dendrite growth predominates accompanied by second- and third-order branching.

1.2.2.2 Frazil slush run

Once formed in supercooled water, frazil particles grow in number and size as the supercooling process proceeds (Daly, 1994; Ye, 2002). In number they grow by secondary nucleation, a phenomenon in which fragments break or are sheared off from existing frazil particles to become nuclei for further ice particles. In size they grow mainly in diameter, while their thickness hardly changes. The growth in size is due to thermal growth, *i.e.*, depends on the transfer rate of latent heat from the crystal to the ambient turbulent flow, and agglomeration (flocculation) as the active frazil particles stick and interlock to each other forming frazil flocks. Gravity is also assumed to remove through buoyancy some particles within the supercooled water. The gravitational removal is assumed to be proportional to the frazil ice concentration.

Numerous mathematical models have been developed to simulate supercooling processes and frazil ice evolution (Daly, 1984; Mercier, 1984; Svensson and Omstedt, 1994; Hammar and Shen, 1995; Ye and Doering, 2004b; Wang and Doering, 2005). When frazil ice crystals grow and attain a state such that their size exceeds the magnitude of the vertical fluctuation rate in a turbulent flow or if the ice discharge exceeds the suspended ice transport capacity of the flow (Shen, 2003), then they rise to the surface of the water and form slush ice sheets, which are variegated forms of strongly porous ice formations. Turbulence may also break up these flocs and entrain them back in to the flow, thus limiting the maximum size of the flocs (this will be discussed in detail later). This slush ice is carried downstream with the flow until it is stopped by blockage, or its density increases so that it covers the surface by

forming a static ice cover. The theory behind the formation and transport of this frazil slush is not clearly understood (Shen, 2003).

1.2.2.3 Skim ice

If the buoyancy (vertical) velocity of the ice crystal is larger than the vertical turbulent fluctuation velocity, frazil particles will remain on the surface of a supercooled surface layer, grow rapidly, and form skim ice, which there by suppresses subsequent ice frazil formation. Skim ice is made up of flat aggregates of ice crystals floating on the surface resembling grease stains or very thin floes (Matousek, 1984, 1990, 1992). As the vertical fluctuation component and buoyancy velocity (which is dependent on the frazil particle size) are stochastic parameters, there could be a phenomena in which a limited amount of skim ice is formed that does not significantly affect the formation of frazil ice (Matousek, 1992, Matousek, 1990). Low wind and flow velocities are ideal conditions for the formation of such sheets, although Marcotte (1984) observed the formation of moving ice sheets with flow velocities of 0.3 m/s -0.4 m/s in moderately cold weather and 0.9-1.0 m/s in very cold weather. The detail of these phenomena will be covered later. Matousek (1984) classified the above two ice run processes as a run of frazil (frazil slush) and skim ice, respectively.

1.2.2.4 Freeze-up

Although not covered in the literature in detail, freeze-up of a water surface is a basic ice process and a frozen water surface is the most frequent phenomena. Freeze-up is occasionally incorrectly referred to as ice bridge formation in the literature. Although

similar, it is important to distinguish these two processes. The initial freeze-up is formed over a very short river reach, where ice bridging occurs (*i.e.*, a bridge occurs from bank-to-bank) and ice motion is stopped (Matousek, 1990). In spite of this it is not sufficiently known for which case an ice cover occurs by bridging and in which cases it does not. Matousek (1984b, 1990) pointed out that freeze-up ice cover is formed in frosty weather on the calm surfaces of standing waters and streams with low flow velocities.

Matousek (1984b, 1990) also hypothesized that the freeze-up process occurs in streams in two ways: the first is freeze-up by the spread of border ice; and the second is the formation of a very thin layer of ice in a supercooled surface layer. (On the quiescent surface of standing waters, the water surface is equally supercooled at its surface area and ice is produced on the whole area of the water surface at the same time). In flowing water the surface freezes-up due to the spread of border ice, if the skim ice does not hinder the spreading of border ice.

The second hypothesis is spontaneous ice cover formation. This is the phenomena where the surface freezes spontaneously over its entire area. Skim ice may appear on the surface, but its movement may be very small and freeze up can occur quickly on the whole width of the surface. Upstream of the Lachine Rapids area of the St. Lawrence River, for example, sheets with lateral dimensions of several hundred meters to more than one kilometer have been formed after traveling only a few kilometers (Marcotte, 1984). Once halted, such sheets can lead to a rapid freeze-over of the complete cross-section.

1.3 Literature Review on Skim Ice

To the author's knowledge the only detailed research carried out to characterize and differentiate the mechanism of formation of skim ice and frazil ice is the research of Matousek (1984, 1992). Another recent supplementary study by Andreasson *et al.* (1998) discussed the importance of surface turbulence on the formation of ice pans. The review of skim ice literature is presented in this section.

1.3.1 Matousek's approach

Matousek (1984, 1990, 1992) developed a semi-theoretical model that predicts the condition for the formation of skim ice and/or frazil ice forms in a natural environment. He tested his theory using field data taken from the Ohre and Labe rivers and laboratory data from the ice engineering laboratory of the CRREL. The basic idea of his approach is to apply the simplified thermal balance equation (Matousek, 1992) to find the coefficient of heat flux and thus the surface temperature. The magnitude of the surface temperature indicates the degree of supercooling, and the degree of supercooling (as discussed above) directly relates to frazil particle size.

1.3.1.1 The surface heat exchange coefficient

During open water conditions some of the components of the total heat transfer at the water surface, especially the long wave radiation, are non-linear functions of air and water

temperatures. The net heat exchange rate at the water surface can be approximated by the following linear relationship (Ashton, 1986)

$$\phi_0 = h_w(T_v - T_a), \tag{1.1}$$

where ϕ_o is the net rate of heat loss from the water surface, T_a is air temperature, T_v is the vertical average water temperature, and h_w is the heat transfer (exchange) coefficient between the air and the water. The heat transfer coefficient can be derived from the energy budget analysis and applied to the temperature difference (Ashton, 1986; Beltaos, 1995).

Matousek (1984, 1990, 1992) applied the same linearization technique on the water surface as

$$\phi_h = \alpha(T_h - T_v), \tag{1.2}$$

where ϕ_h is the heat flux per unit area from the water to the water surface, α is the coefficient of heat transfer between the water and water surface, and T_h is the water surface temperature.

On the surface there is an equilibrium, and therefore, $\phi_o = \phi_h$, which implies

$$\phi_0 = \alpha(T_h - T_v). \tag{1.3}$$

Matousek (1990, 1992) developed an empirical relation to calculate the coefficient of heat transfer and the surface temperature. He found that the coefficient of heat transfer is dependent on the flow turbulence which is entirely dependent on the velocity of the water,

the roughness of the river bed, and the depth of the water. He also pointed out that the heat transfer is also affected by wind which causes waves on the surface. The relation has the form (for wind velocities in the range of 0.4 to 0.5 m/s, *i.e.*, when aw =0)

$$\alpha = \frac{12436U}{(\sqrt{MC}R)^{0.61}} + aw, \tag{1.4}$$

where U is the average flow velocity, M =0.7C+6 for 10 < $C \leq$ 60. For C > 60 M = 48, R is the hydraulic radius, C is the Chezy coefficient, w is the wind speed 2 m above the water surface (m/s), and a is a coefficient dependent on the width of the surface in the direction of the wind. It is recommended to determine 'a' as follows: if the surface width in the direction of the wind is B $\leq$ 15 m, then a = 15, if 15 < B $\leq$ 3800 m, then a = -0.9+5.8logB, and if B > 3800 m , then a =47.

In the model a detailed heat budget analysis at the water surface will be used to compute the surface heat flux and the water surface temperature.

1.3.1.2 Water surface temperature

The water surface temperature plays an important role in the initiation and development of the ice on the water surface. It significantly influences the heat exchange between the water surface and the atmosphere. Therefore it is necessary to accurately measure or model the water surface temperature. Various theoretical and hydrodynamic models are available to determine the water surface temperature of lakes and reservoirs. The problem is more complicated when applying the hydrodynamic equations to streams, where turbulent mixing

due to wind and currents on the top surface layer of streams exist. Later on an energy balance model for the water surface will be developed to predict the surface water temperature. However, it is worth reviewing the empirical approach followed by Matousek (1984, 1990, 1992) to find the surface water temperature.

Matousek (1984, 1990, 1992) derived an empirical relation for the determination of the water surface temperature from the linearized equation, Equation 1.3. Substituting α in equation (1.3) and solving for T_h yields

$$T_h = \frac{\phi_0 \left(\sqrt{MC}R\right)^{0.61}}{12436U + aw\left(\sqrt{MC}R\right)^{0.61}} + T_v, \tag{1.5}$$

It can be seen that the difference between the temperature of the surface and of the water is significantly affected by the water velocity. The heat transfer between the water and the surface is also significantly affected by wind waves. Numerous laboratory measurements by Matousek (1990, 1992) have shown that waves on the surface only occur when a wind velocity, measured 2 m above the water surface, exceed 0.3 m/s, which applies to extensive water surface areas. For water surface widths up to 15 m in the direction of the wind, waves occurred on the surface when the wind velocity exceeded 0.4 to 0.5 m/s. The detail of the effect of wind on the water surface will be discussed later.

1.3.1.3 Skim ice formation

Matousek (1984, 1990, 1992) derived an empirical relation for the rise of these particles (with the assumption that all frazil particles are circular discs) given by

$$u_i = 1.31 \times 10^{-5} \frac{D^{0.29} b^{0.61}}{\nu}, \tag{1.6}$$

where u_i is the buoyancy velocity (or rise velocity of ice particle) (m/s), ν is the kinematic viscosity, of water (m^2/s), D is the diameter of ice particles (m) and b is the thickness of the discs (m).

This rise velocity is compared with the vertical fluctuating component of the water velocity, whose (assumed) relation is also given by (Matousek, 1984, 1990, 1992) as

$$\left|\overline{v'_{zo}}\right| = \frac{0.0121U}{(MC)^{0.305} R^{0.5}}, \tag{1.5}$$

where $\left|\overline{v'_{zo}}\right|$ is the mean value of the vertical component of turbulent fluctuation on the water surface, and R and C are previously defined.

By comparing the buoyancy velocity with the vertical turbulent fluctuation Matousek (1984, 1990, 1992) concluded that frazil is formed in the stream if the following is valid simultaneously:

$T_v < 0^{\circ}C$,

$T_h <$ -0.10 to -0.20°C, and

$U > 0.067(MC)^{0.305} R^{0.5}$,

where T_v is the vertical average water temperature, T_h is the water surface temperature and U is the average stream flow velocity

The third condition is fully valid if the wind velocity at an elevation of 2 m above the water surface is less than 0.4 m/s. With greater wind velocities, frazil forms under lower water velocities than that given by the above condition.

Skim ice will occur in the stream when the following conditions are met simultaneously:

$T_v \geq 0^{\circ}C$,

$T_h \leq$ -0.10 to -0.20°C,

$U < 0.067(MC)^{0.305} R^{0.5}$, and the water velocity does not allow freezing up of the river.

Skim ice can also be formed for the case of frazil slush run.

1.3.2 Andreasson *et al.*, (1998) Approach

Assuming the initial stage (formation and growth) of floating surface ice is mainly determined by turbulent processes, rather than thermal conditions and wind effects, Andreasson *et al.* (1998) studied the effect of flow generated surface turbulence on types of ice runs at and near the surface. They divided the spectral distribution of turbulence at the surface into three turbulent processes: the vertical mixing near the surface, the exposure to turbulent pressure fluctuations at the free surface, and the turbulent shear at the free surface. These processes provided a basis to estimate the size of the minimum ice particles present in the surface layer, the size of the minimum ice particles floating on the surface, and the maximum particle size at and near the surface.

Andreasson *et al.* (1998) used the limiting bed shear velocity criteria of Matousek (1984, 1992), *i.e.*, $u_* = 0.05$ m/s, where skim ice no longer appears on the surface. However, measurements by Matousek (1984, 1992) show that frazil slush and skim ice may appear simultaneously on the free surface when $u_* = 0.05$ m/s. During these conditions it is likely that thermal conditions at the free surface influence the formation of skim ice. It is also known that for calm conditions (where u_* is much less than 0.05 m/s) supercooling might be limited to a thin surface layer, while the temperature over most of the flow depth is slightly above 0°C. During such conditions skim ice growth on the surface is clearly dependent on the heat loss rate. The slope of the energy gradient and mean velocity may easily be found from $S = u_*^2/(gh)$ and $U = h^{1/6}u_*/(ng^{1/2})$.

1.3.3 Experiments on Skim Ice

Matousek (1992) used a tiltable hydraulic flume to test the hypothesis of frazil and skim ice formation presented in section 1.3.1.3. The main purpose of the experiment was to investigate the effect of bottom roughness, discharge (or flow velocity) and to some extent the effect of air temperature on the formation of frazil or skim ice. In all their experiments both skim ice and frazil appeared to form. Skim ice appeared first, even before the supercooling of the water. The first ice particles to form and to be observed ranged from short ice needles up to ice floes with a plane bottom surface. The extent of the skim ice cover at the surface at the time when supercooling has been already reached and frazil has started to form is also shown. From his measurements Matousek (1992) observed that ice particles

begin to form on the surface when the water surface temperature is -0.18°C. The vertical average water temperature and the flow velocity at the instant of ice formation on the surface were the most important parameters observed in the experiment.

Hammar *et al.* (2002) used a re-circulating racetrack flume to study the development of different types of freeze up ice runs. Ice conditions were monitored manually and still photographs were taken to record the ice samples. The water surface was observed to reach -2.5°C while the bulk water temperature still remained slightly above 0°C. They classified the skim ice regime as static skim ice and a skim ice run. Their test results showed, in particular, that the limiting velocity for the formation of skim ice run is much lower than that of Matousek (1984) which indicates that additional theoretical analysis and systematic laboratory studies are needed.

1.4 Aging Mechanism

As the mean diameter of the frazil particles is time dependent, the quantity of ice particles that can exist on the surface is also time dependent. If supercooling is persistent the existing ice particles grow in size and float to the surface and leads to the formation of skim ice and/or frazil slush. The formation of frazil slush is related to the aging of ice crystals. Therefore, it is important to define an aging period to differentiate between frazil slush and skim ice for the purpose of mathematical modeling. Both skim ice (and skim ice run) and frazil slush are types of surface ice runs; the former is formed during the active stage of frazil ice (*i.e.*, during the supercooled period) while the latter is formed at the stage of

residual supercooling. The aging period is, therefore, the time interval in which ice particles float and exist on the surface in such a way that particles float before this period are considered as skim ice (or skim ice run) and particles that grow up and float to the surface after this period are considered to be frazil slush. For convenience this aging period can be taken as the duration of supercooling period as discussed in section 1.2.1. The growth of ice particles before the aging period is mostly due to thermal growth while after the aging period grow is mostly due to flocculation. Therefore, it is reasonable to neglect the effect of flocculation in modeling the growth of skim ice.

Andreasson *et al.* (1998) used the limiting size $D_f = D_r$ (where D_r is the maximum size in which particles of size greater than D_r rise to the surface against turbulent vertical fluctuation) as the criteria for the transition from a skim ice run to a frazil ice run. However, as emphasized by Matousek (1984) there should also be a dependency of this process on the surface heat loss rate. Up to diameter D_f, which is the maximum diameter of the particle to float on the surface against surface pressure fluctuation, particles are not allowed to float on the surface due to turbulent action.

1.5 Objectives of the Research

As discussed in the literature review section there is little understood about the formation and growth of skim ice both in the laboratory and in the field. Therefore, the objectives of this research are:

I. To developed a mathematical model that can predict the formation of surface ice for different hydraulic conditions;

II. To calibrate the developed mathematical model with the available data to make it practical; and

III. To carry out an experimental analysis to study the effect of flow depth, flow velocity, and bottom roughness as turbulence generating parameters, and air temperature on the formation of surface ice.

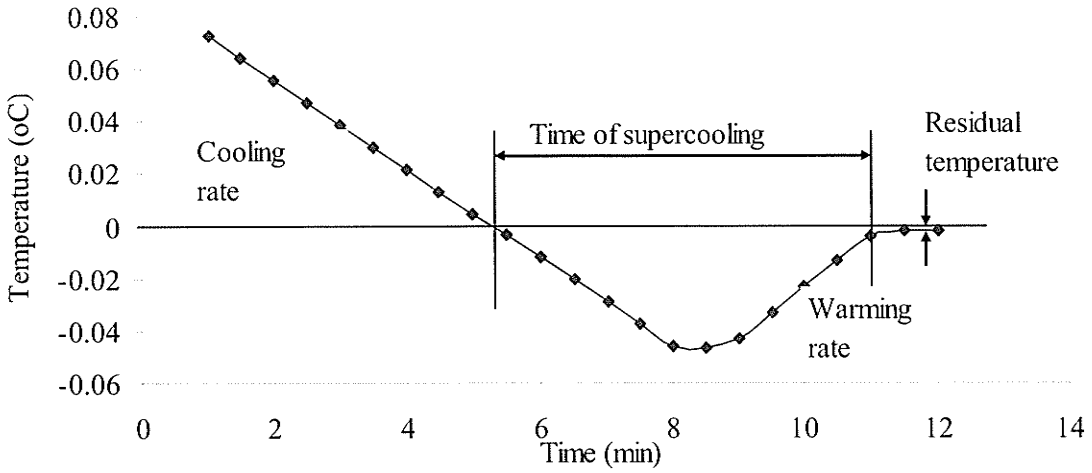

Figure 1.1 Typical supercooling curve.

CHAPTER 2 Turbulence Modeling

2.1 Introduction

The transfer of heat and energy from the river bed to the water, from the water to the water surface and to the air is mainly governed by the presence of turbulence. The turbulent kinetic energy, k, is defined as

$$k = 1/2 \times \left(u'^2 + v'^2 + w'^2\right). \tag{2.1}$$

The turbulent energy spectra has three well-known spectral subranges of velocity fluctuations (Nezu and Nakagawa, 1993; Hinze, 1959): 1) productive, 2) inertial, and 3) viscous subranges, depending on the wave number and turbulent dissipation length scales.

The turbulent structure of open channel flows can be divided into three regions (Nezu and Nakagawa, 1993):

Wall region [y/h < (0.15 – 0.2) where h is the water depth, and y is a vertical coordinate]: This region corresponds to the inner layer of classical boundary layer treatments; length and velocity scales are ν/u_* and u_*, respectively, where ν is the kinematic viscosity of water and u_* is the bed shear velocity. The turbulent energy generation (G) consequently exceeds the dissipation rate (ε), in this region, *i.e.* $G > \varepsilon$.

Intermediate region [$0.15 \leq y/h \leq 0.6$]: This region is not strongly influenced by either wall properties or the free surface. Instead it corresponds loosely to the inertial subrange of the spectral distribution. The length and velocity scales are y and u_*, respectively, where τ is the bed shear stress and ρ is the density of water. This region maintains a near equilibrium turbulent energy budget, $G \approx \varepsilon$.

Free surface region [$0.6<y/h<1.0$]: In this region, the turbulent structure is controlled by the outer variables, with length and velocity scales specified as the flow depth h and the maximum mainstream velocity $U_{max.}$ The turbulent dissipation rate ε becomes larger than the generation rate G. Consequently, turbulent energy must be supplied from the wall region to the free surface region by turbulent diffusion. Such characteristics as the vertical turbulence intensity are strongly affected by the free surface, in contrast to results for closed channel flow.

In open channel flows turbulent energy is extracted from the mean flow in the production subrange. It is transferred to smaller scale eddies in the inertial subrange, and then dissipated into heat in the viscous subrange.

2.2 Governing Flow Equation

The two-dimensional Navier-Stokes equation along the flow direction (x-axis) is written as

$$\rho\left(\frac{\partial u}{\partial t}+u\frac{\partial u}{\partial x}+v\frac{\partial u}{\partial y}\right)=-\rho g\frac{\partial z}{\partial x}-\frac{\partial P}{\partial x}+\frac{\partial}{\partial y}\left(\mu\frac{\partial u}{\partial y}\right), \tag{2.2}$$

where μ is the dynamic viscosity of the fluid, g is the gravitational acceleration, u is the velocity in x-direction, v is the velocity in the y- direction, z is elevation (potential head), ρ is the density of water and t is the time. For steady, uniform flow, with the vertical velocity equal to zero, and $\partial z/\partial x=\sin(\theta)=S$ (where S is the slope of the energy gradient), the above equation reduces to

$$gS=\frac{\partial}{\partial y}\left((\nu_t+\nu)\frac{\partial u}{\partial y}\right). \tag{2.3}$$

Integrating (2.3) with respect to depth, y, yields

$$gSy=(\nu_t+\nu)\frac{\partial u}{\partial y}. \tag{2.4}$$

In the counter-rotating flume, in the Hydraulics Research and Testing Facility at the University of Manitoba, the flow is driven by energy applied by the bed and wall motors of the counter-rotating flume. In this case the driving force is an external force applied to the flow by a motor. Therefore, a constant B_* is set in equation (2.3) to represent gSy (the

potential energy term). This constant B* is a function of u_*, which is entirely a function of the bed roughness, k_s, and needs to be calibrated at the time of running the experiment.

Near the bed of a river, where $y = 0$ and the kinematic eddy viscosity is zero (turbulent generation starts at a distance equal to the thickness of the viscous sublayer as will be explained later), the above equation reduces to

$$gSR = \nu \frac{\partial u}{\partial y} = \frac{\tau_b}{\rho} = u_*^2, \tag{2.5}$$

where R is the hydraulic radius (or flow depth in wide channels), u_* is the bed shear stress velocity, τ_b is the bed shear stress, and ν_t is the kinematic eddy viscosity. In the intermediate region and surface region of open channel flow the value of ν is much smaller than the value of ν_t.

The log-wake logarithmic velocity profile, taking the free surface into account is given by Coles (1956)

$$u^+ = \frac{1}{\kappa} \ln\left(y^+\right) + A + w(y/h), \tag{2.6}$$

where $u^+ = u/u_*$, and $y^+ = y u_*/\nu$ is a dimensionless y-coordinate normalized by the viscous length ν/u_*. Values $\kappa = 0.41$ and $A = 5.29$ are obtained in open channel flow by Nezu and

Rodi (1986). An approximate wake function *w(y/h)* given empirically by Coles (1956) can be described by

$$w(y/h) = \frac{2\Pi}{\kappa}\sin^2\left(\frac{\pi y}{2h}\right). \tag{2.7}$$

For h x $u_*/\nu > 2000$, $\Pi \approx 0.2$.

The above shear stress velocity can be written in a different form as (Carter *et al.*, 1963)

$$u_* = U\sqrt{\frac{f}{8}}, \tag{2.8}$$

where f is a friction factor. For turbulent flow f can be estimated using the Colebrook-White equation (Colebrook, 1939)

$$\frac{1}{\sqrt{f}} = -2\log\left(\frac{k_s}{3.71(4R)} + \frac{2.51}{R_e\sqrt{f}}\right), \tag{2.9}$$

where k_s is representative roughness height. An explicit approximate equation for f can also be written as (Idelchik, 1986)

$$f = 0.1\left(1.46\frac{k_s}{4R} + \frac{100}{R_e}\right)^{0.25}, \tag{2.10}$$

where R_e is the Reynolds number given by $4UR/\nu$, where U is the depth averaged flow velocity and R is the hydraulic radius.

2.3 Turbulence Intensities and the Turbulent Kinetic Energy

The velocity fluctuation in turbulent flow about its mean value is usually expressed on the three fluctuation velocity components: the longitudinal (stream wise) velocity component, usually designated by u, the spanwise velocity fluctuation component, usually designated by w, and the vertical velocity component (normal to the free surface) usually designated by v. In general

$$U = \overline{U} + u', \tag{2.11}$$

where $\overline{U}$ is the mean value of velocity, U is the instantaneous velocity component and u' is the fluctuating component. The turbulence intensity is the root mean square value of these fluctuating components, *e.g.*,

$$u' = \sqrt{\overline{u^2}}, \qquad v' = \sqrt{\overline{v^2}}, \qquad w' = \sqrt{\overline{w^2}}. \tag{2.12}$$

These turbulent fluctuations vary from the inertial subrange to the viscous subrange which shows the distribution of turbulent kinetic energy among the components. Various empirical and semi-empirical relations exist for these turbulence intensities, of which a common form is (Nezu and Nakagawa, 1993)

$$\frac{u'}{u_*} = 2.30\exp(-y/h), \tag{2.13}$$

$$\frac{v'}{u_*} = 1.27\exp(-y/h), \tag{2.14}$$

$$\frac{w'}{u_*} = 1.63\exp(-y/h), \tag{2.15}$$

and

$$\frac{k}{u_*^2} = 4.78\exp(-2y/h), \tag{2.16}$$

where k is the turbulent kinetic energy.

The comparison of the relative magnitude of the turbulent intensities as a function of the non-dimensionalized length is given in Yamamoto *et al.*, 2001. It was concluded that the vertical component of the non-dimensionalized turbulent fluctuation, v'damps near the surface and the spanwise, w', and stream wise, u', component increase near the free surface, which shows the redistribution of the turbulent kinetic energy.

2.4 Surface Turbulence

Turbulence at the water surface could come from different sources. It could come from flow related turbulence, *i.e.*, turbulence generated on the river bed and transported to the surface by diffusion, or wind generated turbulence, *i.e.*, turbulence that is generated due to the presence of wind shear stress on the water surface, or wave related turbulence, *i.e.*, the wave on a water surface can generated turbulence energy at the water surface. The following

section deals with characterizing those turbulence energies and the associated dissipation rates on the water surface.

2.4.1 Flow related turbulence

In the language of interpreters of the turbulent kinetic energy equation, turbulent energy is produced by the shear stress below the surface, and then transmitted by pressure fluctuation and transported (or diffused) by gradients of turbulent kinetic energy to near the surface where it is dissipated by viscous stresses (Ueda *et al.*, 1976). The dissipation rate of turbulent kinetic energy has been studied by many authors. Nezu (1977) proposed an overall dissipation rate function, which as given in Nezu and Nakagawa (1993), has the form

$$\frac{\varepsilon h}{u_*^2} = E_1 (y/h)^{-1/2} \exp(-3y/h), \tag{2.17}$$

where E_1 is approximately equal to 9.8 at moderate Reynolds numbers of 10^4 to 10^5. For any other Reynolds number,

$$\begin{aligned} &E_1 = 12.2K / B_1 \qquad \text{where} \qquad K = 0.691 + 3.98/\sqrt{R_L} \\ &\frac{R_L}{R_*} = 2.3\sqrt{y/h}\exp(-y/h) \qquad \text{where } R_* = \frac{hu_*}{\nu} \end{aligned} \tag{2.18}$$

B_1 is approximately equal to 1.0 for Reynolds number R_* of 1600, and increases slightly as the Reynolds number decreases, *e.g.*, $B_1 = 1.1$ for $R_* = 600$.

As mentioned by Nezu and Nakagawa (1993) the dissipation rate, $\varepsilon h / u_*$, should be slightly larger than the values calculated by the above equation, however, there is not yet an established relation to characterize the dissipation rate near the surface. At the free surface a value of

$$\varepsilon = 4u_*^3 / h \tag{2.19}$$

is used by Andreasson *et al.* (1998).

On the free surface the turbulent kinetic energy value of

$$k = 0.8u_*^2 \tag{2.20}$$

is used by Andreasson *et al.* (1998), where h is the flow depth. Early studies by Komori *et al.* (1987) showed that u'/u_* increases slightly with y/h in the region $y/h > 0.9$; in contrast, v'/u_* decreases strongly with y/h in this region. This contrast indicates the redistribution of turbulent energy among u', v' and w'. The turbulent energy term, k/u_*^2, itself decreases with y/h near the free surface because the turbulent generation is much smaller than its dissipation. However, recent studies by Shi *et al.* (2000) and Yamamoto *et al.* (2001) showed that there is a peak of turbulence kinetic energy in the turbulence production region very near the bed, and away from the bed the turbulent kinetic energy continues to fall until about $y/h = 0.95$ (5% region of the free surface) where it again increases, implying that there is some turbulence production from the behavior of the free surface. According to Yamamoto *et al.* (2001) the effect of the free surface turbulent structure on turbulent kinetic energy (is

negligible and) is not important for heat transfer because the free surface doesn't contribute to the turbulent generation in open channel flow without surface deformation. However, a large horizontal vortex as well as the flow depth scale, which is affected by this free surface turbulent structure, enhances the heat transfer across the free surface.

In the absence of wind-induced shear stress, the water surface can be considered to a first approximation as a plane of symmetry. However, the presence of the free surface should reduce the length scale of turbulence. To account for this damping effect at the free surface Celik & Rodi (1984) as presented by Nezu and Nakagawa (1993) have used the following boundary condition at the free surface for the quantity ε

$$\varepsilon_w = \frac{k_w^{3/2}}{\chi h}, \tag{2.21}$$

where k_w is the value of turbulent energy at the water surface and χ is an empirical constant = 0.18. The use of this boundary condition yields a higher value for ε_w, above the value that would follow from a zero gradient condition. Nezu and Nakagawa (1987) suggested a different boundary condition for k that has basically the same effect as the ε surface condition (equation 2.19), namely a reduction of k near the free surface. They achieved this by multiplying the surface value of k determined from the zero gradient condition by a damping factor D_w. Nezu and Nakagawa (1993) showed that the distribution of k calculated by the k - ε model, using the damping factor of 0.8 at the surface agrees well with the semi-empirical curve of Equation 2.16.

Considering the above review, the following is accepted for turbulent energy and dissipation rate in the absence of wind stress and turbulence on the water surface. Equation 2.16 and 2.17 can be used to sufficiently model the turbulent energy and dissipation rate through out the water depth, respectively. This will give a surface boundary condition (*i.e.*, at $y/h = 1.0$) of $k_w = 0.65u_*^2$ and at $y/h = 0.95$, $k_w = 0.7u_*^2$. However, the data of Shi *et al.* (2000) and Yamamoto *et al.* (2001) shows that there is an increase of the turbulent kinetic energy near the surface due to the presence of the free surface. Therefore, a surface boundary value of $k = 0.8u_*^2$ (as specified by Andreasson *et al.* (1998)) can be taken, which gives comparable result with the findings of Shi *et al.* (2000). Thus, for the region $1 < y/h < 0.95$ a linearly decreasing turbulent energy value of $0.8u_*^2$ to $0.7u_*^2$ is adapted. The boundary condition at the bed is specified at the distance of outside the viscous sublayer equal to ν/u_*, however, the mean velocity follows the logarithmic velocity profile (equation 2.6) when $y^+>30$ where $y^+ = yu_*/\nu$ and, therefore, the boundary condition for k could be set at the grid point $y^+ = 30$. At this point a local equilibrium exists between the turbulent production rate and the turbulent dissipation rate. Taking this local equilibrium as an additional assumption leads to the following relations for k and ε at the first grid point outside the viscous sublayer

$$\frac{k_1}{u_*^2} = \frac{1}{\sqrt{C_\mu}} = 3.33 \qquad \text{and} \qquad \varepsilon_1 = \frac{u_*^3}{\kappa y_1}, \tag{2.22}$$

where 1 denotes values at the first grid point.

If we use the boundary condition of Equation 2.20 for the kinetic energy at the surface and the free surface boundary condition of Celik & Rodi (1984) (Equation 2.21), for $\alpha = 0.18$, gives a boundary condition for ε as

$$\varepsilon = 4u_*^3 / h, \tag{2.23}$$

which is similar to that used by Andreasson *et al.* (1998).

2.4.2 Surface turbulence due to wind shear and wave action

When turbulent wind passes over the water surface different phenomena occur depending on the velocity of the air. At high velocities, waves are produced by wind; at lower velocities the surface is distorted by turbulent eddies in the fluid impinging on it, the deformation being controlled by gravitational and surface tension forces. Since the overall mechanism of turbulence generation and dissipation due to surface waves and wind shear, arising from a wind stress on the water surface, complicates the problem, we neglect the surface turbulence associated with wind shear and surface waves. However, the theoretical formulation and review of wind shear and wave related turbulence on the water surface are discussed in Appendix B.

2.4.3 Total surface turbulence, and eddy viscosity

In natural open channel flow where all the possible effects of turbulent energy production (turbulent energy production due to bed friction velocity, turbulent production due to wind

and wave action) are available, it would be useful to characterize the overall turbulent energy. As the turbulent energy, by definition, is any disturbance coming from eddies of different scales the above discussed turbulence energies and dissipation rates can be combined at a given time and position in the flow field. Once the distributions of k and ε over the flow field are known, the eddy viscosity distribution is calculated from Equation 2.24 (according to the $k-\varepsilon$ turbulence model).

2.5 Turbulence Modeling

Various turbulence models exist in literature to solve for the eddy viscosity term in the governing flow equation. The most common of these models for calculating open channel flow is the $k-\varepsilon$ model. The general $k-\varepsilon$ model is valid for high Reynolds number flow. When the Reynolds number describing turbulence is relatively low, modifications need to be made for the equations of k and ε in the general $k-\varepsilon$ model, which then becomes the low Reynolds Number $k-\varepsilon$ model. The detail description of this model is given in George and Arndt (1989).

In this particular case, the above discussed turbulence energies and dissipation rates can be linearly combined at a given time and position in the flow field. Once the distributions of k and ε over the flow field are known, the eddy viscosity distribution is calculated from the following relation (according to the $k-\varepsilon$ turbulence model)

$$\nu_t = \frac{C_\mu k^2}{\varepsilon}, \tag{2.24}$$

where $C_\mu = 0.09$ is a universal constant for high Reynolds number turbulent flow. The use of a constant C_μ involves the assumption that the ratio of vertical fluctuation to the total kinetic energy, $\overline{v^2}/k$, is constant. However, $\overline{v^2}/k$ drops significantly near the surface, which indicates the damping of C_μ near the surface. A functional dependence of this was obtained by Celik and Rodi (1984).

CHAPTER 3 The energy balance at the water surface

3.1 Introduction

The heat loss from a water's surface is dependent on the temperature difference between the water surface and the surrounding air. With the difficulties of determining the water surface temperature and its dependence on surface heat loss, the use of a heat balance approach to solve heat flow problems is most useful. Most numerical models use a simplified linearized approach to solve energy balance problems; however, this assumption obscures the clear theory of the heat balance and the heat transfer coefficient at the surface. In the following section, a heat balance model at the water surface will be developed to: solve the water surface temperature; estimate the average vertical water temperature, and ice crystal growth rate. In this chapter a general model that is valid for natural conditions will be developed. This model then will be reduced to the closed cell (laboratory condition) in chapter 8, in which case it can be calibrated by the experimental data.

3.2 Water Surface Temperature

Following the cooling of the air temperature during fall, the temperature of a natural water surface decreases until it becomes supercooled. On rivers with low flow velocities and on lakes, which are usually associated with low turbulence characteristics, the surface temperature will not be mixed through the whole depth of the water, which creates a vertical temperature gradient (*i.e.*, a thermocline). This produces a thin cool surface layer with a temperature less than the bulk water. The thickness of this thermal layer and the temperature difference depends on the degree of heat exchange at the surface and the intensity of surface turbulence. See Figure 3.2 for the temperature profile observed in a laboratory counter-rotating flume.

When the surface temperature reaches supercooling, ice crystals are formed at the water surface; the size of these crystals is dependent on the degree of supercooling, the intensity of turbulence, and time. Therefore, the determination of water surface temperature is a key factor in determining the degree of supercooling at the instant of freezing. Moreover, water surface temperature is a key factor affecting the energy exchange at the water surface, particularly net longwave radiation and turbulent energy flux. The water surface temperature and the overall thermal condition in turn is determined by the absorption of radiant energy from the sun, heat exchange with the atmosphere and the bottom, and the redistribution of the heat in the water as result of convection by currents and turbulent mixing.

On lakes and oceans this surface water is continually mixed with the body water by the process of surface renewal. The determining factor for this surface renewal is wind blowing over the water surface. The momentum near the air-water interface due to wind is redistributed among waves, currents and turbulence via such mechanisms as wave breaking and Longmuir circulation (Zhang and Harrison, 2004, Garbe and Jahne, 2002, *etc*). The intensity of the surface renewal event affects the rate of turbulent heat transfer from the water surface to the water body, which entirely affects the temperature profile along the water column. However, in rivers with low to moderate flow velocity, the turbulent heat transfer and the vertical water temperature profile is modified by convection currents and turbulent mixing. While dealing with surface temperature, the turbulence that affects the heat transfer at the surface is surface turbulence. The surface turbulence characteristics of oceans and lakes is mainly associated with the wind flowing on the water surface and has been studied by many authors. The surface turbulence characteristics of open channel flow is complicated as a result of turbulence due to current, turbulence due to waves and wind, and the damping effect of the free surface. Coupling of these turbulence characteristics is not fully understood. It is worth emphasizing here that the bulk Richardson number approach to determine mixing in the upper layer of oceans and lakes can not fully account for the mixing of surface layers in rivers, as the combined turbulence of surface stress and bed stress may be dominated by the bed induced turbulence.

The determination of the surface temperature of rivers was studied by Matousek (1984, 1990). Matousek, developed an empirical relation to determine the surface temperature from the surface heat flux, based on field data from a navigation canal and laboratory data from

flume measurements. Matousek, emphasized the dependence of the surface heat flux coefficient on the velocity of the water, the roughness of the river bed, the depth of the water, and the wind velocity above the water surface. The final form of the water surface temperature is dependent on the overall heat transfer at the water surface, average flow velocity, bed roughness, flow depth, and wind speed.

An energy balance model was used by Pivovarov (1973) to find a theoretical average water temperature as a function of time and depth. He made simplifying assumptions where the flow velocity and temperature are constant over depth, unlike natural rivers which are usually associated with varying velocity and temperature gradients in depth. The detail components of heat balance on the water surface are summarized by several authors (Michel, 1971; Matousek, 1990; Hodges, 1998).

3.3 Heat Balance at The Water Surface

The formation of thermal processes in water is determined by the absorption of radiant energy from the sun, by energy exchange at interfaces with the atmosphere and the bottom, and also by heat redistribution in the water as a result of convection by currents and turbulent mixing of the water masses. The complex interdependence of these factors gives rise to a temperature field that is non uniform in space and unsteady in time. Because this process is complicated we may assume that water is incompressible, the vertical gradient of temperature is considerably greater than the horizontal gradient, and the vertical velocity is

less than the longitudinal velocity. For these assumptions the temperature field in the water is given by (Lal and Shen, 1991b)

$$\frac{\partial T_w}{\partial t} + u\frac{\partial T_w}{\partial x} = \frac{\partial}{\partial y}\left(\frac{\nu_t}{\sigma_t}\frac{\partial T_w}{\partial y}\right) + \frac{\phi_r}{\rho c_p h} - \frac{\phi_o}{\rho c_p h}, \tag{3.1}$$

where T_w is the water temperature, h is the water flow depth, ρ is the density of water, C_p is the specific heat of water, σ_t is the turbulent Prandtl number which is usually equal to unity, u is the velocity in the x-direction, ε_y in the turbulent mixing coefficient in the y-direction. $\phi_o = \phi_B + \phi_E + \phi_H$, where ϕ_o is the total surface heat transfer, which is the sum of the net radiation heat transfer (ϕ_B), the latent heat transfer due to evaporation (ϕ_E), and the sensible heat transfer due to convection and conduction (ϕ_H). ϕ_r is the short wave radiation (that is the penetrative effect).

It is generally presumed that convection, conduction, evaporation and long wave radiation are non-penetrative effects that would appropriately be modeled as surface boundary conditions. However, due to near surface turbulence, the surface heat mixes down to the near surface region. Thus, if the surface heat transfer is simply treated as a temperature boundary condition, the surface may overheat if the net surface heat transfer is into the domain. The mixing due to wave and wind-generated turbulence (as well as the Langmuir circulation) together with current related turbulence can not be easily modeled by turbulence models such as a Richardson number mixing. Hodges (1998) assumed the surface heat to be absorbed

arbitrarily in the upper most grid cell, one meter from the surface. He used an exponential decay to model the distribution of surface heat transfer in the uppermost layer.

Simplified relations for the determination of the total surface heat transfer between the water surface and the atmosphere, (ϕ_o), were given by Matousek (1990, 1992) depending on air and water surface temperatures. These relations are (where parenthesis, ( ) shows non inclusion and brackets, [ ], show inclusion)

1. For $T_a \in (0;-12]$

$$\phi_o = -100 + 12.6T_a - 16T_h + 3.2(0.8T_a - T_h - 1)\mathrm{W} + (318 + 4.6T_a)c_s n_c, \tag{3.2}$$

2. For $T_a \in (-12;-24]$

$$\phi_o = -115 + 11.2T_a - 16T_h + 3.2(0.7T_a - T_h - 2)\mathrm{W} + (326 + 4.6T_a)c_s n_c, \tag{3.3}$$

3. For $T_a \in (-24;-38]$

$$\phi_o = -156 + 9.1T_a - 16T_h + 3(0.6T_a - T_h - 4)\mathrm{W} + (328 + 4.8T_a)c_s n_c, \tag{3.4}$$

4. For $T_a < -38^o C$

$$\phi_o = -175 + 9.5T_o - 16T_h + 3(0.6T_a - T_h - 6)\mathrm{W} + (332 + 4.8T_a)c_s n_c, \tag{3.5}$$

where T_a is the air temperature 2 m above the water surface (°C), w is the wind velocity 2 m above the water surface (m/s), T_h is the water surface temperature, c_s is a coefficient which depends on cloud density and the values in Table 3.1 hold true, n_c is cloudiness *i.e.*, the

extent to which the sky is covered by clouds evaluated by a scale from 0 to 1; clear sky n_c = 0, cloudy sky n_c = 1)

Table 3.1 Values of c_s

Condition	c_s
for thin cloudiness	0.06
for slightly dense cloudiness	0.16
for dense cloudiness	0.27

On lakes and rivers the surface heat transfer (ϕ_o) can be assumed to occur over a layer of thickness that is of the order 0.6 to 1.0 meters with an exponential decay such that (Hodges 1998)

$$\phi_s(y) = \phi_s(h)\exp\{-\eta_s(h-y)\}, \tag{3.6}$$

where $\phi_s(y)$ is the surface heat energy that has not been absorbed at height y (measured from a coordinate base line with y positive in the upward direction), $\phi_o(h)$ is the surface heat transfer penetrating the water surface, η_s is the bulk extinction coefficient for the surface heat transfer, h is the height of the free surface (measured from the same base line as y). If we assume that 90% of the surface heat transfer is absorbed in the first 0.6 meters of the domain, then η_s = 3.84.

The depth of penetration of the shortwave radiation depends on the net shortwave radiation that penetrates the water surface and the bulk extinction coefficient (which is a function of water color, turbidity, plankton concentration, *etc*).

To calculate the shortwave radiation absorbed by water a relation of the form given below is used by Shen (1980)

$$\phi_r = 0.11574\left[a - b(\theta - 50)\right](1-\alpha)(1-0.0065C^2), \qquad (3.7)$$

where ϕ_r is the net solar radiation, θ is the latitude in degrees; a, and b are constants that change from month to month as given in Table 3.7, C is the cloud cover in tenths, α' is the coefficient of reflection or albedo, which depends on the roughness of the water surface and the sun's declination. A value of 10% is assumed here.

Table 3.2 Values of a and b in Equation 3.7.

Month	a [cal/cm^2-day]	b
January	142	11.0
February	228	11.2
March	394	12.7
December	100	8.2

The shortwave radiation ϕ_r decays exponentially from the top surface with increasing depth (Tennessee Valley Authority, 1972; Hodges, 1998). The shortwave radiation at any depth can be found from the relation

$$\phi_r(y) = \phi_r(h)\exp\{-\eta_e(h-y)\}, \tag{3.8}$$

where $\phi_r(y)$ is the short wave radiation absorbed at height y (measured from a coordinate base line with y positive in the upward direction), $\phi_r(h)$ is the net short wave radiation penetrating the water surface, η_e is bulk extinction coefficient, h is the height of the free surface above the same base line as y). Where shortwave radiation reaches the bottom, a complete heat budget model would require: (1) absorption and reflection of the shortwave radiation by the sediment, (2) long wave radiation emission from sediments, and (3) conduction and convection model at the bottom boundary. As a simpler approach, we will consider that any shortwave radiation that reaches the bottom boundary is treated by a model similar to that used for the total surface heat transfer near the free surface (Hodges, 1998). Let $\phi_{sw}(B)$ represents the shortwave radiation that reaches the bottom boundary, and C_r represents the fraction of the shortwave radiation that is returned to the water column. Assuming an exponential decay (in the positive y direction), we have

$$\phi_r(y) = C_r\phi_{sw}(B)\exp\{-\eta_r(y-h)\}, \tag{3.9}$$

where $\phi_{sw}(B)$ is the vertical distribution of the heat energy returned to the water column, and η_r is the bulk extinction coefficient for reflected energy. It is convenient to use the same bulk extinction coefficient used for the total surface heat transfer (*i.e.*, 3.84 m^{-1}). This ensures 98% of the energy returned to the water column is transferred into the first one meter above the bottom.

3.4 Heat Balance in a Closed Cell

The above heat balance equation is written for open water surfaces (natural rivers and lakes. The heat balance equation written in a closed cell during the formation of ice crystals as

$$\frac{\partial T_w}{\partial t} + u\frac{\partial T_w}{\partial x} = \frac{\partial}{\partial y}\left(\frac{\nu_t}{\mathrm{p}_r}\frac{\partial T_w}{\partial y}\right) + \frac{\phi_o}{\rho c_p} + Q_{wi}, \tag{3.10}$$

where $\mathrm{P_r}$ is the Prandtl number and Q_{wi} is the heat loss due to the formation of ice crystals. The linearzed form of 3.10 is

$$\phi_o = h_{wl}(T_h - T_a), \tag{3.11}$$

where h_{wl} is the heat transfer coefficient. T_h and T_a are water surface and air temperatures, respectively. If immediate mixing is assumed the above equation has the form

$$\phi_o = C_p \rho \left.\frac{dT}{dt}\right|_{cooling\,rate}. \tag{3.12}$$

However, in the case of stratified flow the above assumption is not valid (Ashton, 1986). Moreover, both h_{wl} and T_h are unknown and an energy balance has to be used to solve the problem. Inside the laboratory the heat flux associated with evaporation is given by Ryan *et al.* (1974) as

$$\phi_E = \left[3.20\mathrm{W}_z + 2.70\left(\Delta\theta'\right)^{1/3}\right]\left(e_s - e_z\right), \tag{3.13}$$

where ϕ_E is the energy flux in W/m^2, W_z is the wind speed at elevation z above the water surface, e_s and e_z are the saturation vapor pressures and vapor pressure at elevation z, respectively.

The virtual temperature θ' (in K) is defined by

$$\theta' = T_a\left[1+0.378\left(e_a / p_a\right)\right], \tag{3.14}$$

where T_a is the air temperature (K) and e_a and p_a are vapor pressure and atmospheric pressure (mb). The difference $\Delta\theta$ is then

$$\Delta\theta' = \left[T_h\left[1+0.378\left(e_s / p_a\right)\right]\right]-\left[T_a\left[1+0.378\left(e_z / p_a\right)\right]\right], \tag{3.15}$$

where T_h is the water surface temperature (K) and T_a and e_z air temperature and vapor pressure at the 2 m elevation.

The ratio R^* between conductive and evaporative heat loss is known as Bowen's ratio and is given by

$$R^* = c\frac{p_a}{1000}\frac{T_h - T_a}{e_s - e_z}, \tag{3.16}$$

where c is a Bowen's constant estimated to be 0.60 for the units used here; P_a is atmospheric pressure (millibar, mb).

The conductive heat flux is the product of the evaporative heat flux and Bowen's ratio

$$\phi_H = R^* \text{x } \phi_E . \tag{3.17}$$

Therefore, the sum of heat loss due to the above processes is

$$\phi_{EH} = \phi_E (1 + R^*) . \tag{3.18}$$

The heat loss due to the formation of ice particles Q_{wi} is given by the relation

$$Q_{wi} = h_{wi}\left(T_i - T_v\right) = -f\left(M_i\right)T_v = C_p \rho \left(1 - M_i\right)T_v , \tag{3.19}$$

where

$$h_{wi} = \frac{N_u k_u}{l} \tag{3.20}$$

and M_i, the volume concentration of frazil ice formed over time dt, is given by (Ye and Doering, 2004)

$$\frac{dM_i}{dt} = \frac{h_{wi}\left(T_i - T_v\right)}{\rho_i L_i} = \frac{Q_{wi}}{\rho_i L_i} , \tag{3.21}$$

ρ is the density of water, C_p is the specific heat of water, Q_{tw} is the net heat loss per unit volume of water with the surrounding environment, and Q_{wi} is the heat transfer to ice from water. L_i is the latent heat of ice, ρ_i is the density of frazil ice. T_i is the ice surface temperature assumed to be 0°C. T is the ambient water temperature, h_{wi} is the heat transfer coefficient for an individual ice crystal.

h_{wi} is the heat transfer coefficient, which can be expressed in a dimensionless form as a Nusselt number defined by

$$N_u = \frac{h_w l}{k_{wi}}. \tag{3.22}$$

Rearranging

$$h_w = N_u \frac{k_w}{l}, \tag{3.23}$$

where l is the face radius and is calculated based on the surface area of the ice crystal as $l = \left(\left(A_s + A_e\right)/4\pi\right)^{0.5}$; A_s is the surface area and A_e is the edge area. A diameter to thickness ratio of 1:15 is assumed. k_{wi} is the thermal conductivity of water and equal to 0.564. The Nusselt number depends on the flow condition and the particle size. According to Daly (1984)

$$N_u = \left(\frac{1}{m^*}\right) + 0.17\,\mathrm{Pr}^{1/2} \quad \text{if} \quad m^* < \frac{1}{\mathrm{Pr}^{1/2}} \tag{3.24}$$

and

$$N_u = \left(\frac{1}{m^*}\right) + 0.55\left(\frac{\mathrm{Pr}}{m^*}\right)^{1/} \quad \text{if} \quad \frac{1}{\mathrm{Pr}^{1/2}} < m^* < 10, \tag{3.25}$$

where $m^* = r/\eta$, is the ratio between the face radius of the ice crystal and the Kolmogorov length scale.

For large particles, *i.e.* $m^* > 1$

$$N_u = 1.1\left[\left(\frac{1}{m^*}\right) + 0.80\alpha_T^{0.035}\left(\frac{\mathrm{Pr}}{m^*}\right)^{1/3}\right] \quad \text{if} \quad \alpha_T m^{*4/3} < 1000 \tag{3.26}$$

and

$$N_u = 1.1\left[\left(\frac{1}{m^*}\right) + 0.80\alpha_T^{0.24}(\mathrm{Pr})^{1/3}\right] \quad \text{if } \alpha_T m^{*4/3} \geq 1000, \tag{3.27}$$

where $\alpha_T = \sqrt{2k}/U$ is the turbulence intensity indication number, k is the kinetic energy and U is the mean flow velocity. It is noticed that when m^* increases, provided that $m^* > 1$, N_u decreases. Therefore, the thermal growth rate of frazil particles decreases rapidly with an increase in particle size. The Prandtl number Pr is defined as ν/α_r (kinematic viscosity/thermal diffusivity) where the thermal diffusivity is $\alpha_r = k_{wi}/\rho C_p$; note C_p = 4185.5.

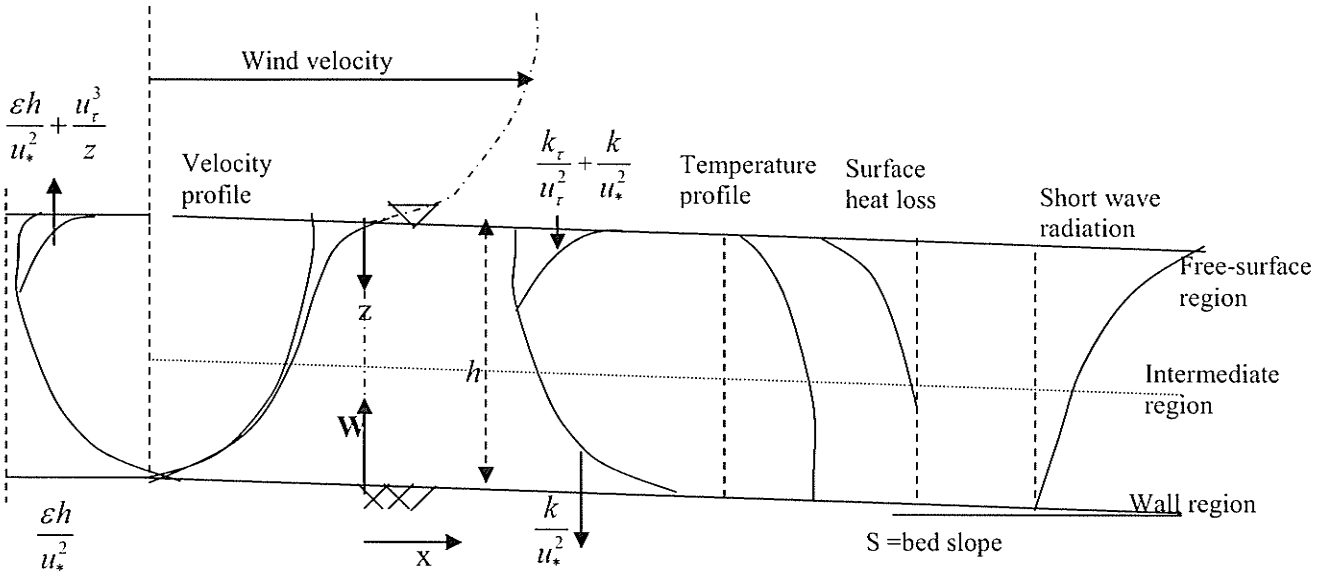

Figure 3.1 Profile of the flow and temperature components.

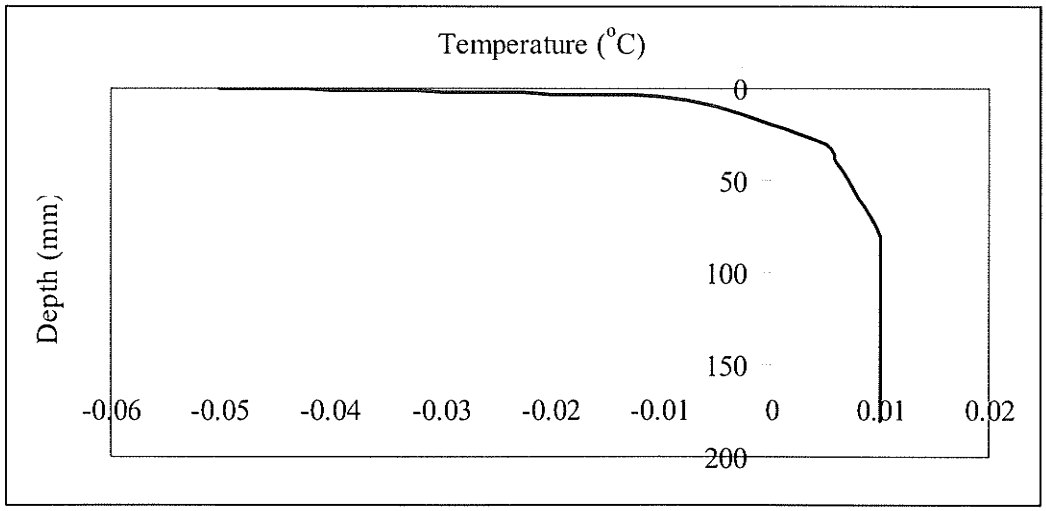

Figure 3.2 Typical vertical temperature distribution in a counter-rotating flume.

CHAPTER 4 Experimental setup and testing

4.1 Introduction

Due to the variability of hydrological and metrological conditions, it is difficult to gather field data to study the formation of surface ice. The only documented field studies carried out to study the formation of skim ice are those reported by Matousek (1984, 1990, 1992). Therefore, it is necessary to carry out experimental studies to determine the effect of different types of hydraulic and hydrologic parameters in the laboratory. For this main reason, therefore, the counter-rotating flume inside a cold room was designed by the HRTF at the University of Manitoba. The ice laboratory is comprised of a cold room, a counter-rotating flume equipped with cameras, peripheral measuring instruments, and digital image processor.

4.2 Experimental Set Up

The counter-rotating flume (Tsang, 1992; Doering and Morris, 2003) to be used in this experiment is shown in Figure 4.1. A brief description of the experimental setting, velocity measuring techniques, and temperature and image acquisition equipment is given below.

4.2.1 Introduction to the counter-rotating flume and cold room

The counter-rotating flume has been designed to simulate open channel flow in terms of Lagrangian theory. It consists of a circular channel supported underneath by a turntable. The bottom of the channel is separate from the channel walls and is supported by an independent overhead structure. This allows the bottom and the walls of the channel to rotate independently and in opposite direction. An air jacket below the base plates circulates warm air to simulate geothermal heat from a river bed. The air pocket is equipped with a heater and fan connected to a PID controller to maintain a constant temperature. The air temperature in this pocket is separated from the flume water by an insulator which is a 5 cm thick layer of UHMW (ultra high molecular weight) plastic. RTD sensors embedded in the UHMW plastic indicate that the temperature of the plastic, just below the embedded gravel bed plates, is 0^{o} C while supercooling occurs. The embedded gravel plates are coated with sand of varying roughness to simulate the roughness of the natural river. A sample picture of different bed plates coated with different sizes of roughness is shown in Figure 4.2. In addition, in order to prevent the side walls of the flume from icing, warm air is used to circulate in ducts surrounding the flume walls. A heater lamp connected to a PID controller is activated

whenever the air temperature in these ducts falls below 2°C. The warm air is circulated through the wall ducts with a fan.

To model the free surface flow in an open channel, the flow in the counter-rotating flume has to be calibrated. The rotation of the bed of the flume has the potential to induce secondary circulation in the fluid due to centrifugal forces. The wall and bed rotation rates must, therefore, be set to balance this centrifugal effect. The net result is the water is stationary in an absolute frame of reference, at a given depth. It is practically impossible to have zero absolute reference velocity at all depths and therefore, a depth of 0.6h (where h is the water depth) was used to calibrate the velocity. The relative rates of rotation required to achieve zero absolute velocity will depend on the bed roughness.

To control the air temperature the counter-rotating flume is located in a cold room which is 4.3 m by 4.3 m by 2.7 m high and is constructed of 4" thick Norbec insulated panels with an insulation value of R30. It is equipped with two Blanchard Ness outdoor air cooled condensing units, each with the capacity of 48000 BTU's. Each condensing unit is coupled with a Blanchard Ness low silhouette evaporator coil via a Sporlan CDS-8 step motor evaporator control valve. The temperature of the cold room is regulated with an Omron E5GN temperature controller mounted outside the cold room. The temperature control system is also equipped with an RS-232 port to allow full computer control and monitoring of the PID controlled compressor systems. The temperature adjustment limit of the cold room can go as low as -30 °C with a variation within ± 0.1° C.

4.2.2 Temperature measuring technique

As mentioned above the temperature of the cold room is controlled by a PID controlled compressor system. Water temperature in the counter-rotating flume is measured by using a Hart Scientific Black Stack thermistor, which measures the water temperature with an uncertainty less than 0.001^0 C and resolution of 0.0001^0 C. The data is directly transferred to a computer in digital form. The temperature of the inner wall, outer wall and bottom duct are recorded using a National Instruments data acquisition system. The relative humidity is detected by a Campbell Scientific temperature and humidity sensor. Two RTDs are installed in the CRF, one near the surface and the other at half of the flow depth to measure the surface temperature and depth average temperature variation.

4.2.3 Velocity measuring technique

The velocity profile, *i.e.*, the magnitude and direction at a given depth, in a counter rotating flume is dependent on the relative magnitude of the bed and the side wall velocity. By setting different wall and bed speeds the average velocity relative to the bed was measured at a depth 0.6h by using a Kent Lea probe (sample of the velocity measured for roughness 0.34 cm and depth 20 cm is shown in Table 4.1). Different values of bed speed and wall speed were varied until the testing velocity for that particular experiment is achieved.

Table 4.1 Bed and wall speed to find relative water velocity, for d = 0.34 mm and h = 20 cm.

bed speed (cm/s)	wall speed (cm/s)	water velocity relative to the bed (cm/s)
15	13	14.0
20	10	16.7
30	0	14.3
30	10	21.0
30	20	27.5
40	20	31.5
40	30	32.5
60	20	34.0
60	30	41.5
60	25	39.0

4.2.4 Image recording

The counter-rotating flume is equipped with two Hitachi KP-F100A CCD cameras each of them having a resolution of 1200 x 1024 pixels. The cameras were located in a box attached to the side walls, which requires them to rotate with the walls. The first camera was set to take images from the top of the water surface and the second camera set to take images from the side to observe the availability and growth of skim ice particles on the water surface and in the water. Two DT-3162 data translation frame grabber boards were used to transfer the data from the cameras to the computer. Images were back lit with one 400 W and one 250 W metal halide bulb producing 40,000 and 20,000 lumens, respectively. The light coming from the bulb was first filtered by a polarizing sheet, then passed through the inner wall, the water, then the outer wall, where it was filtered again by a second polarizer located on the side camera lens. The second polarizer was oriented such that the optic sills are perpendicular to the optic sills of the first polarizing sheet. The camera located on the top of the water surface gets a reflected light from the flume bed where the light bulb was located above the water

surface besides the camera (see Figure 4.4). To get sufficient reflection, the bed plates are painted with black glassy paint. No polarizer was used in the second camera. Using this method it was possible for the camera to "see" the transparent ice particles. The Hitachi cameras permit shutter speeds up to 1/10,000s. These cameras were used to gather images of ice particles in an experiment and the recorded images were automatically saved to the computer mounted in a side wall.

4.3 Testing Procedure

The following experimental procedure is followed in all the experiments. The experimental variables are flow depth (varied as 10 cm, 15 cm, and 20 cm), bottom roughness (varied as d = d_{50} = 1.7 mm, 3.4 mm, and 10 mm), velocity (varied as 0.2 m/s, 0.4 m/s and 0.6 m/s) and air temperature (varied as -10^0C and -15^0C). Specified bed roughness is set on the bed and a certain amount of water equal to the measuring depth is filled in the flume. For this given depth the two cameras are adjusted for clear focus. By varying the side wall and bed speed, a testing velocity is measured at a depth 0.6h by using a Kant lee probe and the bed and side walls are allowed to rotate for that testing velocity. The temperature of the cold room is then set to a testing temperature and the two thermistors are set on the water surface and average depth to read the water temperature at the surface and average depth respectively, by using LogWare II software which gives continuous plot of the water temperature. When the surface water temperature reaches 0.1°C a continuous image acquisition starts and image acquisition ends when the residual water temperature reached approximately -0.002°C. A total of thirty one experiments were conducted by varying the above testing variables and the

data analyzed in the section below. In all the experiments the inner duct temperature, the outer duct temperature, and the bottom duct temperature of the flume kept to a constant value of 3.7°C, 2.64°C and 1.6°C, respectively, and the humidity of the cold room was in the range of 60% to 65%.

Table 4.2 Experiment schedule for different variables.

Temperature (°C)	Roughness (mm)	Depth (cm)	Velocity (m/s)
-15	3.4	20	0.2
			0.3
			0.4
		15	0.2
			0.3
			0.4
		11.5	0.2
			0.3
			0.4
	1.7	11.6	0.2
			0.3
			0.4
		15.7	0.2
			0.3
			0.4
		20	0.2
			0.3
			0.4
			0.6
	10	20	0.2
			0.3
			0.4
		15	0.2
			0.3
			0.13
			0.4
		10	0.2
			0.3
			0.15
-10	10	10	0.2
		15	0.2

Figure 4.1 The counter rotating flume.

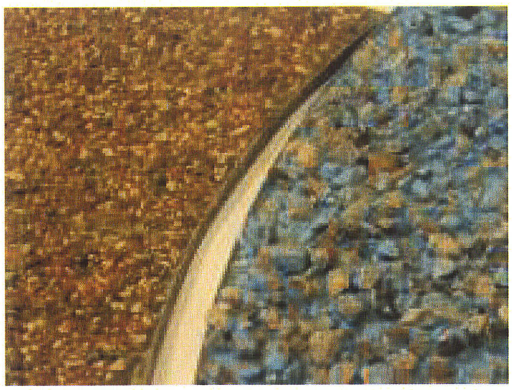

Figure 4.2 Small (D_{50} = 3.5 mm) and large (D_{50} = 10 mm) diameter gravel used for the bed plates.

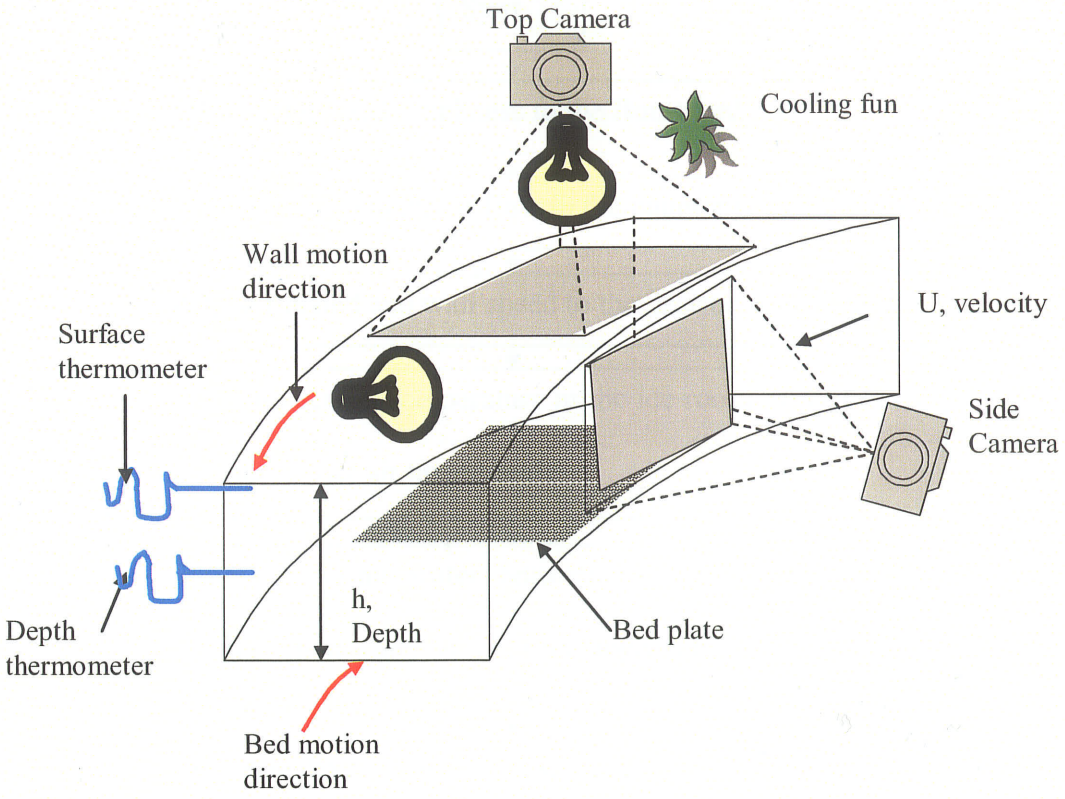

Figure 4.3 Surface camera setting and lighting.

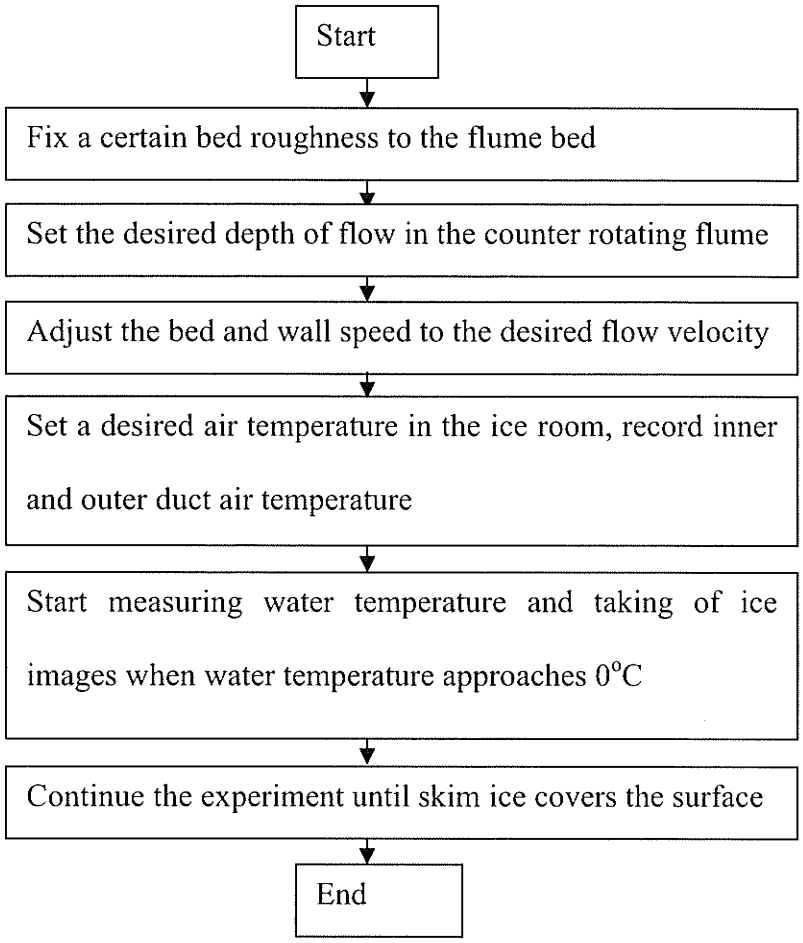

Figure 4.4 Experimental procedure.

CHAPTER 5 Experimental observation: The formation of different types of surface ice runs

5.1 Introduction

The variability of hydraulic and hydrologic parameters on a river system can initiate the formation of different types of surface ice. The types of these surface ice formations, their formation mechanism and their dependence on hydraulic and hydrologic parameters are not yet known. It was presumed that these surface ice formations are related to the flow depth, velocity, bed roughness and air temperature and their formation can be efficiently studied in a laboratory by varying the variables that influence their formation.

The first intention of this chapter is to investigate the types of surface ice formations. Therefore, for each bed roughness, flow depth and air temperature set up the flow velocity was varied in such a way that mixing in a counter rotating flume ranges from a complete

mixing (*i.e*, the temperature readings at the water surface and average depth are nearly equal) to a partial mixing (*i.e*, the temperature reading at the average depth is greater than zero). The observed types of surface ice formations are discussed in section 5.2.

The second intention of the chapter is to examine the combined effect of the testing variables on the types of surface ice formations. For this purpose and for practical application the data sets are combined and converted to different types of dimensionless numbers. The dimensionless numbers that give a meaningful relation with the observed surface ice formations are discussed in section 5.3.

5.2 Observations

The testing procedure described in section 4.3 is used to accomplish testing. It is observed that the types of surface ice formations are mainly dependent on the degree of turbulence. Depending on the degree of turbulence, which is expressed by the combined effect of bed roughness, flow depth and average velocity and entirely affects the degree of mixing, four types of ice formations namely, skim ice that cover the water surface, skim ice run, skim ice and frazil ice run and complete frazil ice formations are observed. Table 5.1 illustrates this observation together with the testing parameters and the following sections elaborate the formation of these ice types.

Table 5.1 Experimental variables and observations

Temperature (°C)	Roughness (m)	Depth (m)	Velocity (m/s)	Observation
-15	0.01	0.20	0.20	skim ice run
			0.30	skim ice + frazil
			0.40	frazil
		0.15	0.20	skim ice run
			0.30	skim ice + frazil
			0.13	skim ice cover
			0.40	frazil
		0.10	0.20	skim ice + frazil
			0.30	frazil
			0.16	skim ice cover
	0.0034	0.20	0.20	skim ice cover
			0.30	skim ice run
			0.40	skim ice + frazil
		0.15	0.20	skim ice + frazil
			0.30	skim ice + frazil
			0.40	frazil
		0.12	0.20	skim ice cover
			0.30	skim ice + frazil
			0.40	frazil
	0.0017	0.20	0.20	skim ice cover
			0.30	skim ice cover
			0.40	skim ice run
			0.60	frazil
		0.16	0.20	skim ice cover
			0.30	skim ice run
			0.40	skim ice + frazil
		0.12	0.20	skim ice run
			0.30	skim ice + frazil
			0.40	skim ice + frazil
-10	0.01	0.15	0.20	skim ice run
		0.10	0.20	skim ice + frazil

5.2.1 Skim ice that covers the water surface (freeze up)

In small to moderate turbulence intensity skim ice particles form at the water surface and grow in number rapidly. The particles formed at the surface may travel with the flow until they cover the water surface; or instantaneous bridging forms on two or three places and then grow farther to cover the surface. In this case no ice particles are observed in the water and all particles are formed at the surface and remain at the surface (see Figure 5.1 and Figure 5.2).

Visual observations show that very thin flat sheets of skim ice particles form on the water surface on early stages of supercooling. These flat sheet ice particles interlock each other so quickly to grow in size or they start to attach with the side walls of the counter rotating-flume to enhance bringing and surface freeze up. On the experiments that lead to the formation of freeze up the testing time is too long compared to the other experiments as the particles on the surface grow in size and number and start to obscure the heat exchange between the water surface and the air.

5.2.2 Skim ice run

When the turbulence intensity increases skim ice particles formed on the water surface form a mesh of dendrites and travel with the flow in the near surface layer. It is observed that the length of the mesh could be as large as 0. 6 m to 1.3 m (see Figure 5.3 and Figure 5.4). The small increase in turbulent intensity is able to submerge some of the particles on the surface

to the near surface layer and the small increase in velocity prevents the bridging and surface freeze up by creating erosion and making the particles travel with the flow.

Visual observations indicate that interlocking of particles start at mid way of the experiment. The small three to four ball-shaped meshes that are formed almost at the same time start to grow in size to finally form one long mesh that is flowing on the near surface layer. The mesh grows in length until the heat exchange between the air and the water surface balances the heat generated due to the ice formation.

5.2.3 Skim ice run and frazil ice run

With the further increase of the turbulent intensity the quantity of skim ice formed on the water surface can not hinder the supercooling of the depth water to the extent enough for the formation of frazil ice. In this case skim ice particles (at the surface and near surface layer) and frazil particles (in the entire flow) travel together with the flow. Their relative quantity is dependent on the degree of turbulence, where the higher turbulence leads to high frazil concentration and the lower turbulence intensity leads to higher skim ice concentration (see Figure 5.5).

5.2.4 Complete frazil ice formation

Finally with the increase of turbulence intensity a complete mixing phenomena, where there is no stratification or a very small amount of stratification (i.e., in the range of 0.01 to 0.001 ^{o}C), is observed. In this case complete frazil ice with no surface ice is formed (see Figure 5.6). The very small disc crystals that are formed almost every where across the flow depth

are start to be observed after few minutes of supercooling. These ice particles grow in size until their buoyancy force is greater than the vertical turbulent fluctuation in which case they float to the surface to form a mesh. Because of a complete mixing, experiments that lead to the formation of frazil ice took much lower testing time than other experiments.

5.3 Data Analysis

For practical purposes the data collected in the laboratory should be expressed in a suitable dimensionless numbers such as the Froude number, F_r, the shear stress Reynolds number R_* and the Reynolds number R_e. The shear stress velocity in a flow can be written as (Carter *et al.*, 1963)

$$u_* = U\sqrt{\frac{f}{8}} \tag{5.1}$$

where f is a friction factor and U is the depth average flow velocity. For turbulent flow f can be estimated using the Colebrook-White equation (Colebrook, 1939)

$$\frac{1}{\sqrt{f}} = -2\log\left(\frac{k_s}{3.71(4R)} + \frac{2.51}{R_e\sqrt{f}}\right), \tag{5.2}$$

where k_s is representative roughness height and for a plane bed is given by equation $k_s = \alpha d_{90}$ where (for sand and gravels) $d_{90} \cong 2d_{50}$ and α is a coefficient ($\alpha = 1$ for stones

$d_{50} \geq 0.1\ m$ and $\alpha = 3$ for sand and gravel material. An explicit approximate equation for f can also be written as (Idelchik, 1986)

$$f = 0.1\left(1.46\frac{k_s}{4R} + \frac{100}{R_e}\right)^{0.25}, \tag{5.3}$$

where R_e is the Reynolds number given by UR/ν and R is the hydraulic radius. The bed roughness can be characterized by a dimensionless number known as shear stress Reynolds number defined as

$$R_* = \frac{u_* k_s}{\nu}, \tag{5.4}$$

where ν is a kinematic viscosity of water at a temperature close to zero and equal to $1.787*10^{-6}$ m^2/s. When R_* is less than 5, the flow is said to be hydrodynamically smooth (HSF), when R_* is greater than 70 the flow is said to be hydrodynamically rough (HRF), when between 5 and 70 the flow is transitional. The Froude number of a flow, F_r, is defined as

$$F_r = \frac{U}{\sqrt{gh}}, \tag{5.5}$$

where h is the depth of flow. The plot of the shear stress Reynolds number versus the Froude number for the experimental variables is given in Figure 5.7, which can be written in equation form as

1. Frazil forms when

$$R_* > -7900Fr + 3000 \tag{5.6}$$

2. Skim ice + frazil forms when

$$-7900Fr + 2200 < R_* < -7900Fr + 3000 \tag{5.7}$$

3. Skim ice run forms when

$$-7900Fr + 1760 < R_* < -7900Fr + 2200 \tag{5.8}$$

4. Skim ice cover forms when

$$R_* < -7900Fr + 1760 \tag{5.9}$$

The same data set can be re-arranged to make a plot of the bed shear velocity and the Reynolds number (Figure 5.8) to investigate the effect of bed shear stress on the type of surface ice formations.

Figure 5.8 can be written in equation form as

1. Frazil forms when

$$R_e > 3\times10^6 u_* - 62000 \tag{5.10}$$

2. Skim ice run + frazil forms when

$$3\times10^6 u_* - 46000 < R_e < 3\times10^6 u_* - 62000 \tag{5.11}$$

3. Skim ice run forms when

$$3\times10^6 u_* - 35000 < R_e < 3\times10^6 u_* - 46000 \tag{5.12}$$

4. Skim ice cover forms when

$$R_e < 3\times10^6 u_* - 35000 \tag{5.13}$$

5.4 Discussion

From the above analysis it can be seen that the experimental results can be reasonably used to study the types of surface ice formations by expressing the experimental variables by dimensionless numbers. Accordingly four different types of surface ice formations are observed: the degree of turbulence was found to be the main factor that affects the stratification level which affects the type of ice formation. It is also observed that the types of ice formations are interdependent on roughness, flow depth and average velocity. The following table shows the limiting values of shear stress velocity and Froude numbers for the different types of ice formations:

Table 5.2 The limiting shear stress velocity and Froude number

Type of ice formation	Minimum shear stress velocity	Maximum Froude number
Skim ice cover		≤ 0.23
Skim ice run	≥ 0.013	≤ 0.28
Skim ice + Frazil	≥ 0.016	≤ 0.38
Complete frazil	≥ 0.022	

It is believed that all the necessary parameters that affect the type of ice formations are incorporated in the chart and it will be useful to investigate the type of ice formations in

natural rivers. Moreover, it can also be concluded that the type of ice formation is independent of the temperature (or surface heat flux).

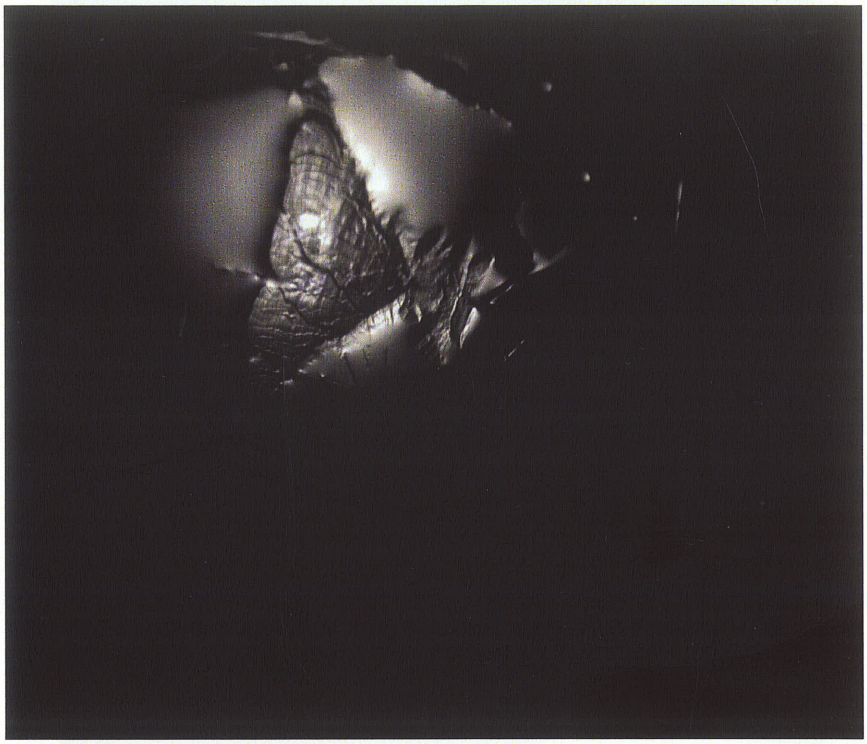

Figure 5.1. Skim ice that covers the surface (top camera) (d=3.4 mm, h=0.2 m, U=0.2 m/s and T=-15°C)

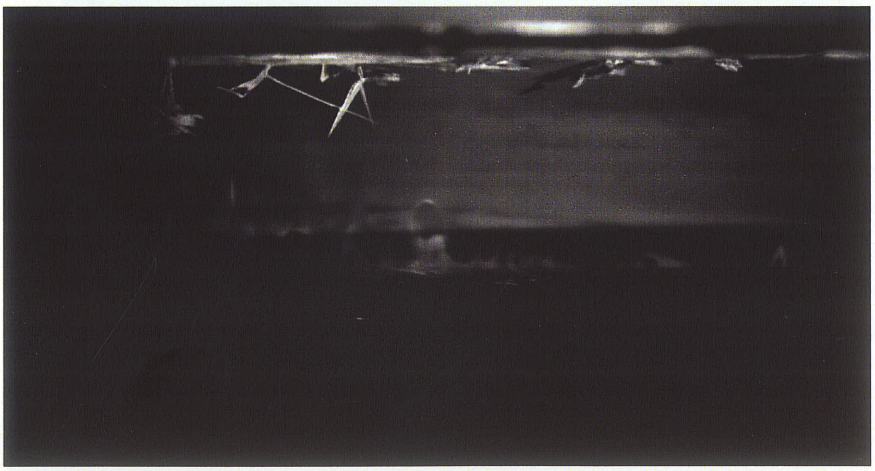

Figure 5.2. Skim ice that covers the surface (side camera) (d=10 mm, h=0.1 m, U=0.155 m/s and T=-15°C)

Figure 5.3. Skim ice run (top camera) (d=10mm, h=0.15 m, U=0.2 m/s and T=-15°C)

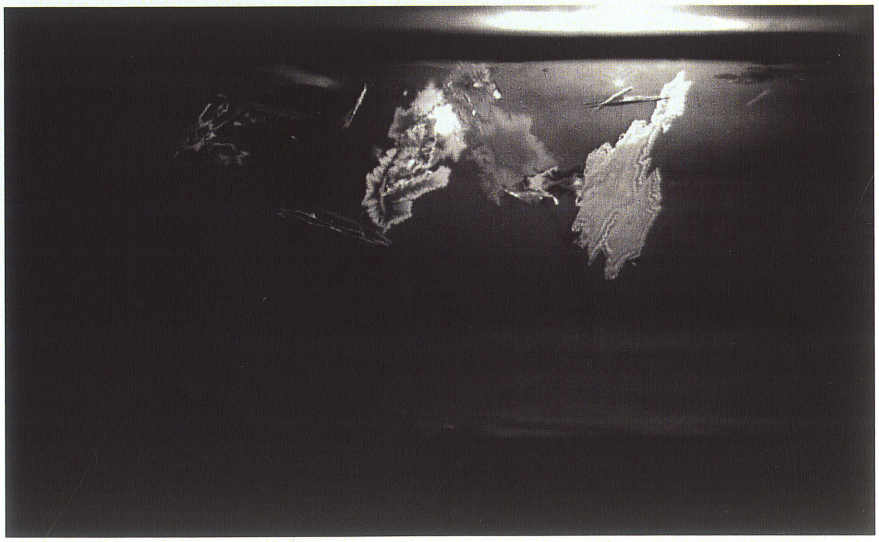

Figure 5.4. Skim ice run (side camera) (d=10 mm, h=0.15 m, U=0.2 m/s and T=-15°C)

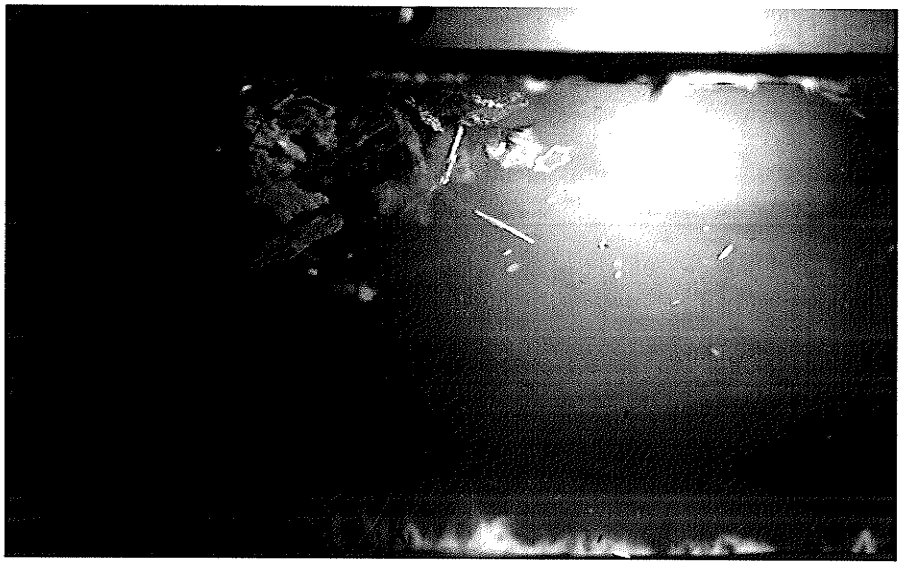

Figure 5.5. Skim ice and frazil run (side camera) (d=3.4 mm, h=0.15 m, U=0.3 m/s and T=-15°C)

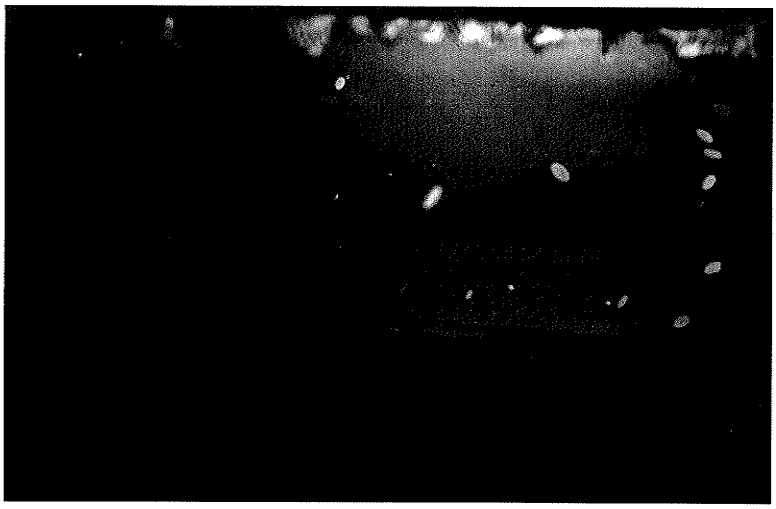

Figure 5.6. Complete frazil formation (side camera) (d=10 mm, h=0.15 m, U=0.4 m/s and T=-15°C)

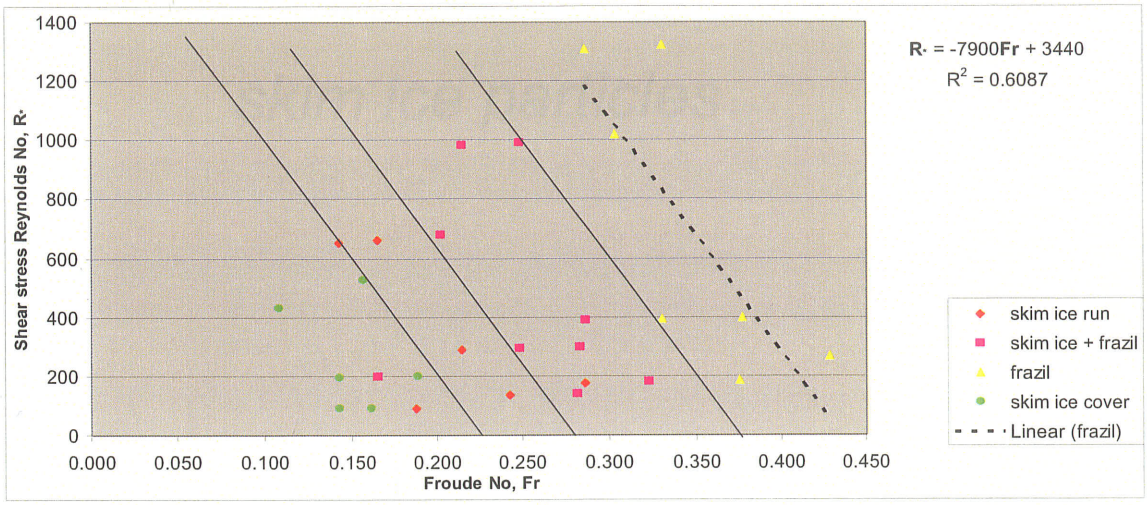

Figure 5.7. Formations of different types of ice runs as a function of Froude number and shear stress Reynolds number

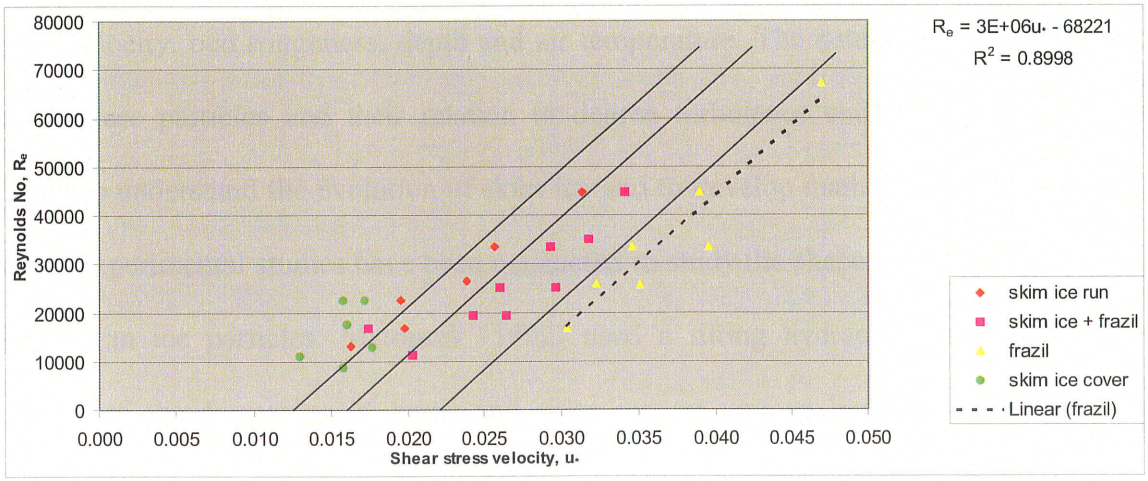

Figure 5.8. Formations of different types of ice runs as a function of Bed shear stress velocity and Reynolds Number

CHAPTER 6 Experimental observation: The skim ice particles

6.1 Introduction

The size and shape of skim ice particles that exist on supercooled water surface depend on the flow velocity, bed roughness, depth and air temperature. The determination of size and shape of these particles and their relation to degree turbulence and surface heat loss is important to understand the evolution of skim ice and to develop mathematical models. Yet, not many experimental studies have been conducted to study the shapes, sizes and properties of these skim ice particles. Matousek (1992) used a tilting hydraulic flume to test the hypothesis of the formation of frazil and skim ice on various bottom roughness, flow velocities and temperature. In his experiment, he observed that the first ice particles to be formed ranged from short ice needles up to ice floes with a plane bottom surface.

In the following sections sizes and types of skim ice particles and their relation to the degree of turbulence will be examined. Moreover, the process of nucleation and the process of surface coverage are discussed in relation to the type of surface ice formed. We will also discuss the fact that skim ice particles are different from frazil ice particles and the fact that skim ice particles are not initiated from frazil crystals. Thirty one experiments were carried out to investigate the formation of skim ice crystals and frazil ice particles and the relation to bed roughness, flow velocity, flow depth and air temperature.

6.2 Observations

After all the experiments were carried out successfully, those experiments that lead to the formation of skim ice were collected and thoroughly examined. It was found that there is no clear relationship between the particles shape and size character with respect to surface heat loss. The following points are discussed depending on the observations and it is worth mentioning that small, moderate and large turbulent intensities are related to the formation of skim ice, skim ice and frazil, and complete frazil (Unduche and Doering, 2007) and given as a function of bed shear stress Reynolds number and the Froude number by the relation

1. $R_* < -7900Fr + 2200$ small turbulent intensity
2. $-7900Fr + 2200 < R_* < -7900Fr + 3000$, moderate turbulence intensity and
3. $R_* > -7900Fr + 3000$, large turbulent intensity.

6.3 Nucleation

It has been noted in the literature that frazil ice is the initiation for the formation of most types of river ice; and skim ice particles are frazil ice particles that float on the surface when the vertical turbulent fluctuation velocity is less than the buoyant velocity. However, our experimental observation indicates that skim ice particles are those ice particles that nucleate at the water surface when the water surface supercools; provided that there is stratification. Frazil ice particles are circular or elliptical discs that nucleate in water at high turbulent intensities. The detail of different types of surface ice formation has been discussed by Unduche and Doering (2007). In a complete mixing scenario, *i.e.*, where there is no stratification, only frazil ice particles are formed. In small to moderate turbulence intensity ice particles first nucleate at the surface to form skim ice particles and grow in size and number and if the turbulent intensity is sufficient to supercool the bulk water then frazil particles start to form. Some of these skim ice particles are submerged in the flow due to the turbulent vertical fluctuation velocity and some remain on the surface and flow with the surface water. Therefore, turbulence is an important factor in determining the type of ice particle formed in a given flow not only by submerging the already formed particles on the surface, but also by affecting the degree of stratification, which affects the location of nucleation.

It is observed that before the particles nucleate, the surface has to deform in the shape of the particle that has to be formed. Figure 6.1(a) shows surface deformation before the formation of circular ice particles and Figure 6.1(b) shows another location on the water surface where the surface deformed and formed a hexagonal shaped particle. From small to moderate

turbulent intensities, the time lag between these two formations can vary from 10 minutes to 5 minutes, respectively. This deformation and initial nucleation were observed to starts at the surface when the surface water temperature was 0.025 to 0.16°C. Even though an attempt was made to measure the water temperature at the interface between the water and the air, it was found to be difficult to measure with the current experimental setup, due to a very high temperature gradient close to the water surface. However, it is still believed that nucleation starts when the temperature on the water surface is few degrees centigrade less than zero.

As surface deformation and surface turbulence attribute to the nucleation on the water surface, the size of skim ice particles is much larger than the size of frazil discs whose nucleation is associated with the external seeding of micrometer size. The initial size of the skim ice particles is dependent on the degree of turbulence, where higher turbulence gives smaller sizes. For small turbulence intensity almost all types of skim ice particle shapes were observed dominated by leaf-shaped and finger shaped particles. For moderate turbulent intensities only needles and diamonds were observed and their quantity on the surface is relatively small.

6.4 Particle Shape and Size

6.4.1 Needle shaped particles

Needle shaped skim ice particles were observed in all experiments where skim ice was formed. Needle shapes were also one of the first skim ice particle shapes to be observed on the water surface. Their initial size ranges from 1 cm to 3 cm for moderate to small turbulent

intensities, respectively, and could grow up to 6 cm to 8 cm before forming any dendrites. Their number on the water surface is also related to the degree of turbulence and air temperature, where smaller turbulence intensity with high negative air temperature produces a large number of particles on the water surface. For small turbulent intensities needle shape particles grow so fast in size and make dendrites on the water surface, which then initiate the formation of bridging. The initial thickness of the needles varies from 0.02 cm to 0.1 cm and can grow up to 0.2 cm to 0.3 cm on later stages; however, their major growth is lengthwise. Figure 6.2(a) shows the images of needle shape particles at the instant of nucleation (when the surface water temperature is in between 0.025 and 0.16) and Figure 6.2(b) shows needle shape particles roughly half an hour after nucleation.

6.4.2 Hexagon, star and circle shaped particles

Hexagon shaped particles are also one of the first particles to be observed on the water surface in almost all the experiments where skim ice was formed. The hexagon shaped particles appeared as hexagonal crystals in small turbulent intensities and as a circle and then transformed to hexagon in moderate turbulent intensities. The initial (nucleation) size, *i.e.* the initial size observed on the water surface, of the hexagon ranged from 0.5 cm to 1 cm, and they could grow up to 2 cm and then submerge in the flow or form a mesh with needle shaped particles. It was difficult to determine the thickness of the hexagon particles but it was observed that they were very thin sheets and their growth was mainly in the radial direction. Star shaped particles are the main particles that were observed submerged in the flow for moderate turbulent intensities. Star shaped particles have the shape shown in Figure 6.3(a) during nucleation and Figure 6.3(e) after nucleation observed by the side camera moving

with the flow. However, sometimes it was observed that there was an interchange of shape from circles to hexagon and later on to stars with high turbulent intensities (Figure 6.3(b)). Figure 6.3(e) shows hexagon shaped particles during nucleation and Figure 6.3(f) shows hexagon shaped particles in the flow taken by the side camera. With the increase of size and turbulence intensity the hexagons formed on the surface may submerge to the flow (see Figure 6.3(c)).

6.4.3 Finger and leaf shaped particles

Finger shaped and leaf shaped particles are one of the dominant types of skim ice particles in small turbulent intensities. They have a common shape of fingers, leafs and triangles. Finger and leaf shaped particles are the dominant cause of surface coverage as they are flat sheets and their size is relatively larger than other types of ice particles. The initial size of fingers and leafs vary from 0.3 cm to 1 cm and they can grow as large as 3 cm to 4 cm before forming a mesh with other particles. Leaf shaped particles start to nucleate as a small circular core, called the center of nucleation, which can have protruding branches in one or two directions (Figure 6.4 (c)). Then they expand and grow from this core to form a triangular leaf or two triangular leafs connected with a core in opposite directions yielding the form of a butterfly. Finger shaped particles can have three to five fingers protruding from one palm and their number can grow to as many as 15 to 20 fingers. Mostly finger and leaf shaped particles were observed just floating on the water surface and occasionally (for moderate turbulent intensities) were observed submerged in the flow. Figures 6.4(b), 6.4(e) and 6.4(h) show initial nucleated and grown finger shaped particles, while Figures 6.4(a) and 6.4(f) show initial and grown leaf shaped particles. Figure 6.4(d) shows triangular shaped particles.

6.4.4 Irregular shaped particles

Irregular shaped particles are rarely formed (skim ice particles) in small turbulence intensities. These particles are mostly started to form as hexagons, circular leafs, or finger shapes and later on change to irregular rounded shapes or irregular branches. Their number in a given experiment is very small compared to the other types of skim ice particles. Their size ranges from 0.5 cm (during nucleation) to 1.5 cm until they sinter to other particles to form a mesh. Figures 6.5(a) & 6.5(b) show irregular shaped particles.

6.5 Particle Growth and Surface Coverage

Once the water surface supercools, skim ice particles form and grow both in size and in number. Their number is much smaller than frazil ice particles, if they would form, and they grow faster in size rather than in number. Therefore, even though their number is small, due to their large size they can easily balance the surface heat loss to prevent further supercooling of the bulk water. Their size and number on the water surface is dependent on the degree of turbulence. Depending on the degree of turbulence they can grow in size and number on the water surface to form either a bridge, a mesh, or a dendrite and cover the surface; or remain on the surface and near surface layer.

When the turbulent intensity is small the skim ice particles (mostly needles, hexagons and finger shapes) grow in size and interlock with each other to form a very long piece of surface ice. This surface ice is then attached to the border and will hinder the transport of other particles on the surface and accumulates particles to form a bridge in that location. Once

bridging is formed, a large sheet of surface ice forms on the water surface and prevents further supercooling of the water surface to form frazil ice.

For moderate turbulent intensities some of the skim ice particles remain on the water surface, however, the majority of the particles will be submerged in the flow and they travel with the flow in the surface layer (within the top 5 cm). These particles grow with time and start to interlock to form a mesh (Figure 6.6). At the beginning many small size dendrites are formed and finally interlock with each other to form a very large mesh of flowing skim ice with a mesh length varying from 50 cm to 130 cm. Once this mesh is formed, any particle nucleated during the later stages will be intermingled with the existing mesh. There is a very unlikely chance for surface coverage at this time and frazil ice may form, if the heat of fusion from the skim ice mesh is insufficient to balance the surface heat loss.

6.6 Section Summary and Discussion

A laboratory study was carried out to investigate the properties of skim ice particles. It is understood that skim ice particles are those ice particles that nucleate at the water surface when the turbulence intensity is insufficient for complete mixing. Whenever there is stratification, the surface supercools faster than the bulk water which initiates the formation of surface ice particles. Surface ice particles start to be observed on the water surface when the measured water surface temperature is in the range of 0.02°C to 0.16°C (non supercooled water surface). However, this does not mean that skim ice particles start to nucleate on a non-supercooled water, but it shows that there is a very high temperature gradient at the air-water

interface which can not be measured with our experimental settings. The water surface has to deform before the nucleation of the particles, which leads to the formation of large ice particles compared to frazil ice. Yet it is not clearly understood what factors contribute to the deformation of the water surface. Four different types of ice particle shapes were observed and their number on a water surface is related to the degree of turbulence. It is not clearly understood what factors attribute to the formation of those fixed shapes but it was observed that turbulence is a factor for the existence of some of the shapes. It is also understood that frazil crystals were either circular or elliptical discs which were formed at large turbulence intensities.

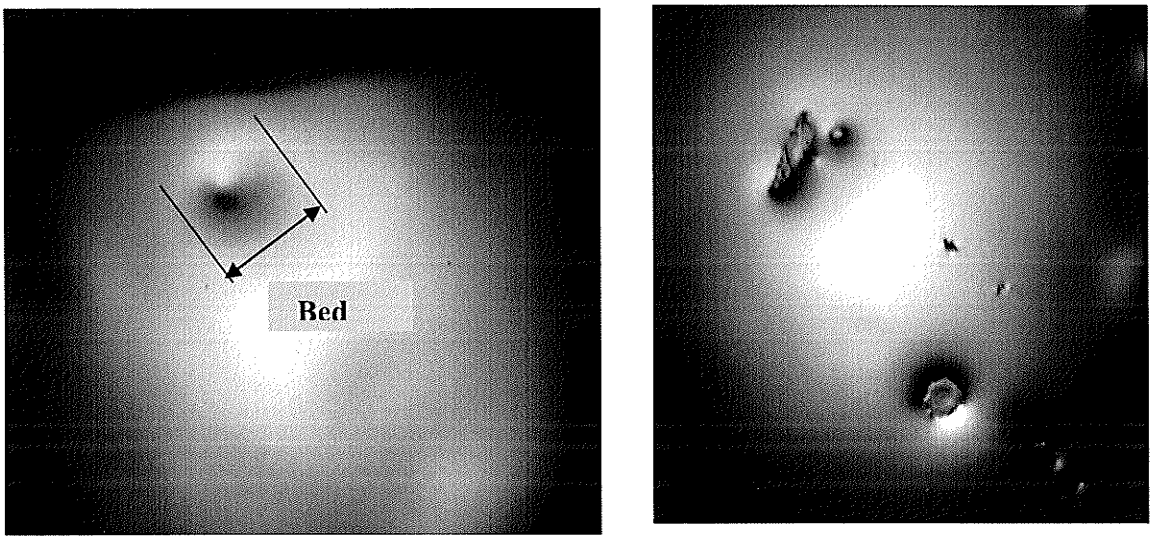

a) Water surface deformation before nucleation

b) A hexagonal and irregular shape during nucleation

Figure 6.1 a) Image of the water surface before nucleation and b) a hexagonal and irregular shape during nucleation on the deformed section of the water surface (plan view).

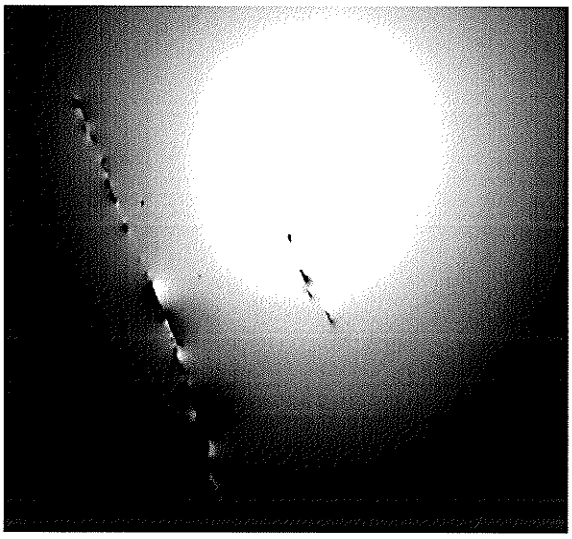

a) A long and short needle, the first to be observed on the surface, (size of the longer particle 3.8 cm and short one 0.8 cm)

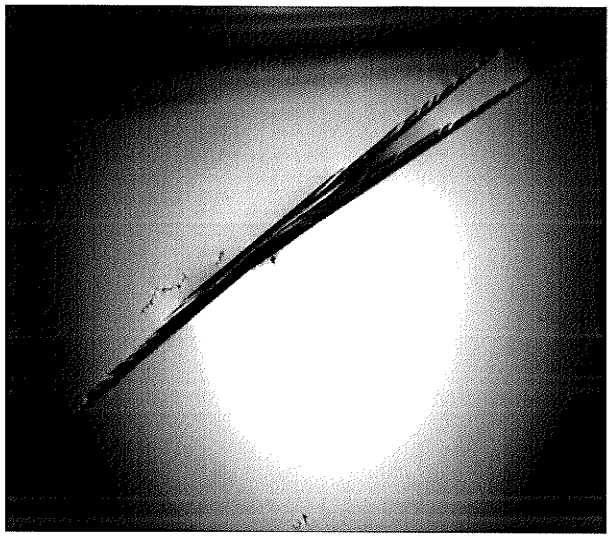

b) Needle shaped particles (size 6 cm)

Figure 6.2 Needle shaped particles a) during the instant of nucleation and b) after nucleation (plan view).

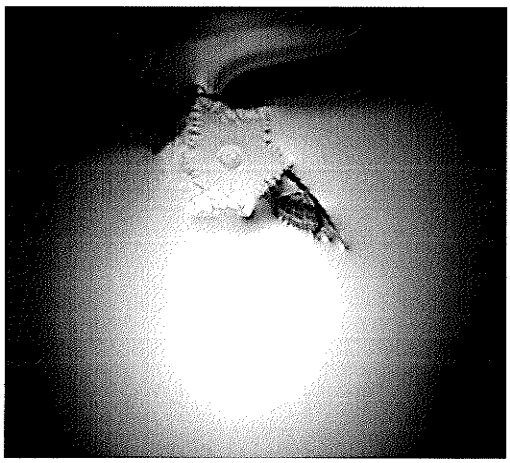

a) Star particle, the first to be observed on the surface, (plan view, size 1.2 cm)

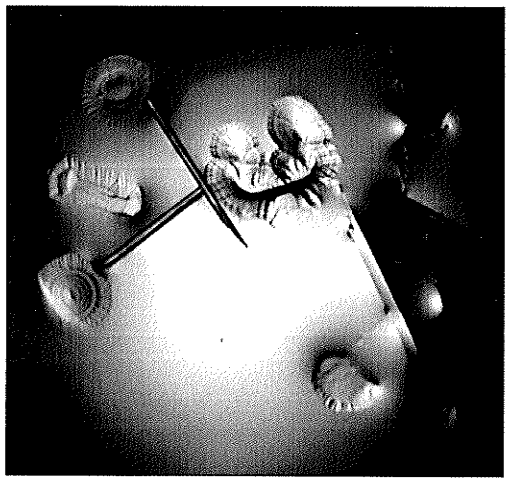

b) Circles (size 0.7 cm), hexagons (0.7 cm) and needles (1.4 cm), plan view

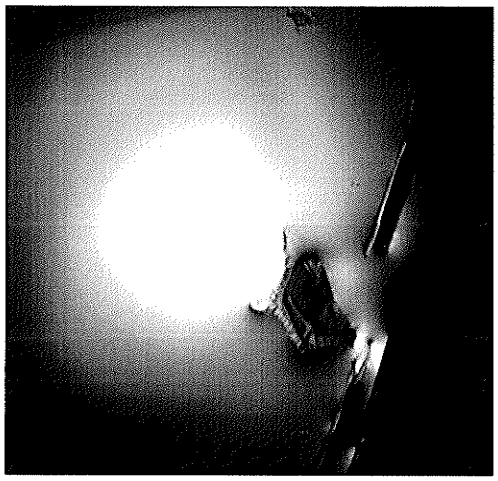

c) Hexagons submerging in the flow (plan view, 1 cm)

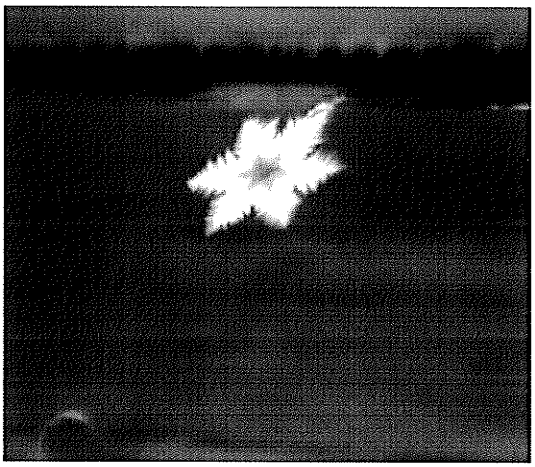

e) Star shaped particle in the flow (1.1 cm)

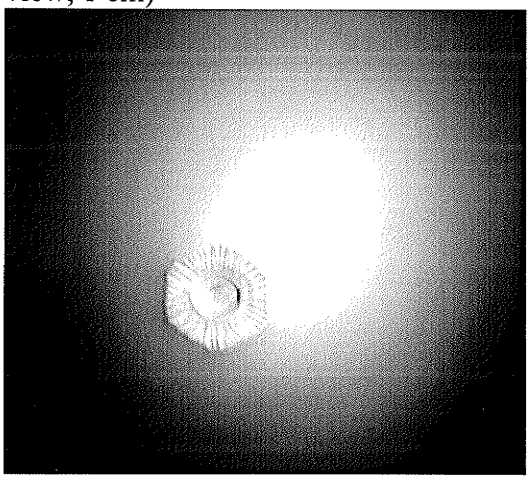

d) Hexagonal shaped particle (plan view 0.8 cm)

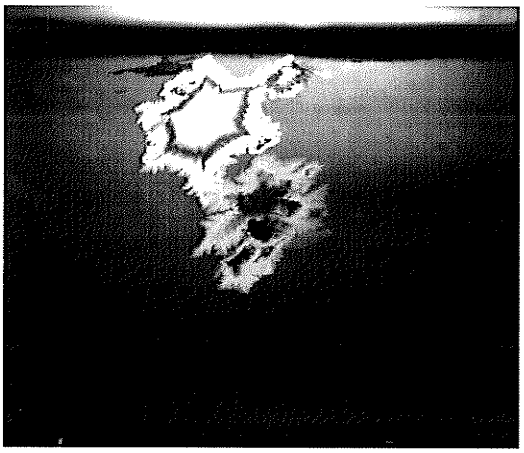

f) Hexagonal shaped particle in the flow (size 1.2 cm)

Figure 6.3 Hexagon, stars, needles and circles (plan views and side views)

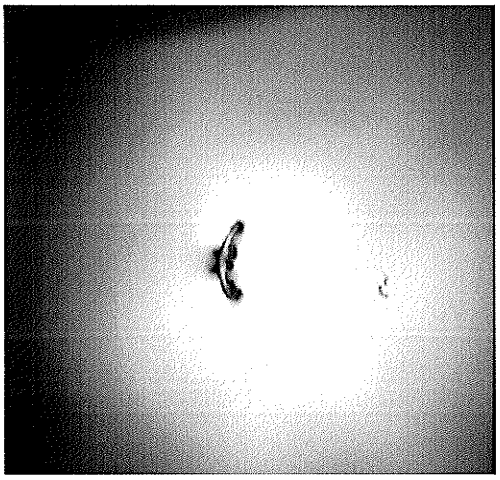

a) Leaf shapes, the first to be observed on the surface, (size 0.5 cm).

c) Start of branched leaf particles (0.5 cm)

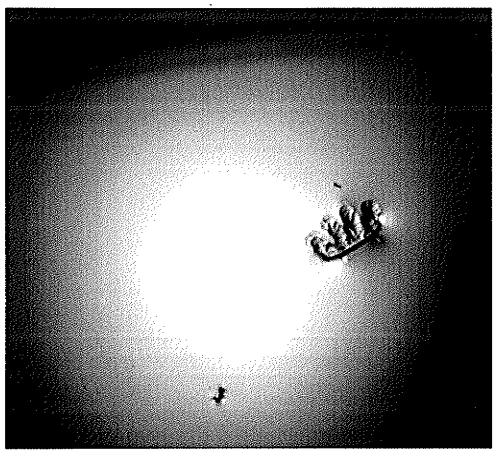

b) Finger shapes, the first to be observed on the surface, (size 0.7 cm, 4 fingers).

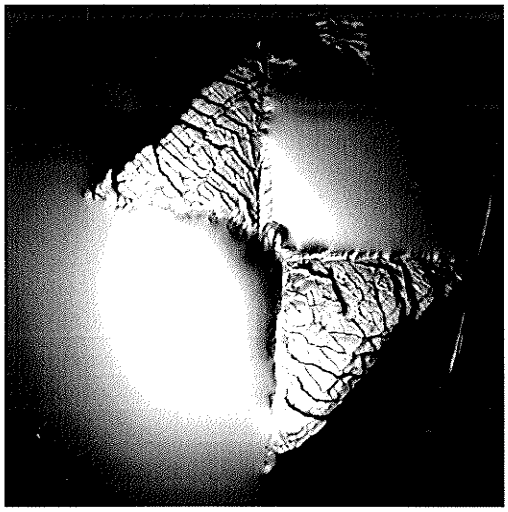

d) Triangular butterfly leaf (size 3.6 cm)

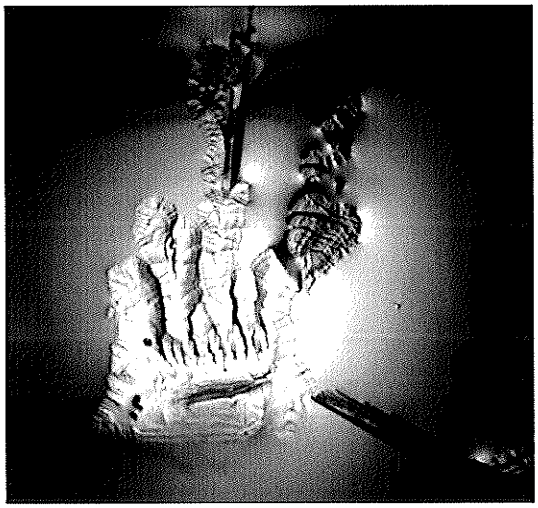

e) Fingers at the middle stage of their growth (size 2.3 cm)

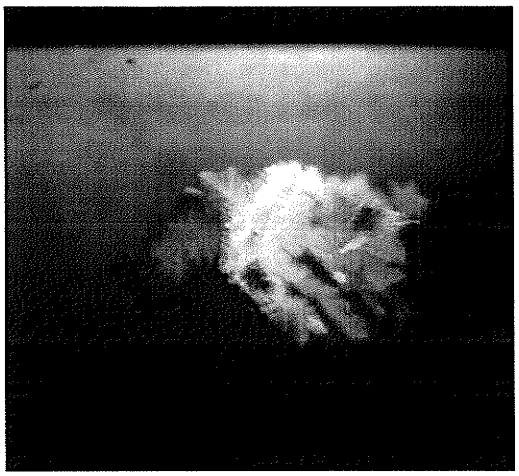

g) Finger shape in the flow (size 2.3 cm)

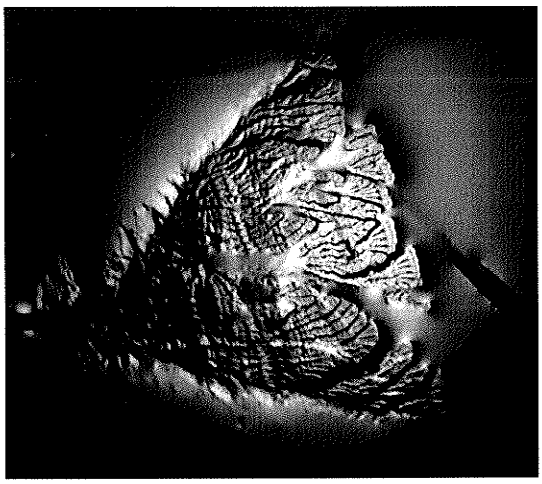

f) Leaf shaped particle (size 3.7 cm)

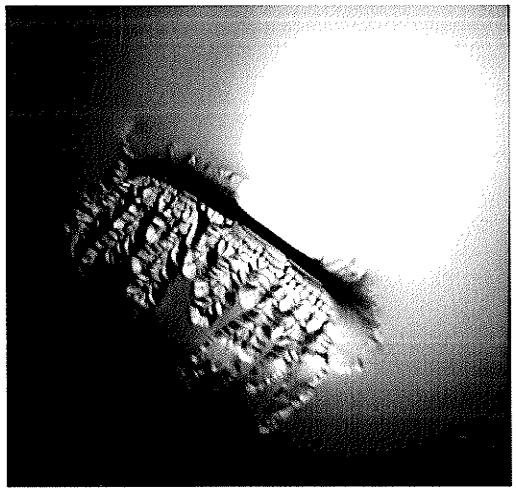

h) Many branching fingers (size 2.8 cm and fingers are 1.5 cm long)

Figure 6.4 Fingers and Leafs (all are plan views except (g))

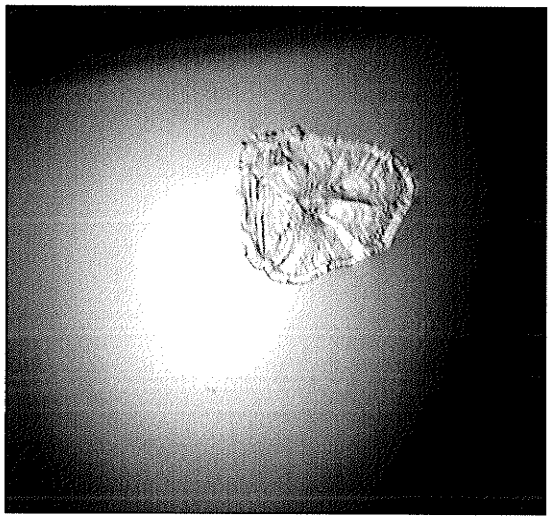

a) Irregular rounded shape (size 1.4 cm).

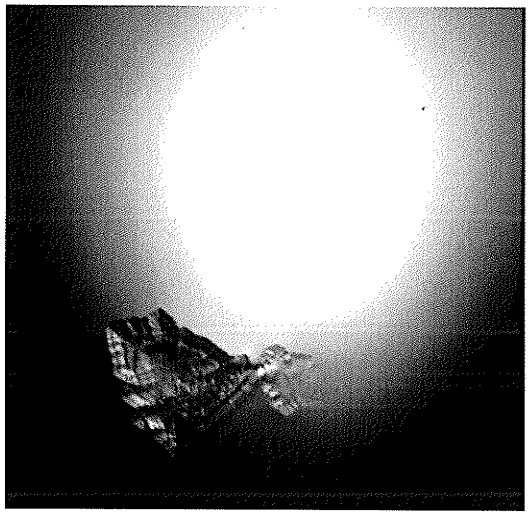

b) Hexagons transformed to irregulars (size 1.2 cm).

Figure 6.5 Irregular shapes (plan view)

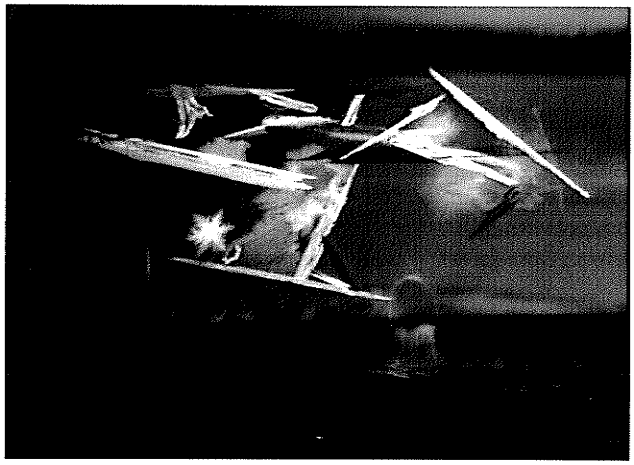

Figure 6.6 Needles, stars and diamond shaped particles interlocking each other to form dendrites.

CHAPTER 7

The minimum supercooling temperature at the average depth as a parameter to classify surface ice run types

7.1 Introduction

The formation of surface ice and frazil particles is linked to the relative difference of the water temperature at the surface and at the average depth (*i.e.*, the degree of stratification). In previous studies of surface ice formation Matousek (1984, 1992) investigated a relationship between the type of surface ice formation and the water temperature at the surface and at the average depth. In general, the higher the degree of stratification the less chance for the water at the average depth to supercool, which indicates a less chance of formation of ice at average

depth. Conversely, the higher the degree of stratification the higher the chance of surface ice cover (freeze up).

In the following section an experimental investigation of the relation of the temperature at the average depth to the type of surface ice cover is investigated. In all the experiments, for the ice to form on the water surface, the minimum supercooling temperature, T_{min}, is in the range of -0.05°C to -0.07°C. The total supercooling time (time to reach from zero to the minimum supercooling curve and from minimum supercooling curve to residual temperature) may change depending on the degree of turbulence and the surface heat loss; however, the minimum supercooling temperature at the water surface remains independent of the above conditions.

The relative temperature difference (ΔT, between the surface, T_h and between the depth, T_v) is dependent on the degree of turbulence and the depth. However, as the turbulent structure is dependent on a dimensionless parameter, y/h), *i.e.*, relative depth, (where, y is the depth measured from the bed and h is the water flow depth), the turbulent structure can be compared at $y/h = 0.5$, for all the experiments. Analogously, the minimum supercooling temperature at the average depth (or at $y/h = 0.5$) is only a function of the degree of turbulence and can be used to evaluate the type of ice formation on the water surface. In the following section the experimentally observed water temperatures at the average depth are used to evaluate the type of surface ice formations.

7.2 Observations

It is observed that the types of surface ice formations are dependent on the degree of turbulence. Depending on the degree of turbulence, which can be expressed by the minimum supercooling temperature at the average depth, four different types of ice formation are observed: skim ice that covers the water surface (freeze up), skim ice run, skim ice run and frazil ice formation, complete frazil ice formation. Due to its simplicity, the minimum supercooling temperature at an average depth was found to be the easiest way to classify surface ice formations. Table 7.1 summarizes the type of surface ice formation with the observed minimum supercooling temperature at an average depth and for the testing variables given in Table 5.1. The following section elaborates the effect of minimum supercooling temperature at an average depth on the type of surface ice formation.

Table 7.1 Experimental variables used in the study and the observed minimum depth supercooling temperature.

Temperature (°C)	Roughness (m)	Depth (m)	Velocity (m/s)	Min. bulk Temp. (°C)	Observation
-15	0.01	0.20	0.20	-0.0069	skim ice run
			0.30	-0.0234	skim ice + frazil
			0.40	-0.0501	frazil
		0.15	0.20	-0.0237	skim ice run
			0.30	-0.0318	skim ice + frazil
			0.13	0.0158	skim ice cover
			0.40	-0.0547	frazil
		0.10	0.20	-0.0296	skim ice + frazil
			0.30	-0.0457	frazil
			0.16	0.0070	skim ice cover
	0.0034	0.20	0.20	0.0114	skim ice cover
			0.30	-0.0125	skim ice run
			0.40	-0.0316	skim ice + frazil
		0.15	0.20	-0.0240	skim ice + frazil
			0.30	-0.0325	skim ice + frazil
			0.40	-0.0366	frazil
		0.12	0.20	-0.0025	skim ice cover
			0.30	-0.0434	skim ice + frazil
			0.40	-0.0738	frazil
	0.0017	0.20	0.20	0.0864	skim ice cover
			0.30	-0.0046	skim ice cover
			0.40	0.0303	skim ice run
			0.60	-0.0316	frazil
		0.16	0.20	0.0039	skim ice cover
			0.30	-0.0109	skim ice run
			0.40	-0.0165	skim ice + frazil
		0.12	0.20	-0.0338	skim ice run
			0.30	-0.0554	skim ice + frazil
			0.40	-0.0410	skim ice + frazil
-10	0.01	0.15	0.20	-0.0141	skim ice run
		0.10	0.20	-0.0356	skim ice + frazil

7.2.1 Skim ice that covers the water surface (freeze up)

Skim ice that completely covers the water surface forms when there is large gradient of temperature (large ΔT) and when the water temperature at the average depth is not supercooled (or the minimum supercooling temperature at the average depth is greater than or equal to zero). The surface supercools from -0.05 to -0.07 ^{o}C and the observed temperature gradient could be as high as 0.30 ^{o}C. A sample of the supercooling curve for a skim ice cover is shown in Figure 7.1 (the blue line shows the supercooling curve at the average depth of the water and the red line shows the supercooling curve at the water surface).

7.2.2 Skim ice run

A skim ice run forms when the temperature at the average depth supercools to an amount 0 to -0.02 ^{o}C. In this case unstable skim ice that flows with the flow is observed. The excess heat of fusion that comes from the formation of skim ice particles is enough to balance the further supercooling of the water temperature at the average depth up to the extent of formation of frazil ice. Figure 7.2 shows sample of the temperature profile for skim ice run (the blue line shows the supercooling curve at the average depth and red line shows the supercooling curve at the water surface). It can be noticed that the temperature at the average depth supecooled almost after an hour later than the surface which gives sufficient time for the surface particles to grow in size and number to form a mesh.

7.2.3 Skim ice run and frazil ice run

Skim ice and frazil ice run forms when the water temperature at the average depth supercools to an amount -0.02 to -0.04 °C. In this case skim ice, which can not hinder the formation of frazil ice, is formed. Figure 7.3 shows a temperature profile on a particular experiment for a skim ice run and frazil formation (the blue line shows the supercooling curve at the average water depth and the red line shows the supercooling curve at the water surface). It can be seen from the figure that the temperature at the average depth supercools roughly after fifteen minutes later than the surface, which shows the surface particles can not get sufficient time to grow in number and size to either cover the water surface (skim ice cover) or flow with the water and establish an equilibrium temperature by the heat of fusion (the case of skim ice run) to hinder frazil formation. It is also important to mention that frazil ice particles are only observed during and after the minimum supercooling temperature at the average water is reached, or $T_{min} \leq -0.02^{o}C$, (*i.e.,* after time $t \approx 4.15$ hr in Figure 7.3).

7.2.4 Complete frazil ice formation

Finally with the increase of turbulence intensity a complete mixing phenomenon, where there is no stratification (or significantly small stratification), where there are no skim ice particles (or very small number of skim ice particles dominated by frazil particles) are observed. In this case the supercooling temperature at the average depth is less than -0.04 °C. Figure 7.4 shows the temperature profile for the complete frazil ice formation. It can be seen that the temperature at the average depth and at the surface supercools almost at the same time, which leads the formation of ice particles of the entire flow. Unlike the above three cases, frazil particles start

to form when the temperature at the average depth starts to supercool, (*i.e.,* at time t ≈ 1.35 hr in Figure 7.4). During the start of their formation frazil particles have a disc shape and form in a relatively large number compared to the skim ice particles. Their size and number grows rapidly until the water temperature at the average depth reaches the minimum equilibrium temperature (mostly equals to -0.005°C) where by then the frazil particles form slush and float on the surface.

7.3 Effect of Air Temperature

From the experimental analysis it was observed that the type of surface ice formation is weakly dependent of surface heat loss (air temperature). The variation in air temperature only affects the cooling rate. The type of surface ice formation is mainly dependent on ΔT (*i.e.*, the temperature difference between the surface and the average depth) and the minimum supercooling temperature at the average depth which are entirely dependent on turbulence intensity. It is also worthy to mention here that the quality of the water under the test affects the minimum supercooling temperature and in this particular study Winnipeg tape water was used and any conclusion made is regard to this water quality. Figure 7.5 illustrate experiments with the same bed roughness, depth of flow and velocity, but with air temperatures of -15°C and -10°C. It can be seen that the experiment with an air temperature of -15°C shows steep cooling rate compared to the experiment with an air temperature of -10°C; however, the minimum supercooling temperature at the average depth and the temperature gradient, ΔT, roughly remained the same which indicate the same type of surface ice formation. In both the experiments observations show that the type of surface ice formed is a skim ice run and frazil

ice. Observations show that with increase in negative air temperature, the cooling rate increases and the ice particles grow faster in number and size, which limits the extra cooling of the temperature at the average depth of water for the same hydraulic properties but increased negative air temperature.

In general, from the above analysis, it can be concluded that the experimental result can be reasonably used to study the types of surface ice formations by expressing the experimental variables by dimensionless numbers. Accordingly four different types of surface ice formations are observed; the degree of turbulence was found to be the main factor that affects the stratification level, ΔT, and the minimum supercooling temperature at the average depth, which affect the type of ice formation. It was also observed that that the types of ice formations are interdependent on roughness, flow depth and average velocity. The following table shows the limiting values of the minimum supercooling temperature at the average depth for the different types of ice formations.

Table 7.2 The limiting values for the minimum supercooling temperature at the average depth.

Type of ice formation	The minimum supercooling temperature at the average depth
Skim ice cover	$T_{min} \geq 0.0$
Skim ice run	$-0.02 < T_{min} \leq 0$
Skim ice + Frazil	$-0.04 < T_{min} \leq -0.02$
Complete frazil	$T_{min} < -0.04$

Moreover, it can also be concluded that the type of ice formation is weakly dependent of the air temperature (or surface heat flux). The air temperature only affects the rate of cooling, and not the degree of stratification, ΔT. Therefore, types of ice formations are strongly affected by

hydraulic parameters and river properties rather than metrological parameters. The minimum supercooling temperature at the average depth is found to be directly related to the types of ice formation and can be used as a guide to differentiate the types of ice formation in river ice simulation models. It is believed that all the necessary parameters that affect the type of ice formations are incorporated in the chart and it will be useful to investigate the type of ice formations in natural rivers.

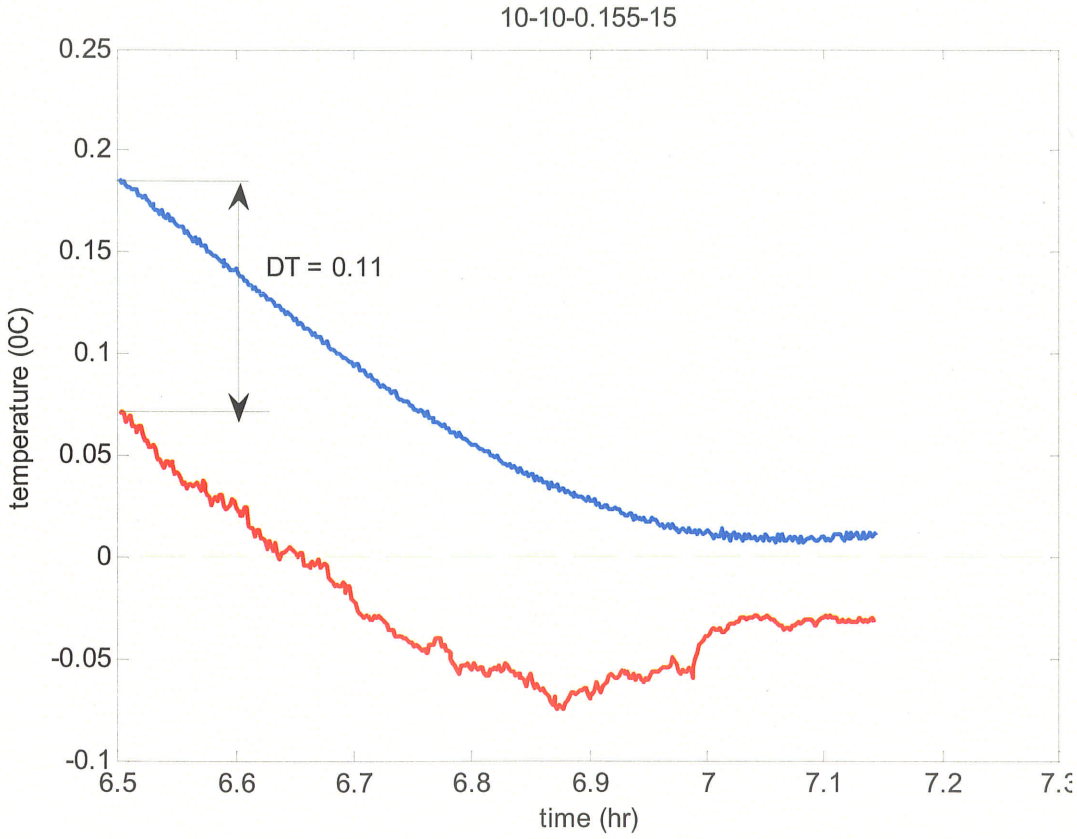

Figure 7.1 Complete skim ice cover for experiment d = 10mm, depth 10cm, velocity 0.155m/s, and temperature -15 °C.

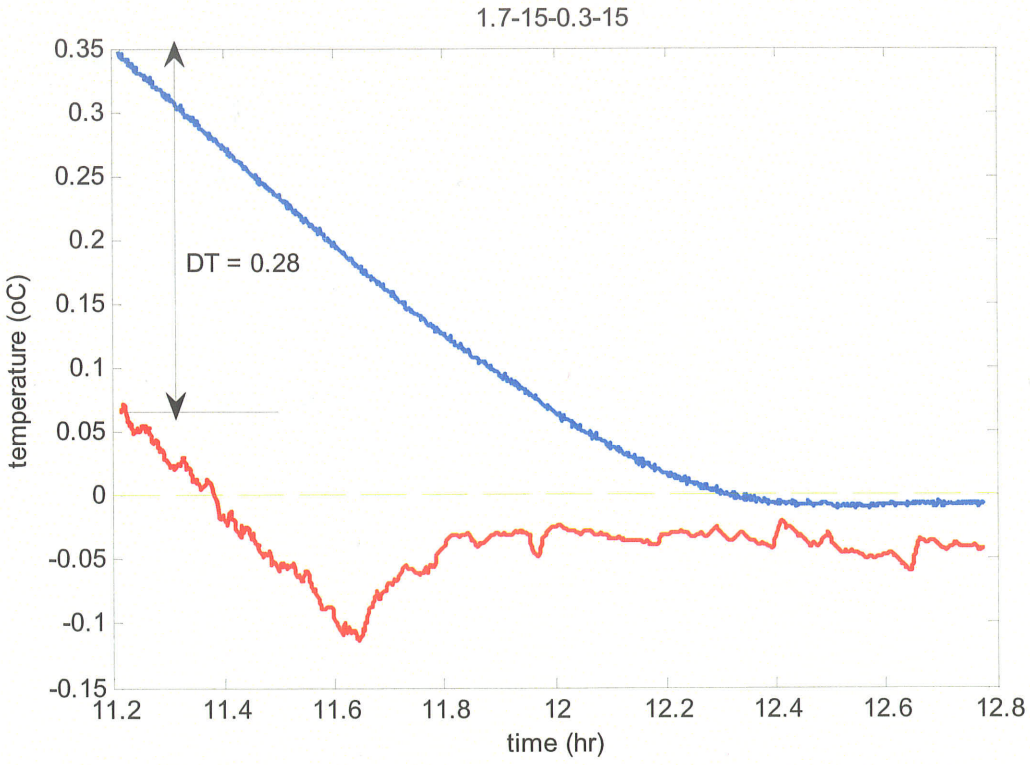

Figure 7.2 Skim ice run, roughness 1.7 mm, depth 15.7 cm, velocity 0.4 m/s, temp -15°C.

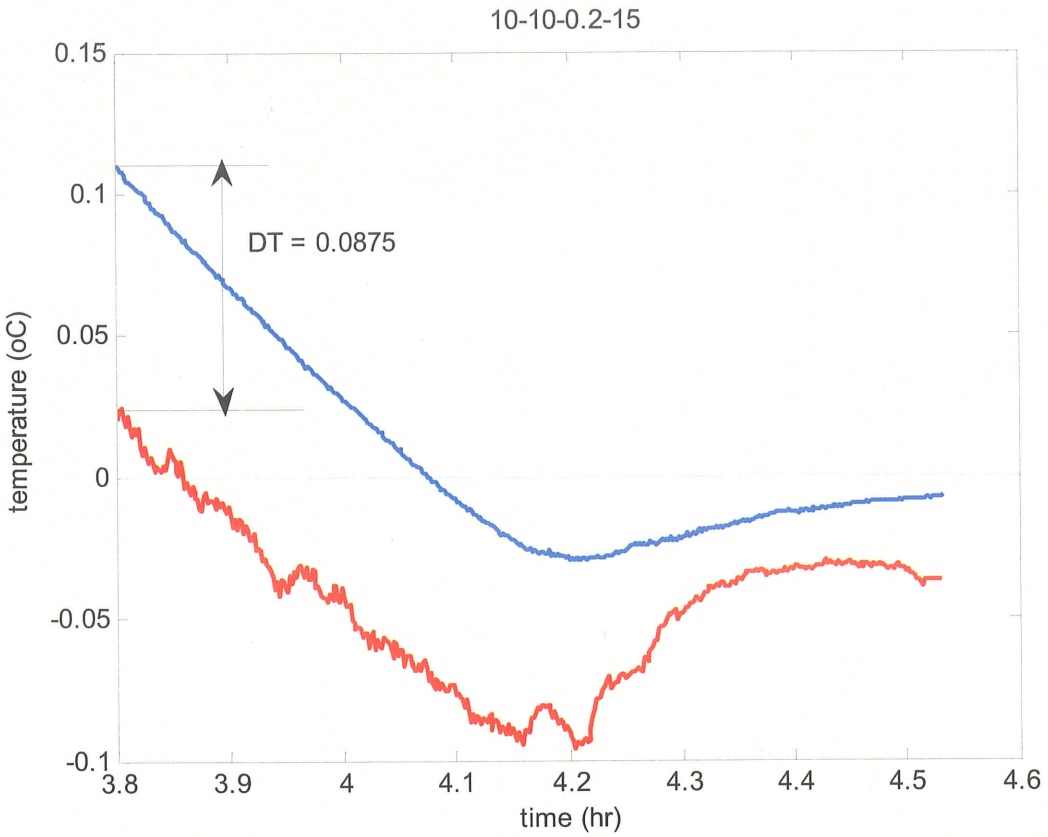

Figure 7.3 Skim ice and frazil ice run, d =10mm, depth 10cm, velocity 0.2m/s, temp -15°C.

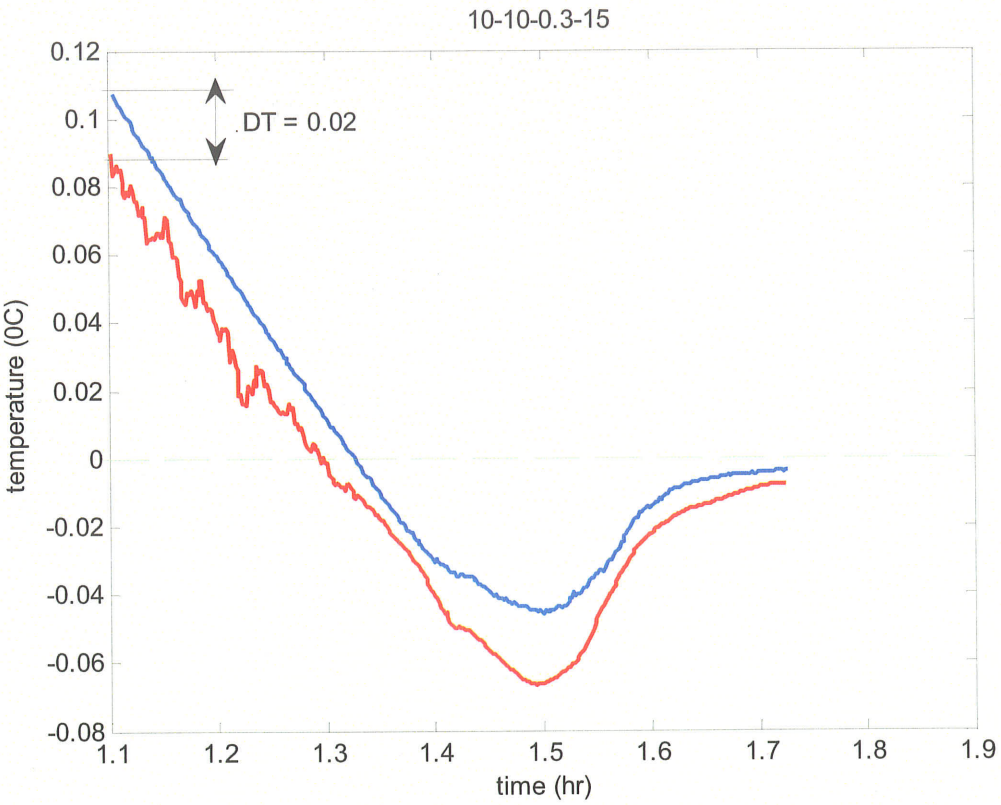

Figure 7.4 Complete frazil formation, d = 10mm, depth 10 cm, velocity 0.3m/s, temperature -15°C (blue line is supercooling curve at the average depth and the red line is supercooling curve for surface water).

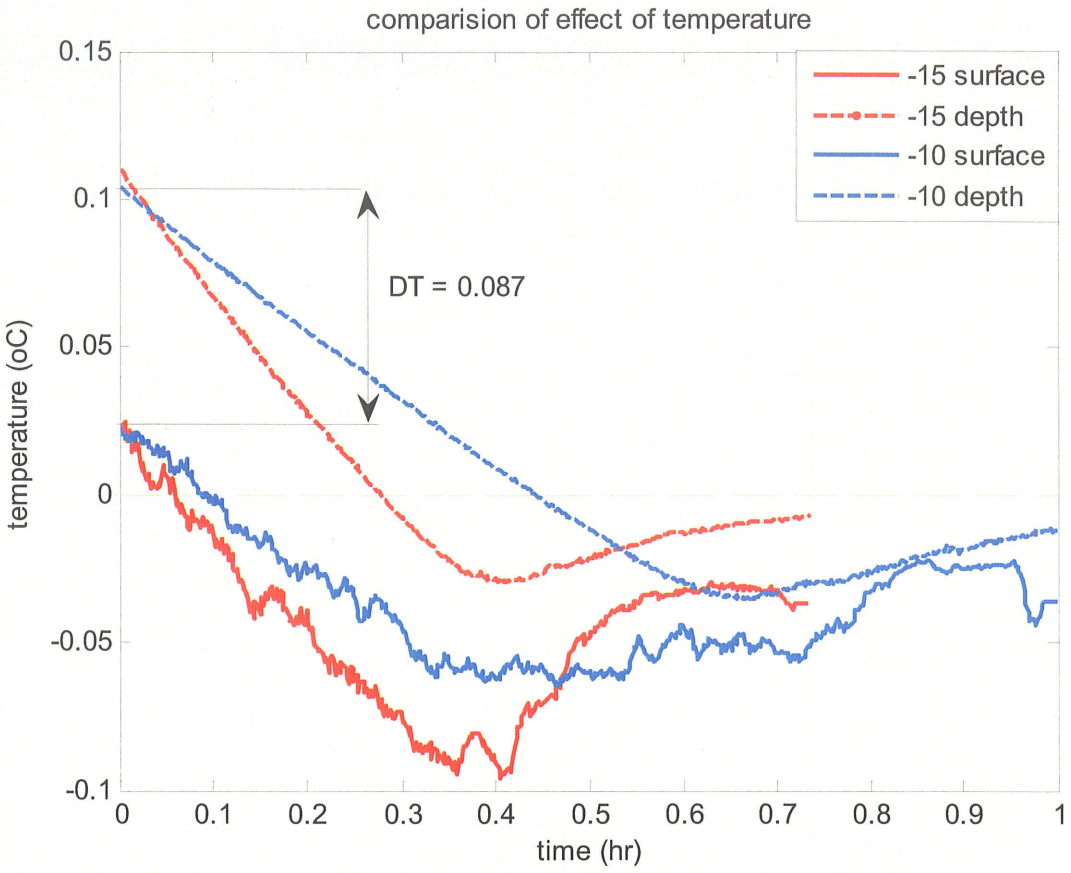

Figure 7.5. Comparison of the effect of air temperature on the type of ice formation, d = 10mm, h = 10 cm, and U = 0.2m/s for the air temperature of -15°C and -10°C.

CHAPTER 8 Mathematical modeling of the evolution of surface ice

8.1 Introduction

If the water flow velocity is low, supercooled water surfaces can cause stratification. The degree of stratification depends on the turbulent intensity and the hydraulic properties of the river. Depending on the degree of stratification the surface ice runs can have four different forms: skim ice cover, skim ice run, skim ice and frazil ice run, and frazil ice run (Unduche & Doering, 2007). It is essential to study the evolution of these ice run types as their presence on the water surface could affect the operation of many hydraulic structures and could hinder the further supercooling of the bulk water. Due to the difficulties and challenges that face conducting field studies, it was found to be easier and reasonable to carry out experimental studies and mathematical modeling of the natural processes to understand the evolution of surface ice runs. Some of such relevant experimental studies were conducted by Unduche and Doering (2007) and Hammar *et al.* (2002). However, the availability of a comprehensive mathematical model is essential due to its flexibility on boundary conditions and efficiency on

time and money. Unlike frazil ice, where numerous mathematical models have been developed to simulate supercooling processes and frazil ice evolution (Daly, 1984; Mercier, 1984; Svensson and Omstedt, 1994; Hammar and Shen, 1995; Ye and Doering, 2004; Wang and Doering, 2005), there are no sufficient reported studies conducted on the mathematical modeling of surface ice run types.

In the following sections a mathematical model for the evolution of surface ice is developed. The model applies the heat balance on the water surface together with the turbulence, hydraulic properties of the river and the ice growth model to simulate the temperature distribution in the water body. The mathematical model is calibrated by the experimental studies conducted at the Hydraulic Research and Testing Facility at The University of Manitoba.

8.2 The Heat Balance on the Water Surface

The detail of the heat balance on the water surface is given in chapter 3. To recapitulate, the heat balance at the open water surface as given by equation 3.1 (Lal and Shen, 1991), is written as

$$\frac{\partial T_w}{\partial t} + u\frac{\partial T_w}{\partial x} = \frac{\partial}{\partial y}\left(\frac{\nu_t}{\sigma_t}\frac{\partial T_w}{\partial y}\right) + \frac{\phi_r}{\rho c_p h} - \frac{\phi_o}{\rho c_p h}, \tag{8.1}$$

where T is the water temperature, h is the water flow depth, ρ is the density of water, C_p is the specific heat of water, σ_t is the turbulent Prandtl number, which is usually equal to unity, u is the velocity in the x-direction. ϕ_o is the total surface heat transfer which is the sum of the net

radiation heat transfer, the latent heat transfer due to evaporation, and the sensible heat transfer due to convection and conduction, ϕ_r is the short wave radiation (that is the penetrative effect).

And for a closed laboratory room during the formation of ice particle on the water surface, the above equation is written as equation 3.2,

$$\frac{\partial T_w}{\partial t} + u\frac{\partial T_w}{\partial x} = \frac{\partial}{\partial y}\left(\frac{\nu_t}{\mathrm{p}_r}\frac{\partial T_w}{\partial y}\right) + \frac{\phi_o}{\rho c_p} + Q_{wi}, \tag{8.2}$$

where $\mathrm{P_r}$ is the Prandtl number and Q_{wi} is the heat loss due to the formation of ice crystals and ϕ_o is the surface heat loss. The linearzed form of ϕ_o as given in equation 1.3 is

$$\phi_o = \alpha(T_h - T_a), \tag{8.3}$$

where α is the heat transfer coefficient that will be calibrated by the experimental data during the simulation. T_h and T_a are water surface temperature and air temperature, respectively. Equation 8.2 can be re-written in Lagrangian form as

$$\frac{\partial T}{\partial t} = \frac{\partial \nu_t}{\partial y}\frac{\partial T}{\partial y} + \frac{\nu_t}{\mathrm{P}_r}\frac{\partial^2 T}{\partial y^2} + \phi_o + Q_{wi}, \tag{8.4}$$

where T is the instantaneous water temperature.

8.3 Ice Formation and Growth on the Water Surface

Unlike frazil ice crystals which are characterized by tiny disc shapes, surface ice particles have a large but very varying size with different shapes. The four main types of surface ice particles that were observed during the experimental study are needle shaped particles, hexagonal shaped particles, finger and leaf shaped particles, and irregular shaped particles. Almost all of these shapes of particles were observed in all experiments where surface ice was formed and their number on a given experiment depends on the degree of turbulence. Even though these particles grow both in size and in number, they grew dominantly by their size, unlike the frazil discs. The detail of experimental observation of surface ice particles is presented by Unduche and Doering (2007b). Due to their complex behavior of size and number, it is difficult to express their size and number by the usually used methods. Therefore, the growth of surface ice particles can be modeled by the total volumetric growth with time. If M_n is the volume concentration of surface ice formed over time t and dM_n is the volume concentration of surface ice formed over time dt, dM_n is given in equation 3.21 by (Ye and Doering, 2004)

$$\frac{dM_n}{dt} = \frac{H_w(T_i - T_v)}{\rho_i L_i} = \frac{Q_{wi}}{\rho_i L_i}, \tag{8.5}$$

where

$$H_w = f(M_n) = \mathbf{k} \times M_n. \tag{8.6}$$

An established curve is used for H_w, Ye and Doering (2004). From those results we can make an assumption that $H_w = f(M_n)$. $\mathbf{k}$ is the constant determined by calibrating $M_{n=0}$. ρ is the density of water, C_p is the specific heat of water, and Q_{wi} is the heat transfer to ice from water. L_i is the latent heat of ice, ρ_i is the density of frazil ice,. T_i is the ice surface temperature

assumed to be 0°C. T_v is the ambient water temperature in which case has to be replaced by T_h for surface ice formations, H_w is the heat transfer coefficient for the total volume of ice formed. The above equation numerically solved as

$$
\begin{aligned}
H_{w,i=0} &= \mathbf{k} \times M_{n=0} \\
dM_{n=0} &= \frac{dt}{\rho_i L_i} H_{w,i=0}(T_i - T_{h,i=0}) \\
Q_{w,i=0} &= \frac{\rho_i L_i}{dt} dM_{n=0} \\
M_{n+1} &= M_{n=0} + dM_{n=0}
\end{aligned}
\tag{8.7}
$$

As the surface ice particles formed and remain on the water surface or on the near surface layer, Q_w is be applied on the first grid point of the numerical model.

8.4 The Turbulence Model

Various turbulence models exist in the literature to solve for the eddy viscosity term in the governing flow equation. The most common of these models for calculating open channel flow is the $k-\varepsilon$ model (as described in chapter 2). In this model, the turbulent kinetic energy and the dissipation rate will be linearly combined at a given time and position in the flow field to find the viscosity term in Equation 8.1. Various empirical and semi-empirical relations exist for turbulent energy in the flow, of which a common form is (Nezu and Nakagawa, 1993), as given in equation 2.16

$$\frac{k}{u_*^2} = 4.78\exp(-2y/h), \tag{8.8}$$

The shear stress velocity is given in equation 2.8. The dissipation rate of turbulent kinetic to be used in the model is given in equation 2.17. The boundary conditions set at the free surface are given in 2.19 and 2.20 for the dissipation rate and turbulent kinetic energy, respectively. The eddy viscosity distribution is calculated from equation 2.24, for C_μ=0.09.

8.5 Numerical Solution of the Governing Equations

Because of its compatibility with the spatial and temporal grid and because of its second-order accuracy in space, the Crank-Nicolson method is used to solve the numerical formulation of the governing equations. Using the Crank-Nicolson method (Kim and Chapra, 1997), equations 8.3, 8.4 and 8.5 can be solved numerically. The partial derivative in time and the first and second derivative in space can be determined at the mid point by averaging the difference approximation at the beginning and at the end of the time increment, *i.e.*,

$$\frac{\partial T}{\partial t} = \frac{T_j^{n+1} - T_j^n}{\Delta t} \tag{8.9}$$

$$\frac{\partial \nu_t}{\partial y} = \frac{\nu_{j+1} - \nu_j}{\Delta y} \tag{8.10}$$

$$\frac{\partial T}{\partial y} = \frac{1}{2}\left[\frac{T_{j+1}^{n+1} - T_{j-1}^{n+1}}{2\Delta y} + \frac{T_{j+1}^{n} - T_{j-1}^{n}}{2\Delta y}\right] \tag{8.11}$$

$$\frac{\partial T^2}{\partial y^2} = \frac{1}{2}\left[\frac{T_{j+1}^{n+1} - 2T_j^{n+1} + T_{j-1}^{n+1}}{\Delta y^2} + \frac{T_{j+1}^{n} - 2T_j^{n} + T_{j-1}^{n}}{\Delta y^2}\right] \tag{8.12}$$

Substituting equations 8.9 to 8.12 into equation 8.4, and rearranging gives the following expression

$$\left(\frac{1}{\Delta t} + \frac{\nu_j}{\Delta y^2}\right)T_j^{n+1} - \left(\frac{\nu_{j+1} + \nu_j}{4\Delta y^2}\right)T_{j+1}^{n+1} - \left(\frac{3\nu_j - \nu_{j+1}}{4\Delta y^2}\right)T_{j-1}^{n+1} - \phi_o - Q_{wi}\Big|^{n+1}$$

$$= \left(\frac{1}{\Delta t} + \frac{\nu_j}{\Delta y^2}\right)T_j^{n} + \left(\frac{\nu_{j+1} + \nu_j}{4\Delta y^2}\right)T_{j+1}^{n} + \left(\frac{3\nu_j - \nu_{j+1}}{4\Delta y^2}\right)T_{j-1}^{n} \tag{8.13}$$

In the above equation, if (L has to be modified for the temperature at n+1 source component)

$$L = \left(\frac{1}{\Delta t} + \frac{\nu_j}{\Delta y^2}\right); J = \left(\frac{1}{\Delta t} - \frac{\nu_j}{\Delta y^2}\right); H = \left(\frac{\nu_{j+1} + \nu_j}{4\Delta y^2}\right), \text{ and } I = \left(\frac{3\nu_j - \nu_{j+1}}{4\Delta y^2}\right),$$

then equation 8.13 can be written as

$$LT_j^{n+1} - HT_{j+1}^{n+1} - IT_{j-1}^{n+1} - \frac{\phi_o - Q_{wi}}{\rho c_p}\Big|^{n+1} = JT_j^{n} + HT_{j+1}^{n} + IT_{j-1}^{n}. \tag{8.14}$$

This unconditionally stable and consistent equation can be solved for each time step for all grid points.

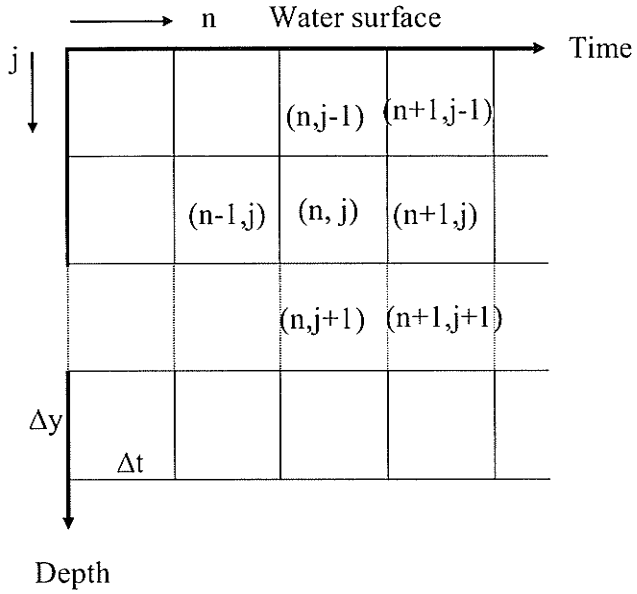

The boundary condition for the above equation is set at the surface as

$$\nu_{t(i=1)} \frac{\partial T}{\partial y} = \frac{\phi_o}{\rho c_p}. \tag{8.15}$$

and no heat flux boundary condition is set at the bed as

$$\nu_{t(j=m)} \frac{\partial T}{\partial y} = 0 \tag{8.16}$$

A no heat flux condition is set as the boundary condition on the bottom of the counter-rotating flume. The simulation starts usually three to four hours before the start of ice formation (*i.e.*, before the surface temperature reaches zero degrees).

8.6 Model Calibration

The model is calibrated with the experimental data that was collected during the study period. Thirty-one experiments were collected at the Hydraulic Research and Testing Facility where the testing variables are shown in Table 4.2. Depending on the type of surface ice formation, the turbulent parameters and the air temperature were set according to the table. A time step of Δt = 1 s and spatial step of Δy = 1 cm is used in the simulation (note that the simulation is implicit and the results are independent of grid space). The main calibration parameters in the model are M_o, *i.e.*, the magnitude of the initial seeding and α, *i.e.*, the surface heat loss coefficient. M_o is calibrated by the minimum supercooling temperature and α is calibrated by the rate of temperature fall before the formation of ice crystals.

It is observed in the experiment that the temperature falling rate decreases as the temperature gets closer to 0°C. Therefore the heat loss coefficient α is calibrated for the falling rate between 1 °C and 0 °C. The literature value of α for natural river is 20 W/m^2, where as the calibrated values of α lie in the range of 18 W/m^2 to 25 W/m^2. The model is calibrated to the four different types of ice run types, *viz.*, are: skim ice cover, skim ice run, skim ice and frazil run, and complete frazil ice formation. The calibration of the initial seeding takes account of the minimum supercooling temperature and the coefficient **k** of Equation 8.6. During the experiments surface ice particles were observed at the surface when the surface temperature was 0 °C to 0.1 °C. In the model a constant initial temperature of 0.007 °C is used as the starting temperature of ice formation.

8.7 Model Simulation and Results

The simulation results for the four different types of surface ice formations are shown below. The simulation of the formation of skim ice and frazil formation for experiment roughness 0.0034m, depth 0.2m, velocity 0.4m/s and air temperature of -15°C is shown in Figure 8.1. This simulation shows a good match in the simulation of the depth average temperature. The simulation of complete frazil ice formation for experiment roughness 0.01m, depth 0.10m, velocity 0.30m/s and air temperature -15°C is also shown in Figure 8.2. Skim ice cover formation simulation is also shown in Figure 8.3 for experiment with roughness 0.01m, depth 0.10m, velocity o.155m/s and air temperature -15°C. Finally, the fourth case, which is the formation of skim ice run is simulated for experiment roughness 0.01m, depth 0.15m, velocity 0.2m/s and air temperature -15°C and shown in Figure 8.4.

In most cases the minimum supercooling temperature of the surface temperature shows a deviation with the simulated result. Ice particles that occasionally form on the surface of the surface thermometer would indicate a lower temperature than the actual temperature. Figure 8.5 indicates the simulation result plotted at each grid point in the depth and Figure 8.6 shows the variation of temperature at depth at different times. Figure 8.7 and Figure 8.8 show the turbulent kinetic energy and the dissipation rate at depth. Figure 8.9 shows the growth rate of the concentration with time. It can be observed that the volumetric growth rate is very small during the initial periods and will maintain a uniform growth rate during later times. The plot of Q_w (surface heat loss), which is shown in Figure 8.10, indicates that the heat loss is nearly constant during later stages. It is also observed in the simulation that the rate of growth of surface ice concentration is very low for small turbulent intensities and small negative air

temperature. During this time Equation 8.5 can not give a good result and, therefore, a better comprehensive theoretical model that incorporates the effect of degree of turbulence and surface heat loss is needed.

8.8 Discussion

The developed mathematical model reasonably simulates the water cooling rate during the formation of four different types of surface ices. A good correlation exists between the simulated and measured supercooling curve at the average depth although some discrepancy exists at the surface. This discrepancy of the surface temperature simulation is attributed to the effect of ice formed on the surface of the surface thermometer and the difficulty of measuring the precise temperature at the water surface during an experiment. This model did not consider the influence of wind and waves on the water surface, which would create surface turbulence and enhance surface heat loss. Therefore, the model can be further developed to simulate the natural condition, provided that there is measured data for the calibration. It was also observed that the volumetric growth rate of surface ice reduces as the turbulent and surface heat loss reduce and a better comprehensive model that incorporates the degree of turbulence and surface heat loss is needed to simulate rate of surface ice growth.

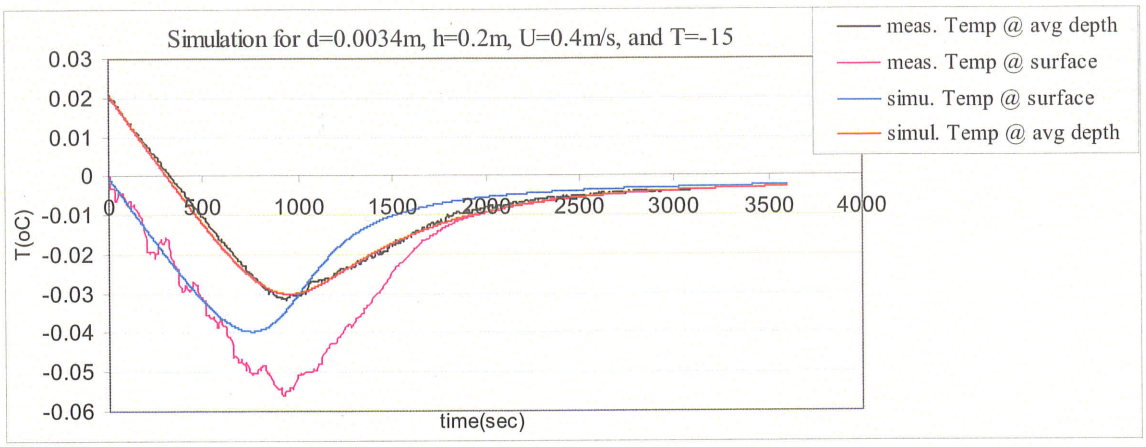

Figure 8.1 Simulation and comparison with the measured data for bed roughness, d = 0.0034 m, depth h = 0.20 m, velocity U = 0.40 m/s and air temperature T = -15 °C.

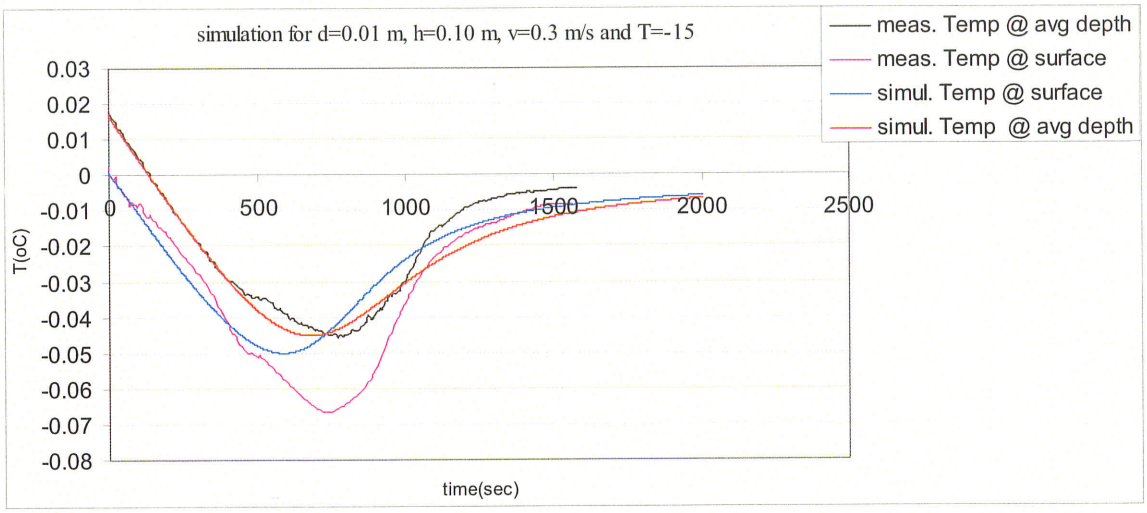

Figure 8.2 Simulation and comparison with the measured data for roughness, d = 0.01 m, depth h = 0.10 m, velocity U = 0.30 m/s and air temperature T = -15 °C..

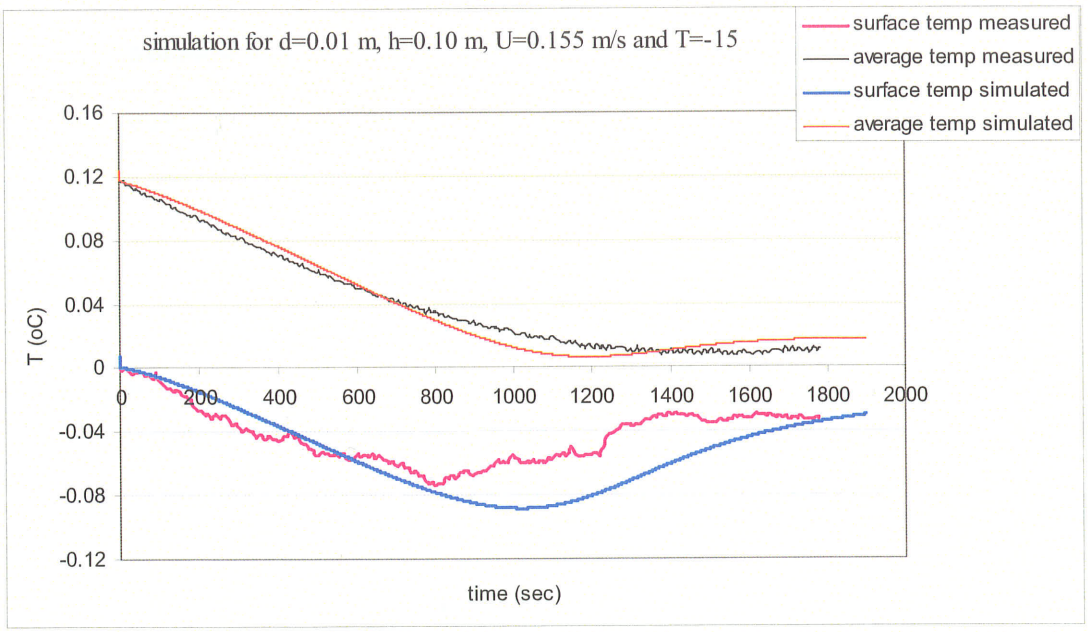

Figure 8.3 Simulation and comparison with the measured data for roughness, d = 0.01 m, depth h = 0.10 m, velocity U = 0.155 m/s and air temperature T = -15 °C.

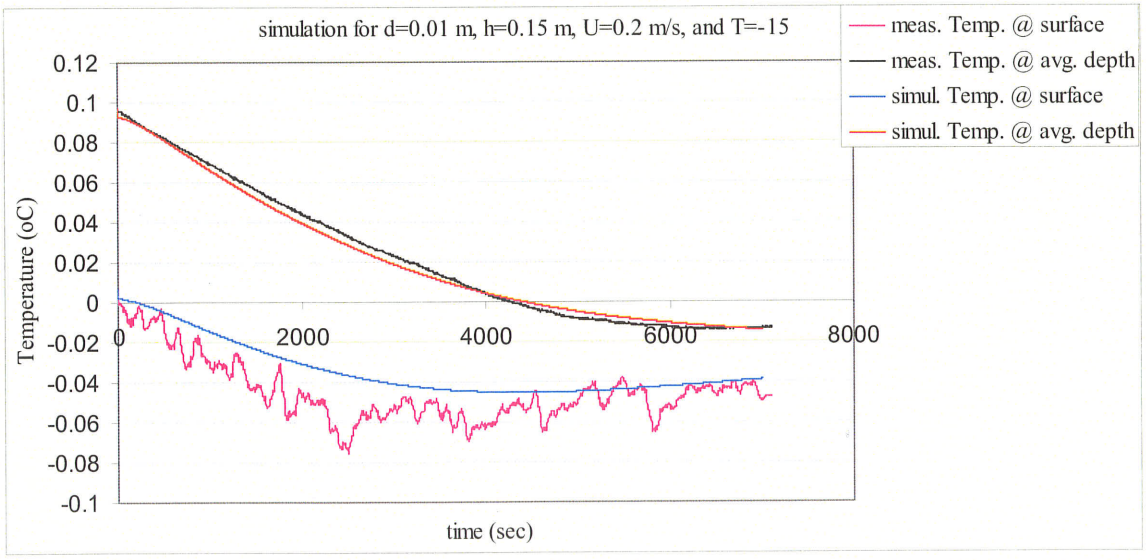

Figure 8.4 Simulation and comparison with the measured data for roughness, d = 0.01 m, depth h = 0.15 m, velocity U = 0.2 m/s and air temperature T = -15 °C.

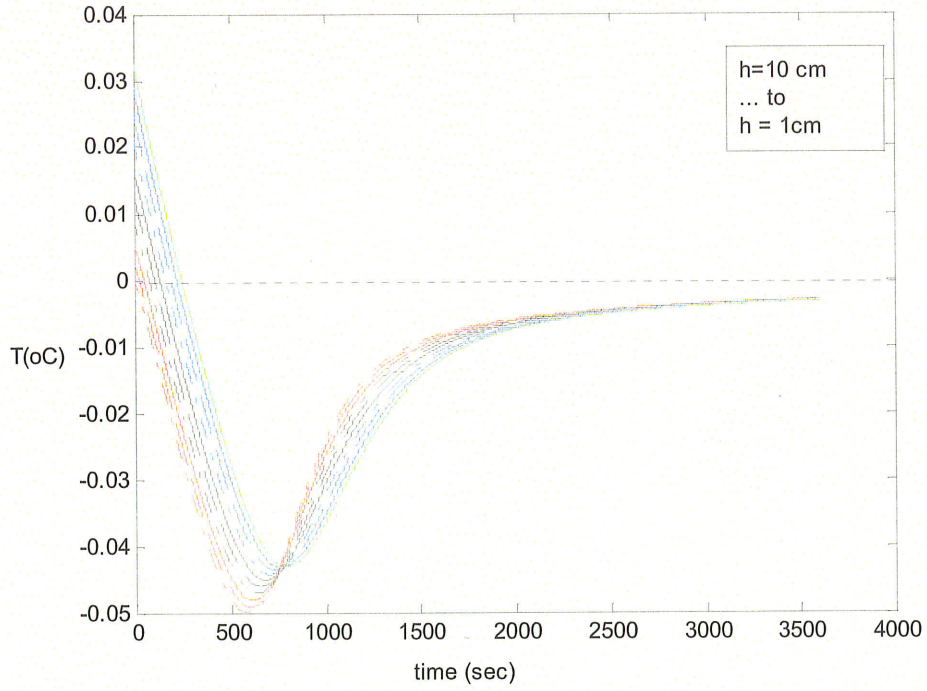

Figure 8.5 Simulation of water temperature at different depths. (Simulation for depth 10 cm, roughness 0.1 cm and velocity 30 cm/sec)

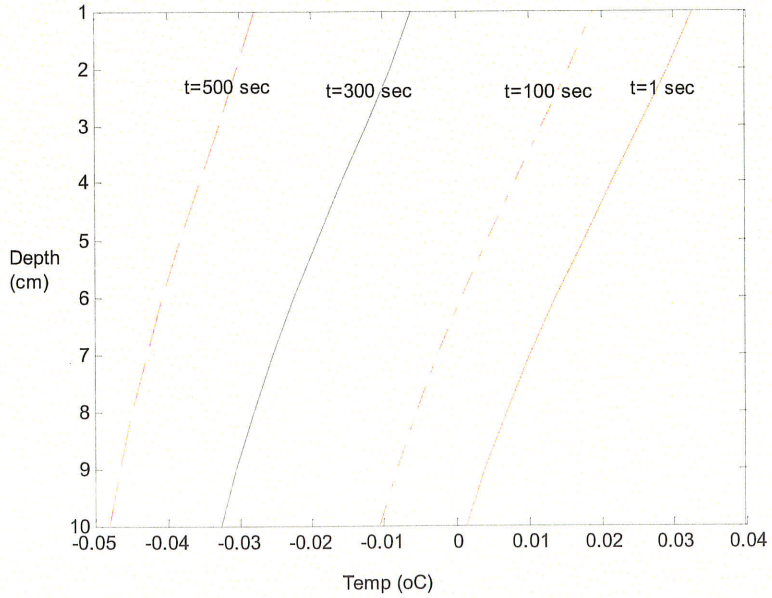

Figure 8.6. Simulation of water temperature at a depth for different time interval. (Simulation for depth 10 cm, roughness 0.1 cm and velocity 30 cm/sec)

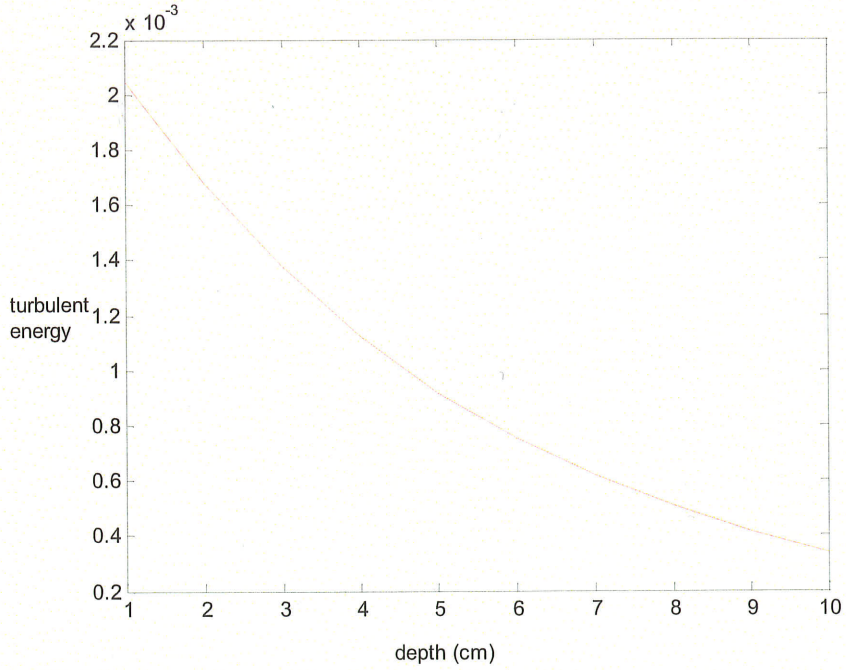

Figure 8.7. The turbulent energy profile in a depth. (Simulation for depth 10 cm, roughness 0.1 cm and velocity 30 cm/sec)

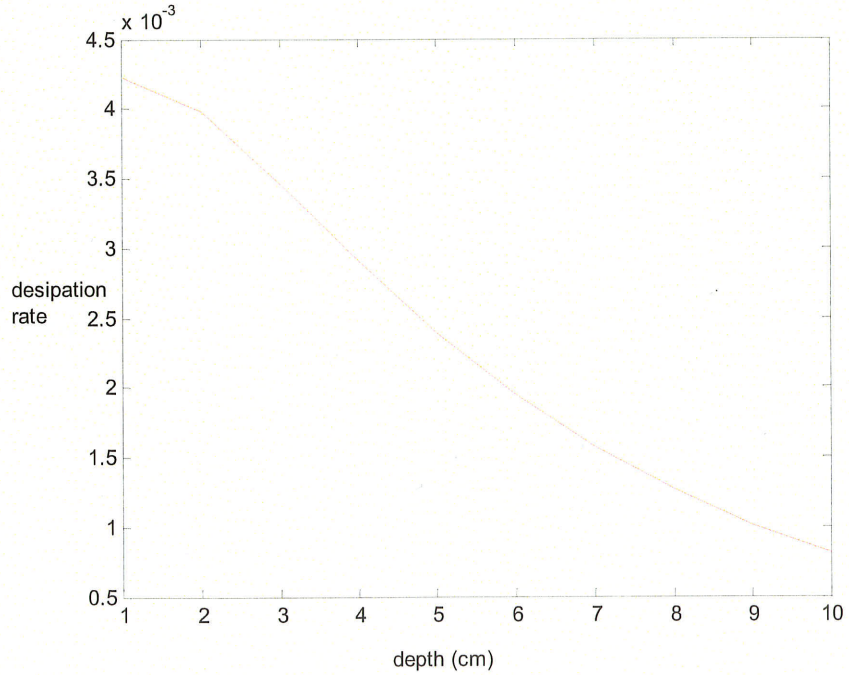

Figure 8.8. The variation of the dissipation rate in a depth. (Simulation for depth 10 cm, roughness 0.1 cm and velocity 30 cm/sec)

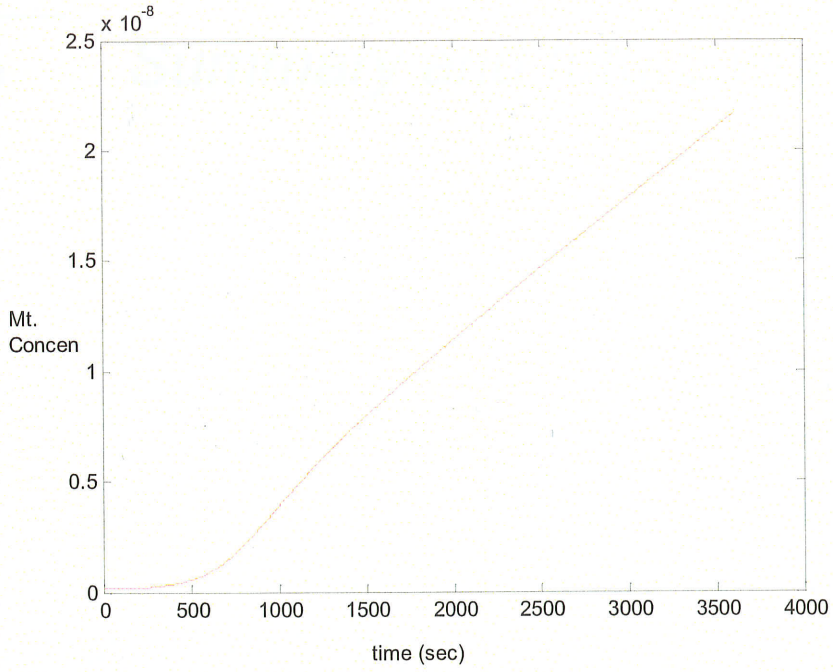

Figure 8.9. The volumetric concentration as a function of time. (Simulation for depth 10 cm, roughness 0.1 cm and velocity 30 cm/sec)

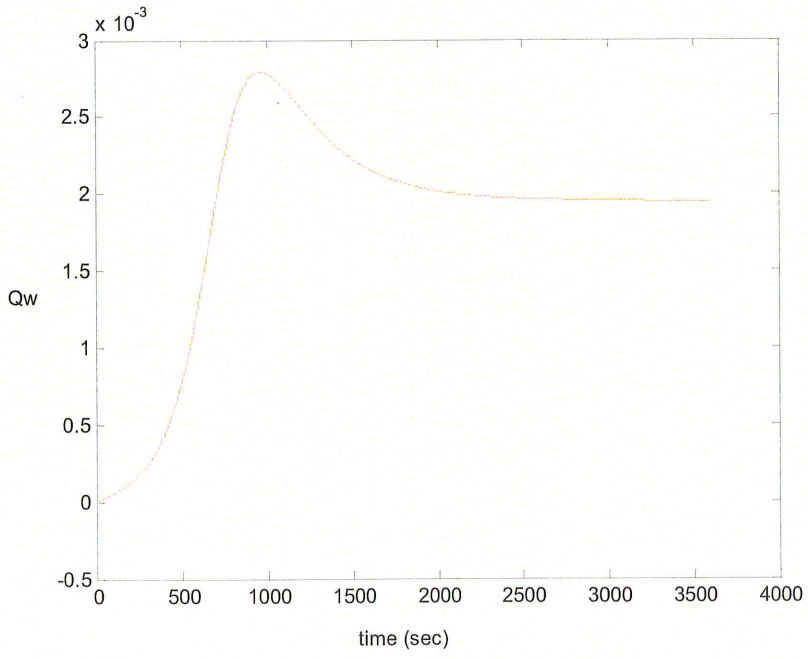

Figure 8.10. The heat flux from the ice surface as a function of time. (Simulation for depth 10 cm, roughness 0.1 cm and velocity 30 cm/sec)

CHAPTER 9 Summary and future work

9.1 Summary of the Study

An extensive experimental and theoretical study has been conducted in an attempt to understand the formation and growth of surface ice. The following section summarizes the over all study. The counter-rotating flume at the Hydraulic Research and Testing Facility is used to undertake the experimental study and a mathematical model is programmed using MATLAB.

From the understanding of the hydraulic and hydrologic parameters that govern the formation of surface ice, it was believed that the type of surface ice formation is dependent on the degree of turbulence and the surface heat loss. Therefore experimental variables were selected to represent these two parameters, *i.e.*, turbulence and surface heat loss. Turbulence was expressed by the combined effect of bed roughness, flow velocity, and depth; and surface heat loss is represented by the air temperature.

Thirty-one experiments were carried out continuously by varying the above testing variables. The measured values and outputs of an experiment are: the supercooling curve at the average depth, the supercooling curve at the water surface, ice images at the water surface, and ice images in the flow. These data help to predict the specific type of ice formation in the flow. The surface camera also revealed the shape and size characteristics of the skim ice particles.

In the mathematical model it has been attempted to include all the vulnerable parameters that govern the surface ice formation. Due to the variable shape and size characteristics of skim ice particles, it was found to be difficult to model the growth of the mean size of the surface ice particles. Therefore, a simplified model that simulates the volumetric growth of surface ice is used. A linear relationship between the heat flux coefficient and the volumetric growth rate was found to be reasonable.

The mathematical model is calibrated by two different calibrating parameters, namely the surface heat loss coefficient and the quantity of the initial seeding. The magnitude of the initial seeding is calibrated by the measured minimum supercooling temperature at the average depth and the surface heat loss is calibrated by the measured temperature falling rate prior to the formation of ice crystals. The mathematical model was calibrated for the four different types of surface ice formations; *i.e.*, skim ice cover, skim ice run, skim ice and frazil run, and frazil formation, and found to give a good correlation with the measured data.

9.2 Discussions and Comparison with Literature Values

As the experimental study has been conducted in the laboratory and the mathematical model has been calibrated by the experimental data, it is essential to compare the observed results with previous studies and to apply the obtained results to a practical situation to see the sensitivity and practicality of the results. Some of the major conclusions of the thesis are summarized by the charts shown in Chapter 5 (Figure 5.7 and Figure 5.8) and chapter 7, which states that the type of surface ice formation is weakly dependent on surface heat loss. In this section the above conclusions will be compared to the previously obtained literature studies and practical field data.

Matousek (1992) has developed a chart that shows the types of ice formations are dependent on the degree of surface heat loss and river flow velocity. In his chart it is clearly observed that the type of surface ice formation is strongly dependent on velocity but weakly dependent on surface heat loss. Moreover, the observation of Hammer *et al.* (2002) also shows the experimental observation that the type of surface ice formation is weakly dependent on air temperature but strongly dependent on velocity. Even though, the investigation in chapter 7 (Figure 7.5) shows the type of ice formation is independent of surface heat loss, it can not be generalized as the experiment is carried with only two different temperature sets and the effects of long wave and short wave rations are not considered. However, it clearly indicates that the type of surface ice formation is weakly dependent on the surface heat loss.

The results of Figure 5.7 and Figure 5.8 show that the surface ice formations are dependent on the combined effect of bed roughness, velocity, depth, and bed shear stress which are

represented by dimensionless numbers as Reynolds number, Froude number, shear stress, and Reynolds number. Previous studies of Matousek (1986, 1990, 1992) also show strong dependence of surface ice formation on velocity, bed roughness, and Reynolds number. Studies of Andreasson *et. al.*, (1998) also indicate that the types of surface ice formations are dependent on depth and bed shear stress.

The result from charts Figure 5.7 and Figure 5.8 are applied to Nelson River and compared with the results of Matousek (1992). Two different sections of a river with depths of 4.15 m and 13.17 m, with a velocity of 1.16 m/s and 0.38 m/s, respectively, are selected. These two sections of the river have two k_s (Nikurades Roughness Coefficient) values of 0.046 and 0.082. Matousek (1984, 1990, 1992), as described in section 1.3.1.3, concluded that frazil is formed in the stream if the following is valid simultaneously:

$T_v < 0^{\circ}C$,

$T_h <$ -0.10 to -0.20°C, and

$U > 0.067(MC)^{0.305} R^{0.5}$,

where T_v is the vertical average water temperature, T_h is the water surface temperature and U is the average stream flow velocity. Skim ice will occur in the stream when the following conditions are met simultaneously:

$T_v \geq 0^{\circ}C$,

$T_h \leq$ -0.10 to -0.20°C,

$U < 0.067(MC)^{0.305} R^{0.5}$,

Where, $M = 0.7C+6$ for $10 < C \leq 60$. Therefore, application of these formulae will give us Matousek (1984, 1992) results of the type of ice formed. If we calculate the Reynolds number,

Froude number, shear stress Reynolds number, and shear stress velocity as mentioned in Chapter 5, will give us two different ways of predicting the type of ice formed according to charts Figure 5.7 and Figure 5.8. The results are summarized in Table 9.1 and both predictions give similar answers.

In the first case the Matousek (1984, 1992) relation gave the formation of frazil ice. According Figure 5.7, the computed values of R_* and R_e are greater than the limiting values determined by the charts (or plot of R_* versus Froude number) which indicate the formation of frazil ice. According to Matousek (1984, 1992) the second case shows the formation of skim ice and Figure 5.8 tells us that the minimum shear stress for the formation of frazil is 0.022. In table 9.1 the calculated shear stress is 0.02 which is less than 0.022 and indicates frazil is not forming but rather indicates the formation of skim ice. It is also noted that the Reynolds number calculated in the flume is much less than the Reynolds number observed in reality. These shows that for the selected river, on the selected section, the observed results match with the literature values and the effect of the flume size is controlled by the dimension less numbers.

Table 9.1 Comparison of the Matousek (1984, 1992), Figure 5.7 and Figure 5.8 and the prediction of the type of surface ice formed.

									Limiting criteria's		
	Ks	h	U	R_e	R_*	u_*	F_r	Matousek	R_*	R_e	Conclusions
I	0.046	4.15	1.16	2683194	3711	0.08	0.18	Frazil Ice	1570	164613	Frazil / Frazil
II	0.082	13.17	0.38	2822669	993	0.02	0.03	Skim ice	1494	25651	Skim ice / Skim ice

9.3 Conclusions

From the overall study (*i.e.*, the experimental analysis and the mathematical modeling) the following points are concluded:

I. The type of surface ice formation is found to be weakly dependent on the surface heat loss (*i.e.*, the air temperature)

II. Turbulence is the dominant factor that governs the type of surface ice formation.

III. Depending on the degree of turbulence four different types of surface ice formations could form in a flow; namely, skim ice cover (freeze-up), skim ice run, skim ice and frazil ice run, and complete frazil formation.

IV. The minimum supercooling temperature at an average depth is an excellent guide to classify types of surface ice formations.

V. The minimum supercooling temperature at the water surface is found to be independent of the degree of turbulence, however, the supercooling time is found to be dependent on the degree of turbulence. Higher turbulence intensity leads to lower supercooling time.

VI. Experimental analysis indicated that the types of surface ice formations can be determined by the relationship of the dimensionless parameters, shear stress Reynolds number, Reynolds number, Froude number and the bed shear stress velocity.

VII. Skim ice particles do not originate from frazil ice particles; and in fact skim ice are different from frazil ice particles by their shape, size and total number.

VIII. Skim ice particles are particles that nucleate on the water surface at low turbulence intensities (or provided that there is stratification).

IX. Skim ice particles predominantly grow by their size unlike frazil discs whose growth is dominated by their number to balance the surface heat loss.

X. Four different types of skim ice particle shapes were observed; namely needle shaped particles, hexagonal shaped particles, finger and leaf shaped particle and irregular shaped particles.

XI. Skim ice particles have large size and small number compared to frazil ice particles.

XII. Frazil ice particle are circular or elliptical discs that nucleate in the bulk flow at moderate to high turbulence intensities.

XIII. Surface coverage and freeze-up is caused either by bridging and further propagation of ice accumulation on the surface or by dendrites and mesh formed at the water surface.

XIV. A mathematical model with two calibrating parameters, *i.e.*, the surface heat loss coefficient and the magnitude of the initial seedling, was developed.

XV. The mathematical model prediction gave a good correlation with the measured supercooling curve at the water surface and at the average depth.

9.4 Future Work

Despite an overall effort to improve the experimental set up and mathematical modeling to get the best out of it, it is believed that some improvements and modifications could still be done. The experimental set up can be modified by the installment of newer and better equipment and the mathematical model can be improved by the better understanding of the theory and calibration. The following points are discussed to give insights for further study to understand the formation of surface ice run types.

The thermometers used in the experiment are of high precision and accuracy. However, it was observed during the experiment that there is a very high temperature gradient near the water surface and can not be precisely measured with the current thermometer setting. A very slight motion of the thermometer on the vertical direction gives readings that change in the range of 0.01 to 0.001 ^{o}C. Moreover, the thermometer on the water surface creates local turbulence during highly turbulent flows and could cause some extent of mixing at the surface. Therefore, it is recommended that a point temperature measuring technique, that can measure the water temperature right at the interface between the air and water, should be applied.

The presence of wind on the water surface aggravates the heat loss from the water surface and creates a surface turbulence due to wind waves and wind shear stress developed on the water surface. Even though the study revealed that surface heat loss does not affect the type of surface ice formations it is worth to study the experiment by the presence of wind on the water surface to see the effect of wind related turbulence on the type of surface ice formation. The wind related turbulence is a local effect that occurs on the surface, but it could affect the type of surface ice formation depending on the intensity of the wind and the magnitude of the developed waves.

A considerable attempt was carried out to get a better ice images by the surface camera. The observed images were found to be clear, however, a modification can be done to improve the extent of the area coverage by the surface camera. As the lighting that comes reflected from the bed is insufficient to light the entire surface, images near to the border (wall) are not very clear. Therefore, a better lighting set up could be installed if further study has to be attempted.

Besides turbulence and mixing, the minimum supercooling temperature is found to be slightly dependent on some other factors that are not yet investigated. It is hypothesized that this phenomena is attributed to the quality of the water, the humidity of the air and some other factors. Therefore a detailed study is important to figure out this process and to find out the experimental results practical. The water and air quality at the experimental conditions could be different than the practical conditions and the above unforeseen reason might bring different result than expected in practice.

References

Andreasson, P., Hammer, L., and Shen, H. T. 1998. The influence of surface turbulence on the formation of ice pans. Ice in surface waters, Shen (ed.) Balkema, Rotterdam, pp 69 – 76

Andres, D. (1995) Floe development during frazil generation in large rivers. Procc. & Workshop on the hydraulics of ice covered rivers, Canadian Geophysical union

Ashton, G. D. ed. (1986) River and lake ice engineering, Water resources publications, Littleton, Colorado, USA

Beltaos, S. (1983) River ice jams: Theory, case studies and applications. J. Hydr. Eng. 109(10), 1338-1359

Beltaos, S. ed. (1995) River ice jams. Water Resources Publication, LLC, Colorado, USA

Borue, V., Orszag, S. A., and Staroselsky, I. (1995) Interaction of surface waves with turbulence: direct numerical simulation of turbulent open channel flow. J. Fluid Mech. 286:1-23

Carter, R. W., Einstein, H. A., Hinds, Julian, Powell, R. W. and Siberman, E. (1963) Friction factors in open channels. J. Hydr. Div., ASCE, 89HY2, 97-143

Clark, S. and Doering, J.C. (2002) Laboratory Observations of Frazil Ice. IAHR International Symposium on Ice, 127-133.

Clark, S. and Doering, J. C. (2004) A laboratory study of frazil ice size distributions. IAHR, 17 Int. Sym. Ice Saint Petersburg, Russia, 291-297

Colebrook, C. F. (1939) Turbulent flow in pipes with particular reference to transition region between the smooth and rough pipe laws. Journal of the institute of Civil Engineers, 1938-1939

Daly, S. F. (1984) Frazil ice dynamics. CRREL Monograph 84-1, U.S. Army CRREL, Hanover, N.H.

Daly, S.F. and Colbeck, S.C. (1986) Frazil Ice Measurements in CCREL's Flume Facility. IAHR Ice Symposium, Iowa City, Iowa, 427-438.

Daly, S. F. (1994) Report on frazil ice. US army Corps of Engineers Cold Regions research & Engineering laboratory, Special report 94-23

Doering, J.C., and Morris, M.P., 2003. A digital image processing system to characterize frazil ice. Canadian Journal of Civil Engineering, Vol. 30, No.1, pp 1-10

Fulgosi, M., Lakehal, D., Banerjee, S., amd De Angelis, V. (2003) Direct numerical simulation of turbulence in a sheared air – water flow with a deformable interface. J. Fluid Mech., Vol 482, pp 319-345

George, W. K. & Arndt, R. (1989) Advances in Turbulence. Hemisphere Publishing Corporation USA

Grass, A. J. (1971) Structural features of turbulent flow over smooth and rough boundaries. J. Fluid Mech., 50: 233-255

Hammar, L. and Shen, H. T. (1995) Frazil evolution in channels, J. of Hyd. Res., Vol.33, 291-306

Hammer, L., et al. (2002) A laboratory study on freezeup ice runs in river channels. "Ice in the environment: Proc., 16th IAHR Int. Symp. on ice, 3, Dunedin, New Zealand, 22-29

Hanley, T.O., and Rao, S.R., 1982. Acoustic Detector for Frazil. in IAHR 1981, vol. 1.pp. 81-85.

Hinze, J. O. (1959) Turbulence: An introduction to its mechanics and theory McGraw-Hill Book company, INC

Idelchik, I. E. (1986) Hand book of hydraulic resistance. 2nd revised and augment edn. (Hemisphere: New York, USA)

Kim, K. S. and Chapra, S. C. (1997) Temperature model for highly transient shallow streams. J. of Hydr. Eng. Vol. 123, No.1 pp 30-40

Lal, A. M. W., and Shen, H. T. (1991a) A mathematical model for river ice process. J. Hydr. Eng. 117(7), 851-867

Lal, A. M. W., and Shen, H. T. (1991b) A mathematical model for river ice process. Report

Lia, L. (1998) Snow and ice blocking of tunnels. IAHR symposium on ice, Postdam N.Y

Marcotte, N. (1984) Anchor ice in Lachine Rapids, results of observations and analysis. Proc. IAHR Int. Symp. On ice , Hamburg, Germany, Vol. 1, 151-159

Matousek, V. (1984) Types of ice runs and conditions for their formation. Proc., IAHR Ice Symp., Delft, The Netherlands, 315-327

Matousek, V. (1984) Regularity of freeze-up and heat exchange between water body and water surface. Proc. IAHR Int. Symp. On ice , Hamburg, Germany

Matousek, V. (1990) Thermal processes and ice formation in rivers. Papers and Studies, No. 180. Published by Water Resources Institute in the State Agricultural publishing house, Prague

Matousek, V. (1992) Frazil and skim ice formation in Rivers, IAHR Ice Sym. Banff, Alberta

Mercier, R., 1984. The Reactive Transport of Suspended Particles: Mechanisms and Modeling. Ph.D. Dissertation, Cambridge: Joint Committee on Oceanographic Engineering, Massachusetts Institute of Technology (unpublished).

Nezu, I. and Nakagawa, H. (1993) Turbulence in open channel flows, IAHR Monograph, A. A. Balkema, Rotterdam

Nezu, I. amd Azuma, R. (2004) Turbulence characteristics and interaction between particles and fluid in particle laden open channel flows. J. Hydr. Engg. Vol. 130, No. 10, pp 988-1001

Osterkemp, T. E. (1978) Frazil ice formation: A review. J. Hydr. Div., Am. Sc. Civ. Eng., 104(9), 1239-1255

Osterkamp, T.E. and Gosink, J.P. (1983) Frazil Ice Formation and Ice Cover Development in Interior Alaska Streams. Cold Regions Science and Technology, 8, 43-56.

Ramseir, R. O., (1970) Formation of primary ice layers. IAHR, Proc. Of Ice Symp. Reykjavik

Ryan, P. J., Harleman, D. R. F., and Stolzenbach, K. D. (1974) Surface heat loss from cooling ponds. Water Resources Research, Vol. 10, no. 5 pp 930-938

Shen, H. T. (2003) Research on River ice process: Progress and Missing Links. Journal of Cold Regions Engineering Vol. 17 No. 4

Svensson, U. and Omstedt, A. (1984) Modeling supercooling and ice formation in a turbulent Ekman layer. J. Geoph. Res., 89 (C1):735-744

Svensson, U. and Omstedt, A. (1994) Simulation of supercooling and size distribution in frazil ice dynamics. Cold Regions Science and Technology, 22:221-233

Svensson, U., Billfalk, L., and Hammer, L. (1989) A mathematical model of border ice formation in rivers. Cold regions science and technology, 16, 179-189

Tennekes, H. and Lumley, J. L. (1972) A first course in turbulence. The MIT Press Cambridge, London

Tsang, G. (1988) A theory for frazil distribution in turbulent flow. IAHR ice Symposium, Sapporo

Tsang, G. (1992) Laboratory investigation of frazil evolution, flocculation and the formation of anchor ice, Progress Report No.3, National Hydrology Research Institute, Environment Canada Saskatoon, SAsk. NHRI contribution No. CS-92057

Unduche, F.S., and Doering. J. C. 2007a. Laboratory observation of skim ice particles. Submitted to the 14th workshop on the committee on river ice and the environment CRIPE, Quebec City, Canada

Unduche, F.S., and Doering. J. C. 2007b. Experimental study of the formation of different types of ice runs. Submitted to the 14th workshop on the committee on river ice and the environment CRIPE, Quebec City, Canada

Wang, S. and Doering, J. C. (2005) Numerical simulation of the supercooling process and frazil ice evolution. Submitted to J. Hydr. Eng..

Ye, S. Q. (2002) A physical and Mathematical study of the supercooling process and frazil evolution, Ph.D. dissertation University of Manitoba, Civil Engineering department

Ye, S. Q. and Doering, J. C. (2004) Simulation of the supercooling process and frazil evolution in turbulent flows. Submitted to Can. J. Civil Eng.

Ye, S. Q. and Doering, J. C. and Shen, H. T. (2004) A laboratory study of frazil evolution in a counter rotating flume. Can Journal of Civil Eng.

Appendix A: Water temperature measurements

The following section summarizes the water temperature measurements for the thirty one experiments conducted. In all the figures the red line indicates the measurement of the temperature at an average depth and the blue line indicates the measurements of the water temperature at the surface. The temperature measurement at the water surface fluctuates greatly due to the sensitivity of the thermistor and the un-even surface of the water due to small waves. To get an smooth plot a smoothing window of the form given in equation A-1 is used on most of the surface temperature measurements.

$$T_i = \frac{1}{13}(T_{i-6} + T_{1-5} + T_{i-4} + T_{i-3} + T_{1-2} + T_{i-1} + T_i + T_{i+1} + T_{i+2} + T_{i+3} + T_{i+4} + T_{i+5} + T_{i+6}) \quad \text{(A-1)}$$

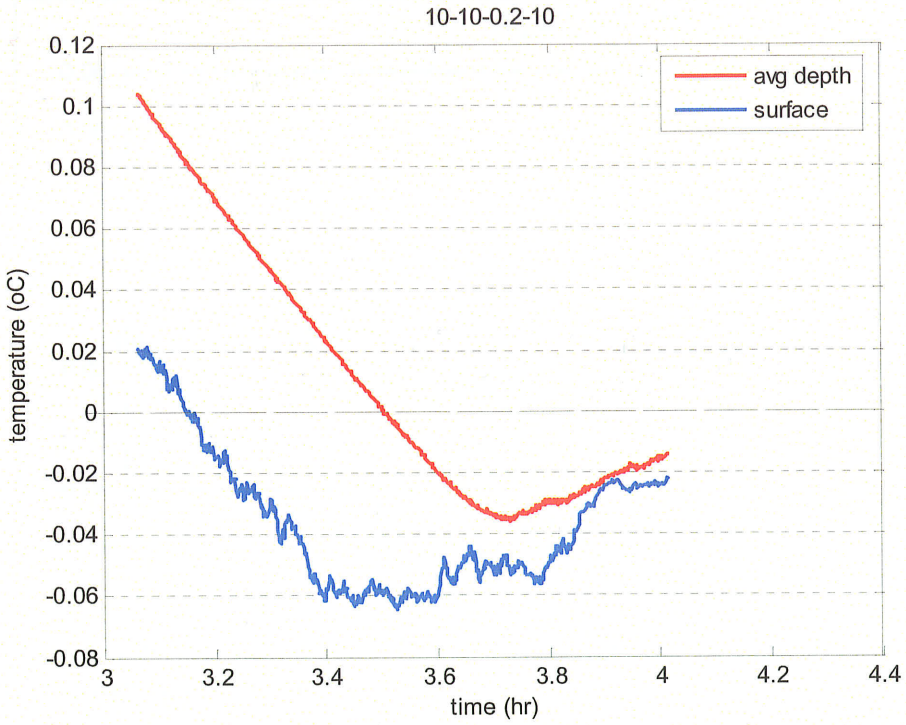

Figure A-1 Water temperature plot of bed roughness 10 mm, depth 10 cm, velocity 0.2 m/s and air temperature -10 °C.

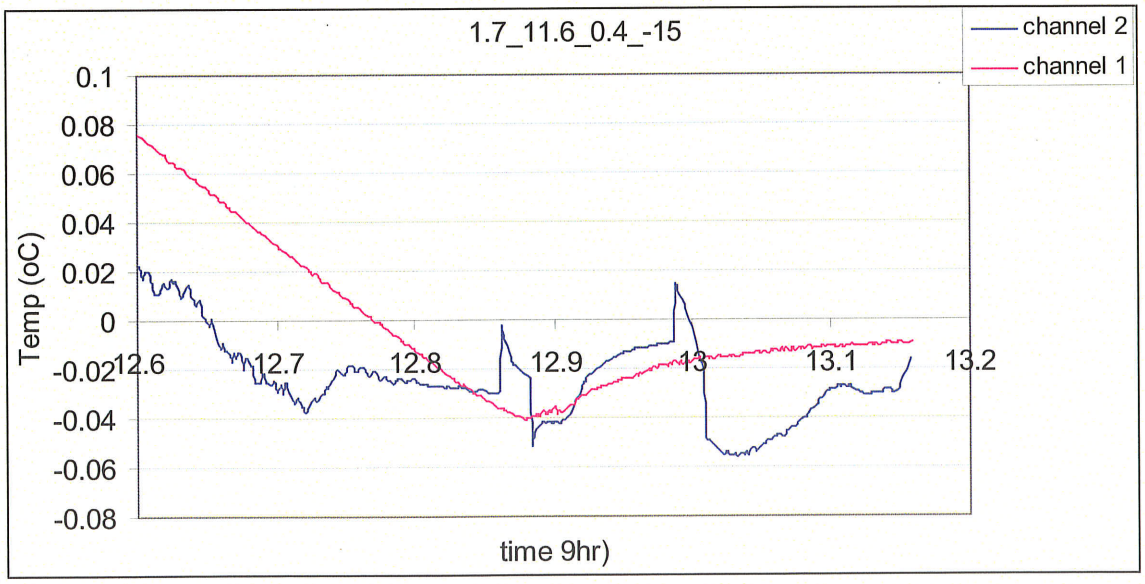

Figure A-2 Water temperature plot of bed roughness 1.7 mm, depth 11.6 cm, velocity 0.4 m/s and air temperature -15 °C.

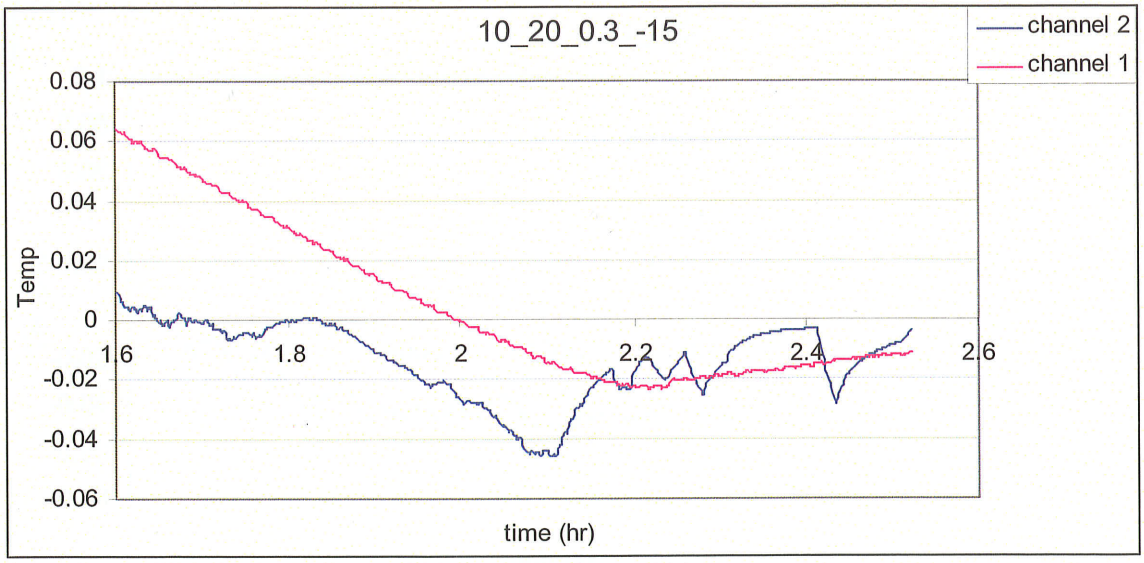

Figure A-3 Water temperature plot of bed roughness 10 mm, depth 20 cm, velocity 0.3 m/s and air temperature -15 °C.

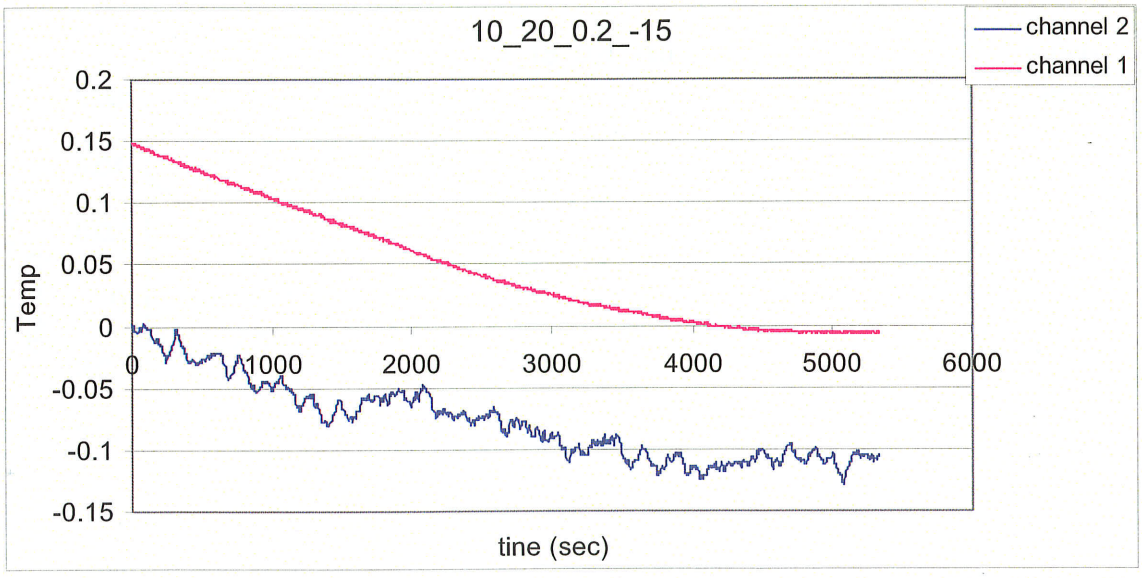

Figure A-4 Water temperature plot of bed roughness 10 mm, depth 20 cm, velocity 0.2 m/s and air temperature -15 °C.

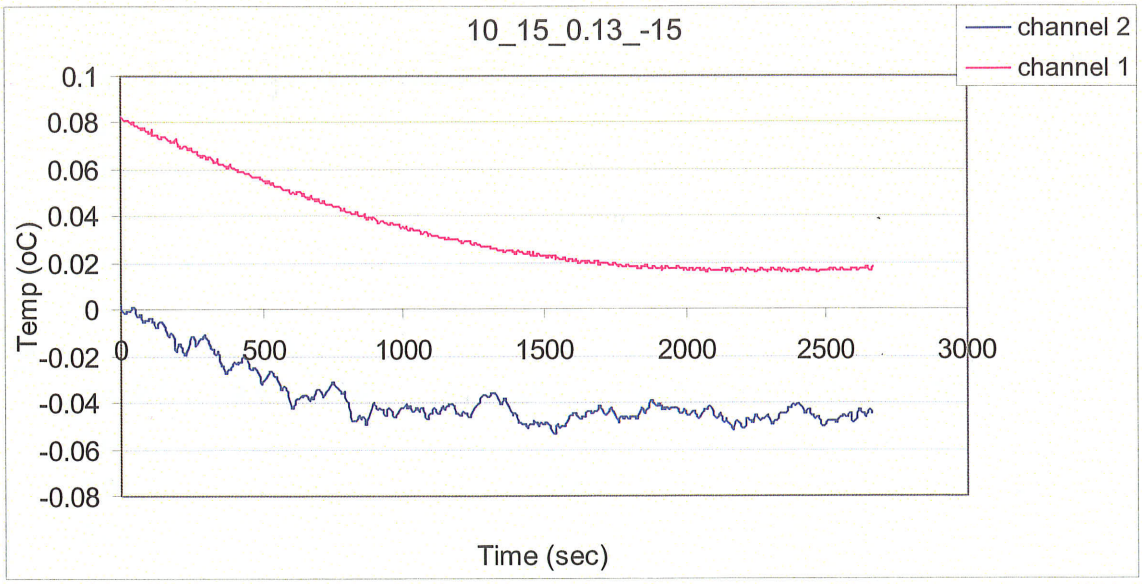

Figure A-5 Water temperature plot of bed roughness 10 mm, depth 15 cm, velocity 0.13 m/s and air temperature -15 °C.

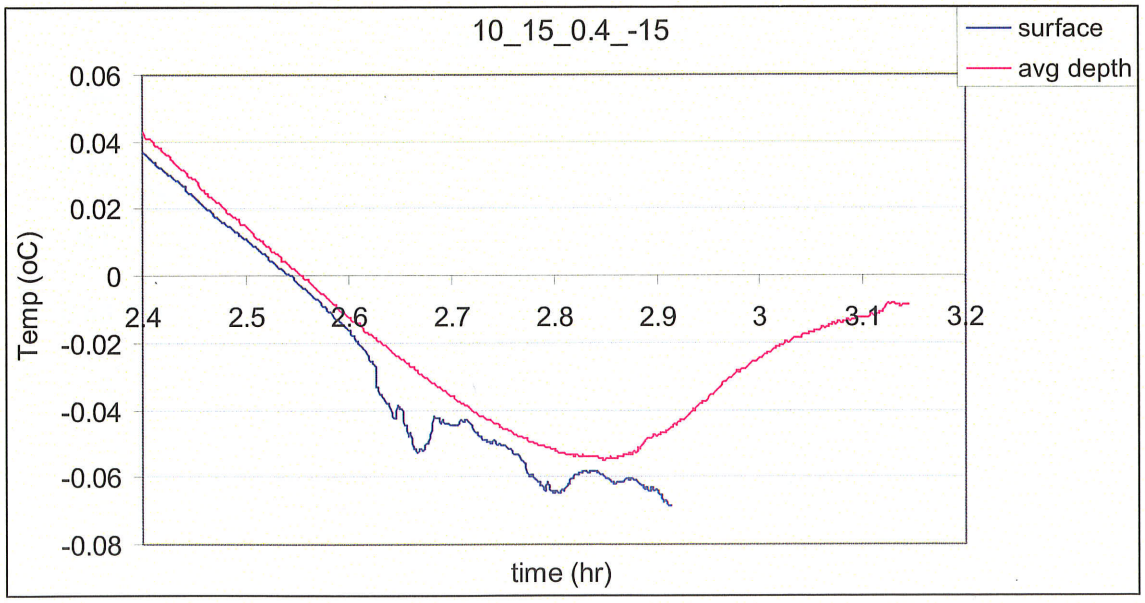

Figure A-6 Water temperature plot of bed roughness 10 mm, depth 15 cm, velocity 0.4 m/s and air temperature -15 °C.

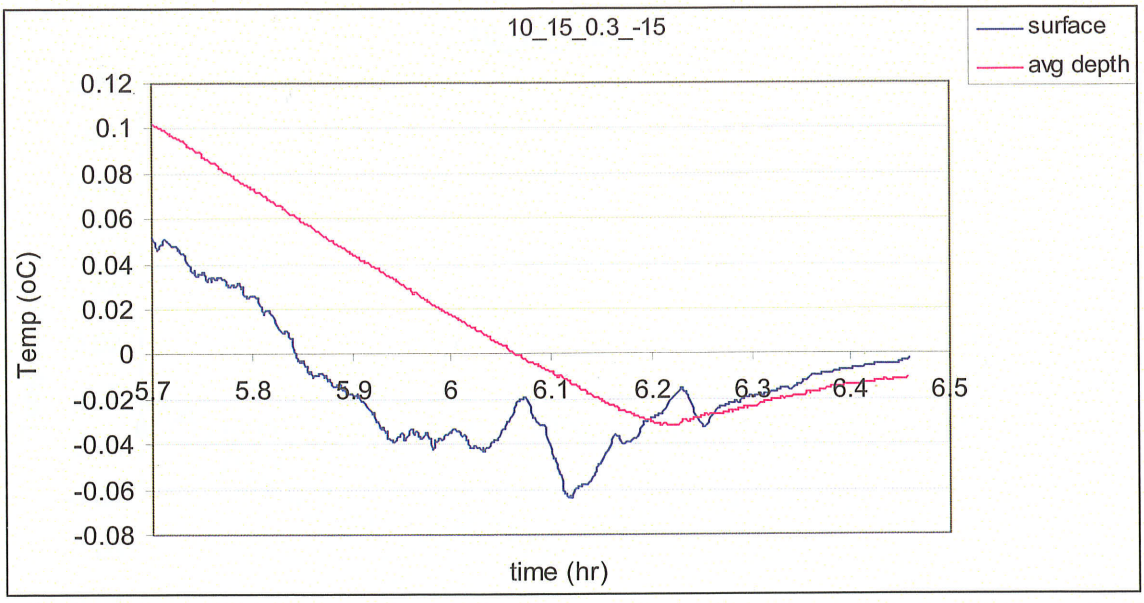

Figure A-7 Water temperature plot of bed roughness 10 mm, depth 15 cm, velocity 0.3 m/s and air temperature -15 °C.

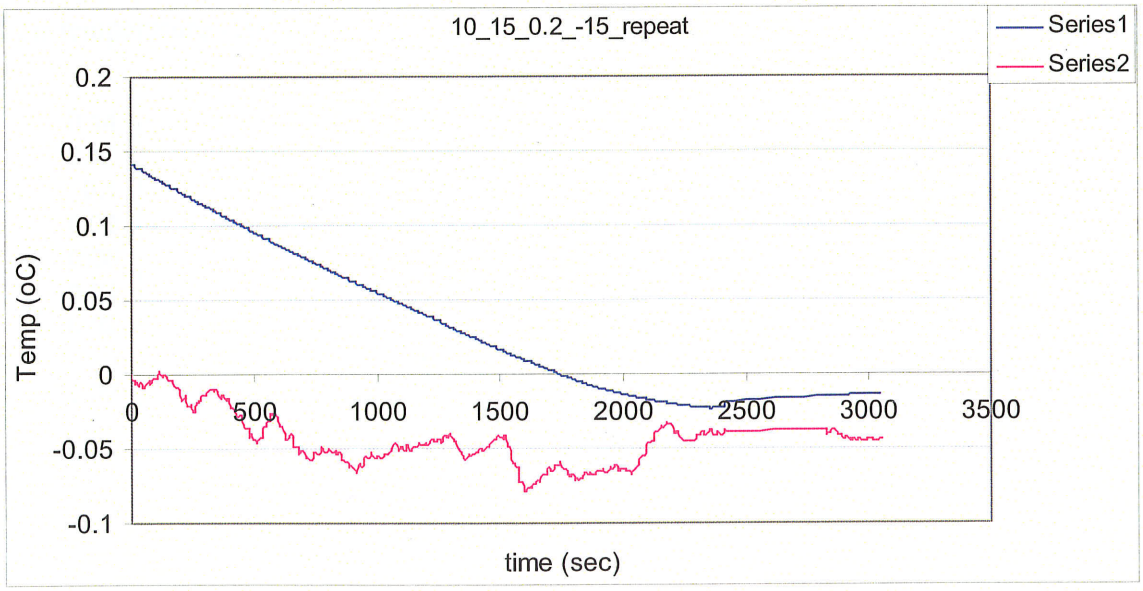

Figure A-8 Water temperature plot of bed roughness 10 mm, depth 15 cm, velocity 0.2 m/s and air temperature -15 °C (repeated experiment).

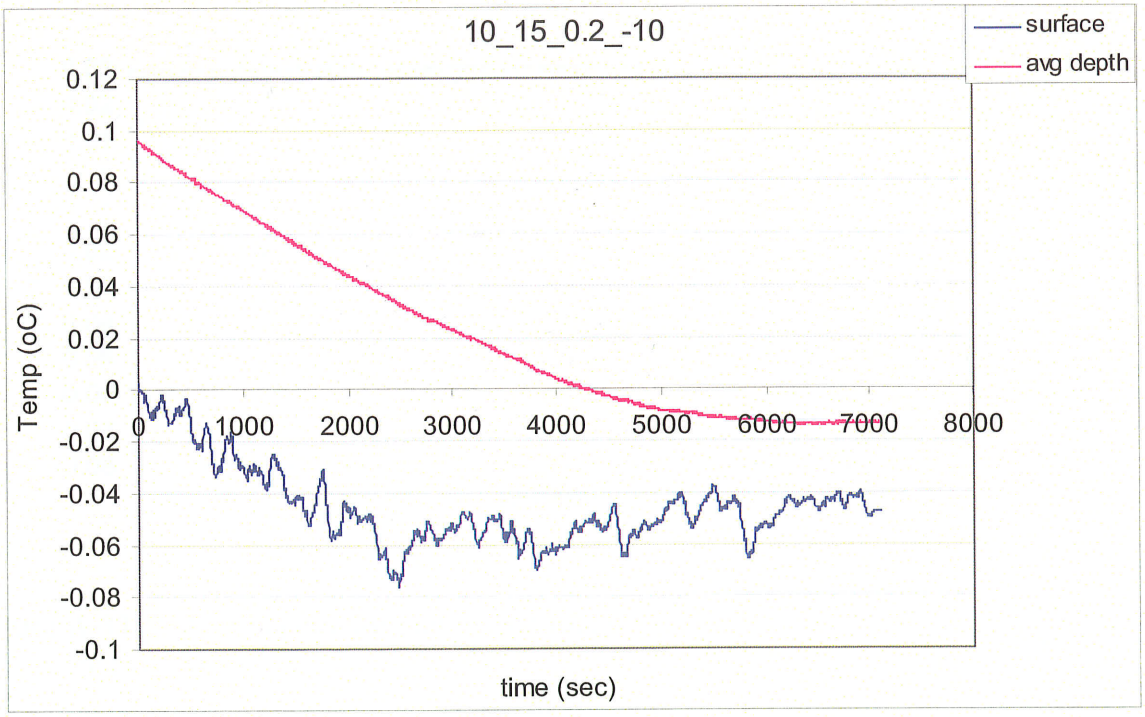

Figure A-9 Water temperature plot of bed roughness 10 mm, depth 15 cm, velocity 0.2 m/s and air temperature -10 °C.

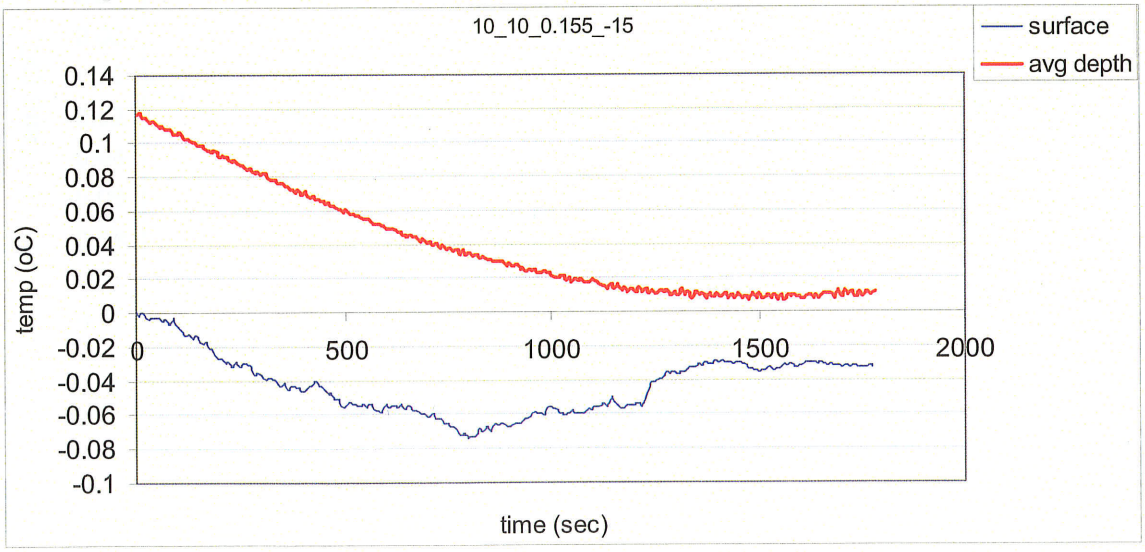

Figure A-10 Water temperature plot of bed roughness 10 mm, depth 10 cm, velocity 0.155 m/s and air temperature -15 °C.

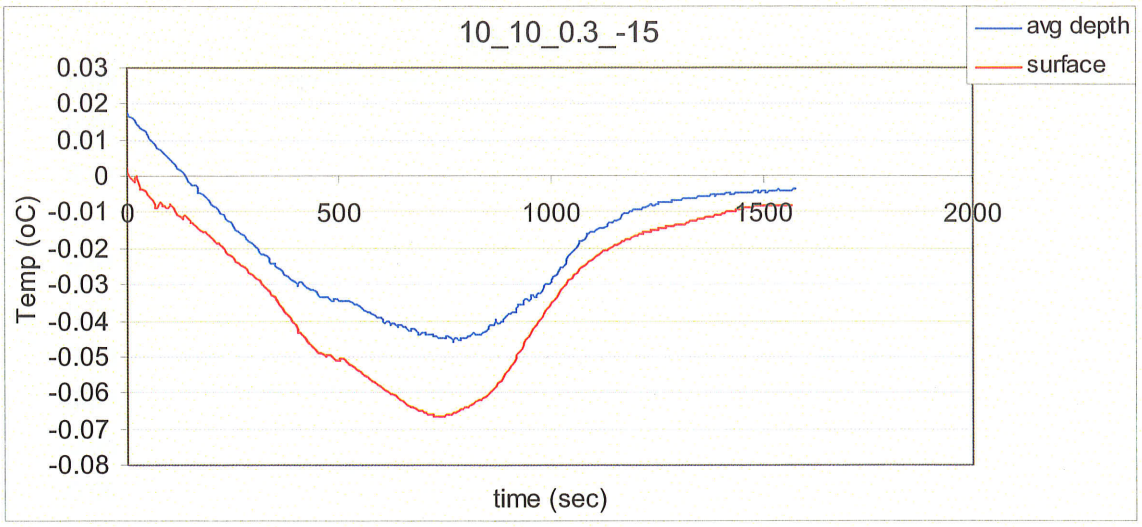

Figure A-11 Water temperature plot of bed roughness 10 mm, depth 10 cm, velocity 0.3 m/s and air temperature -15 °C.

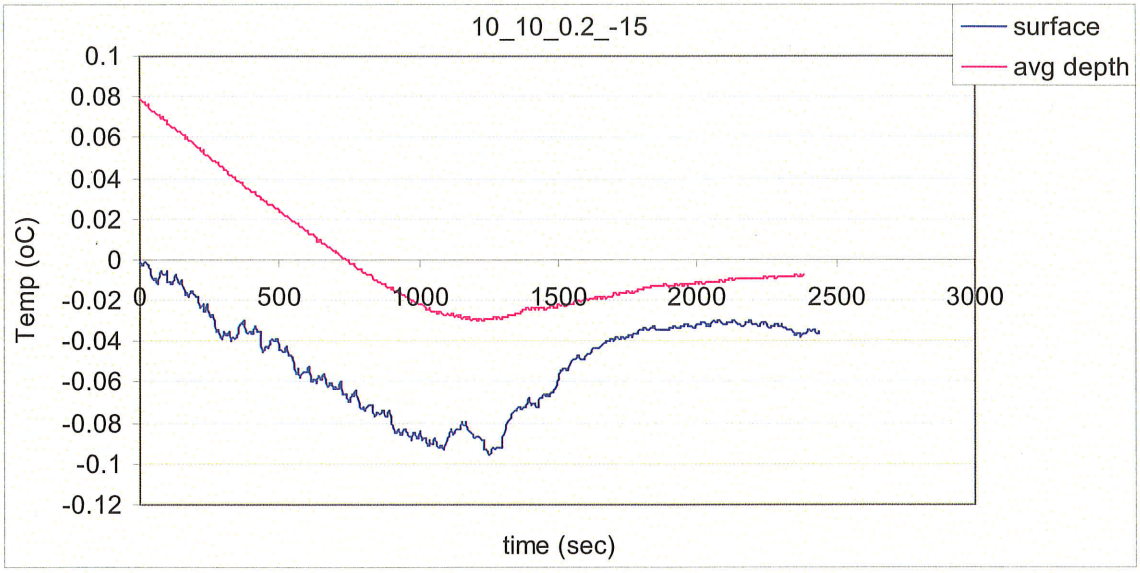

Figure A-12 Water temperature plot of bed roughness 10 mm, depth 10 cm, velocity 0.2 m/s and air temperature -15 °C.

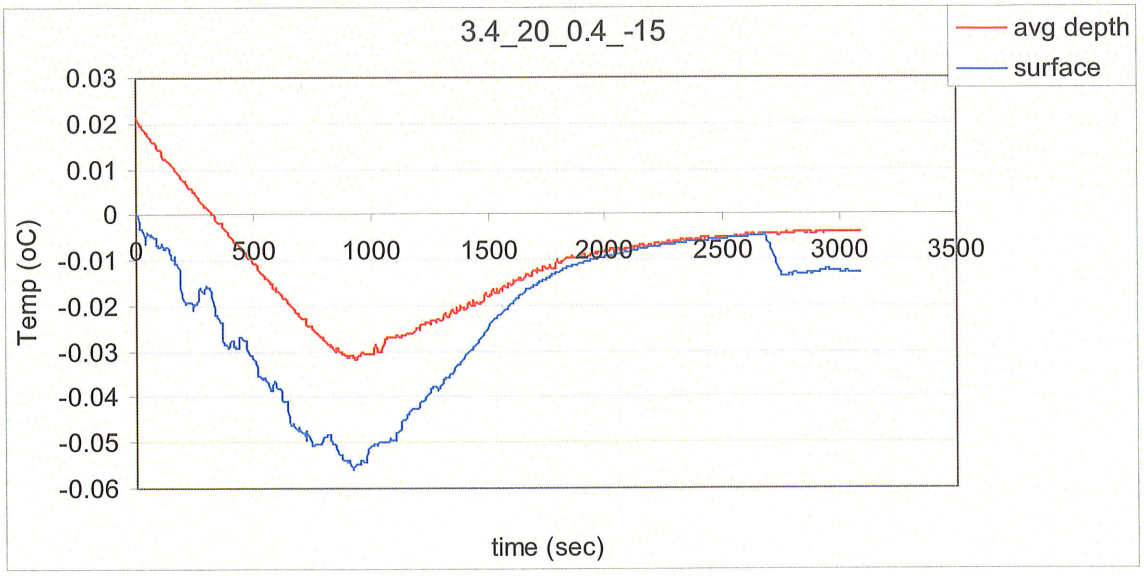

Figure A-13 Water temperature plot of bed roughness 3.4 mm, depth 20 cm, velocity 0.4 m/s and air temperature -15 °C.

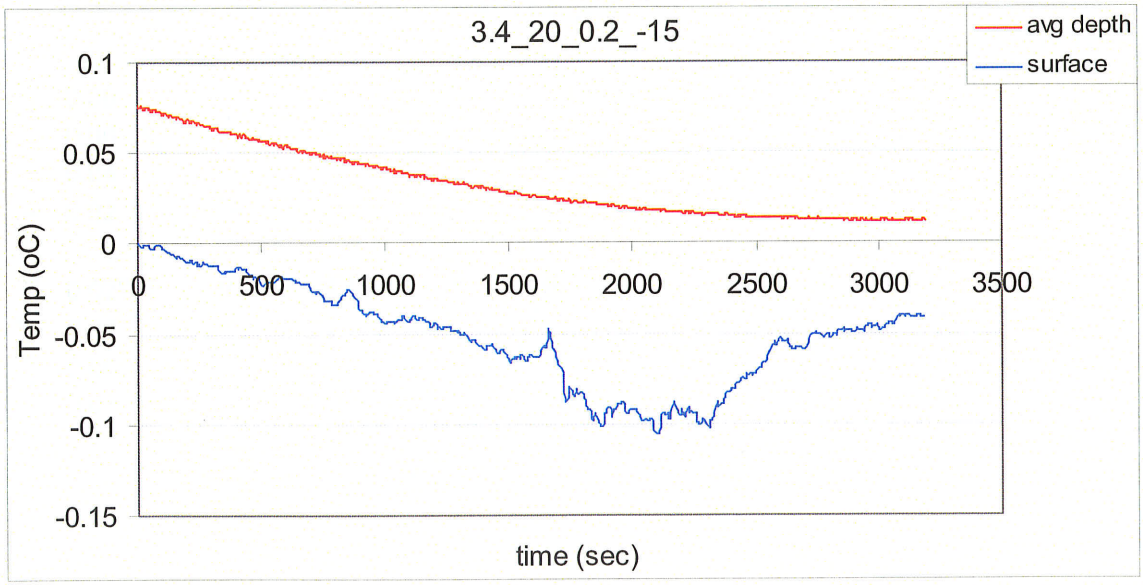

Figure A-14 Water temperature plot of bed roughness 3.4 mm, depth 20 cm, velocity 0.2 m/s and air temperature -15 °C.

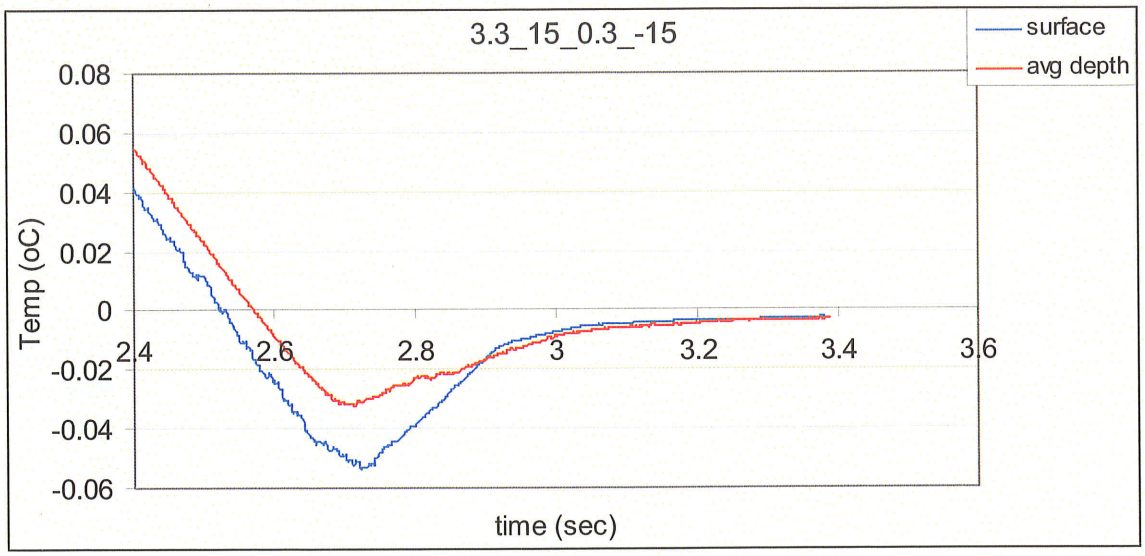

Figure A-15 Water temperature plot of bed roughness 3.4 mm, depth 15 cm, velocity 0.3 m/s and air temperature -15 °C.

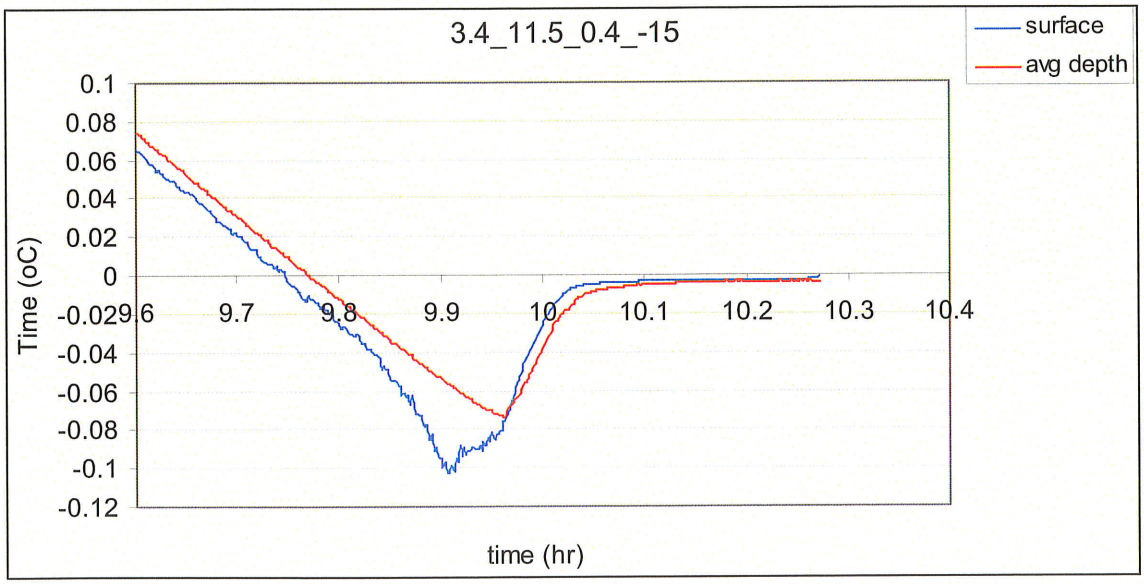

Figure A-16 Water temperature plot of bed roughness 3.4 mm, depth 11.5 cm, velocity 0.4 m/s and air temperature -15 °C.

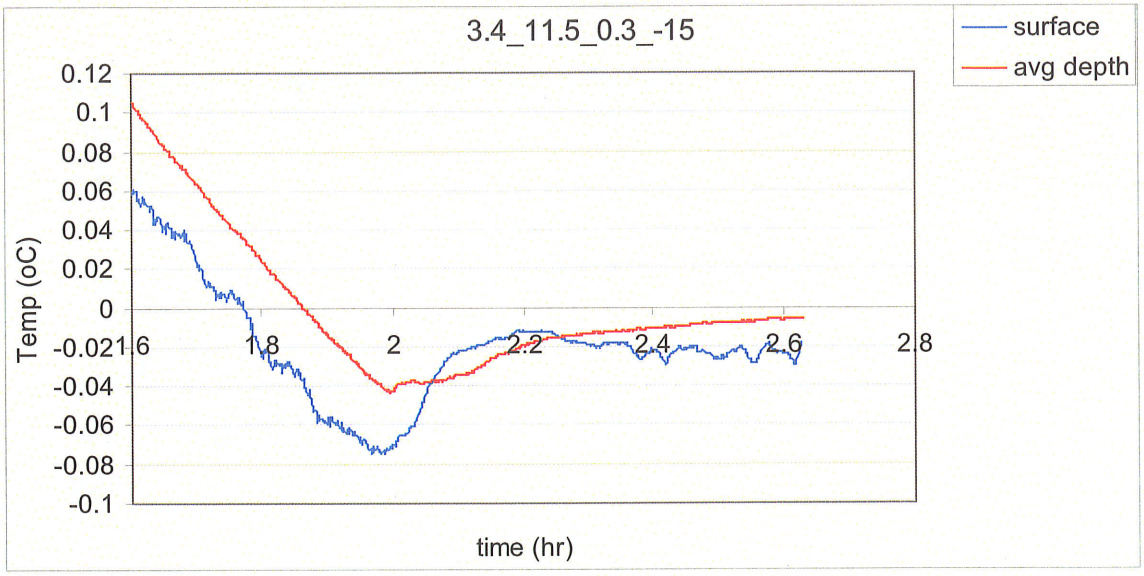

Figure A-17 Water temperature plot of bed roughness 3.4 mm, depth 11.5 cm, velocity 0.3 m/s and air temperature -15 °C.

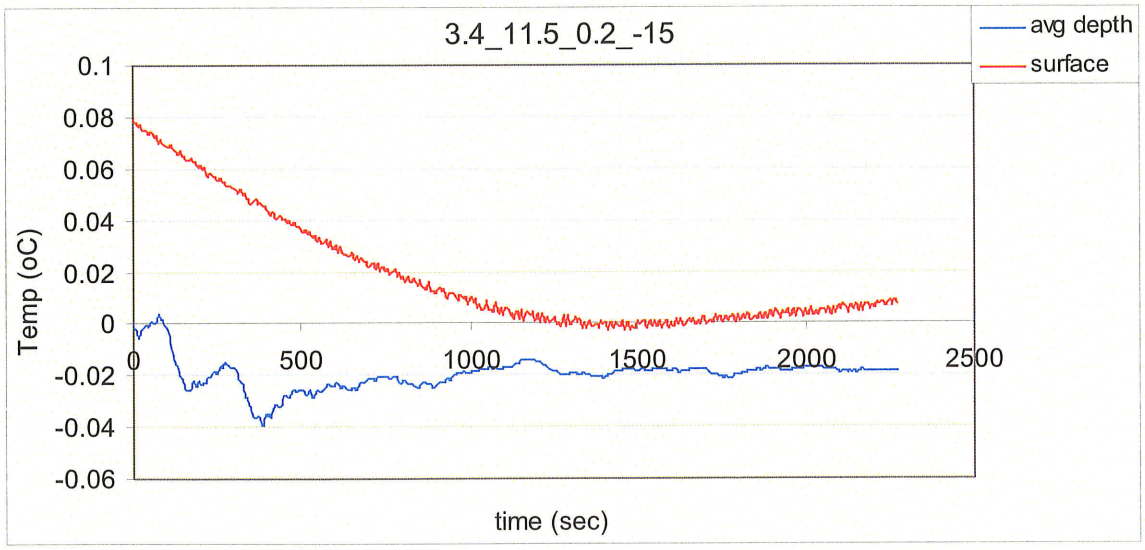

Figure A-18 Water temperature plot of bed roughness 3.4 mm, depth 11.5 cm, velocity 0.2 m/s and air temperature -15 °C.

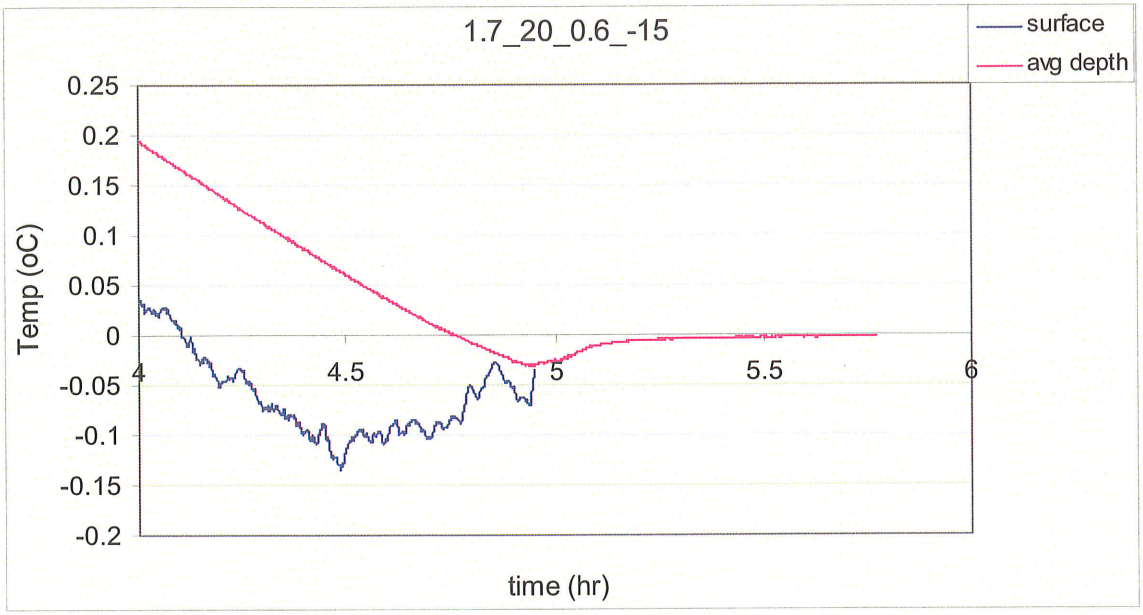

Figure A-19 Water temperature plot of bed roughness 1.7 mm, depth 20 cm, velocity 0.6 m/s and air temperature -15 °C.

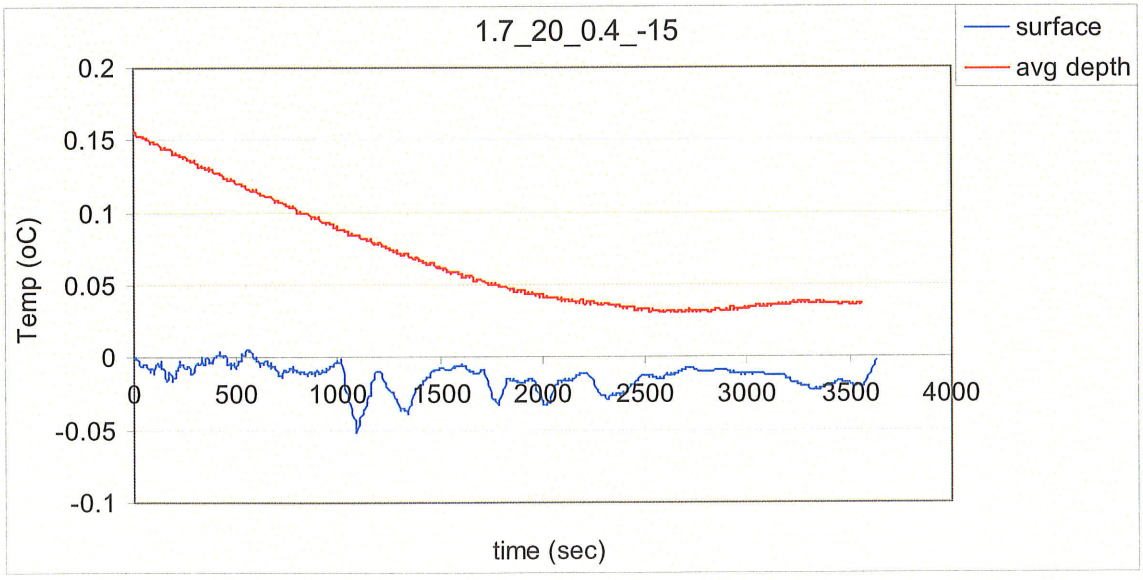

Figure A-20 Water temperature plot of bed roughness 1.7 mm, depth 20 cm, velocity 0.4 m/s and air temperature -15 °C.

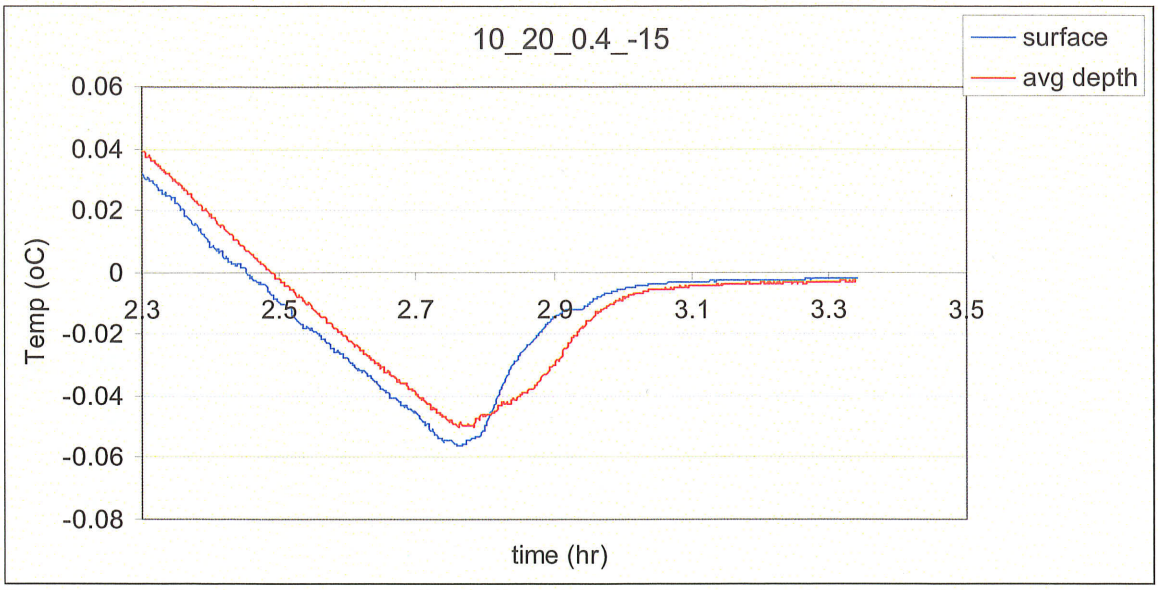

Figure A-21 Water temperature plot of bed roughness 10 mm, depth 20 cm, velocity 0.4 m/s and air temperature -15 °C.

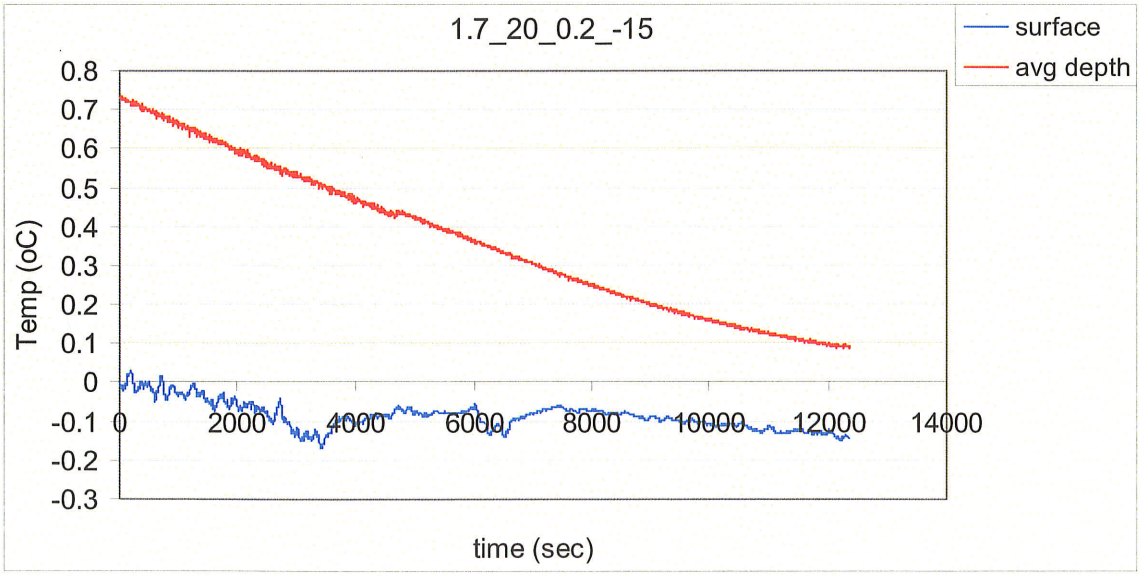

Figure A-22 Water temperature plot of bed roughness 1.7 mm, depth 20 cm, velocity 0.2 m/s and air temperature -15 °C.

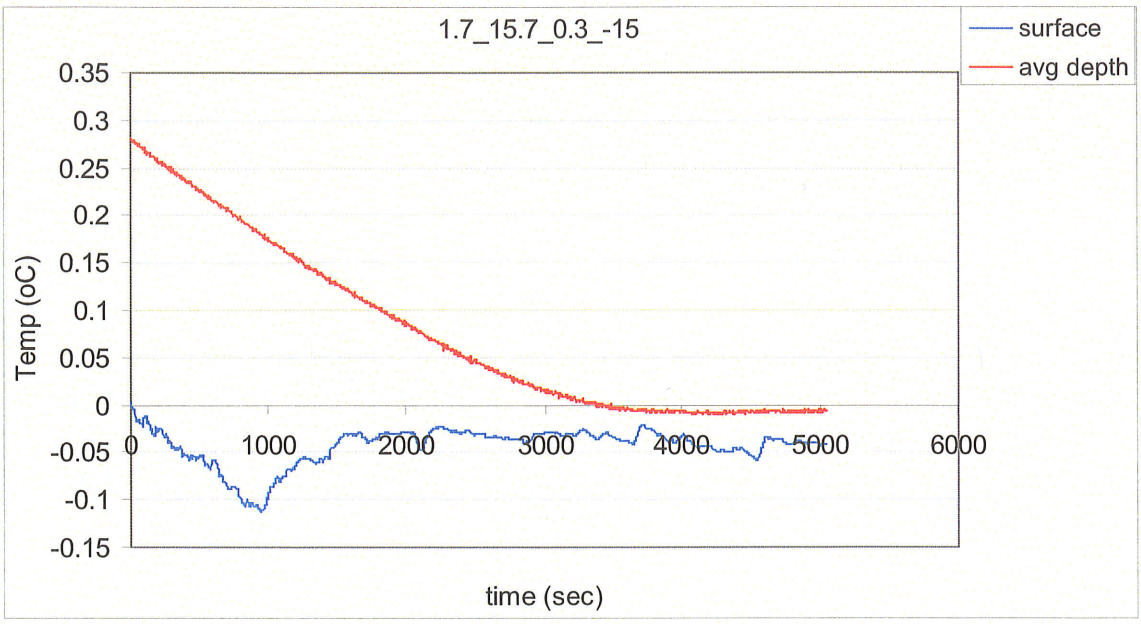

Figure A-23 Water temperature plot of bed roughness 1.7 mm, depth 15.7 cm, velocity 0.3 m/s and air temperature -15 °C.

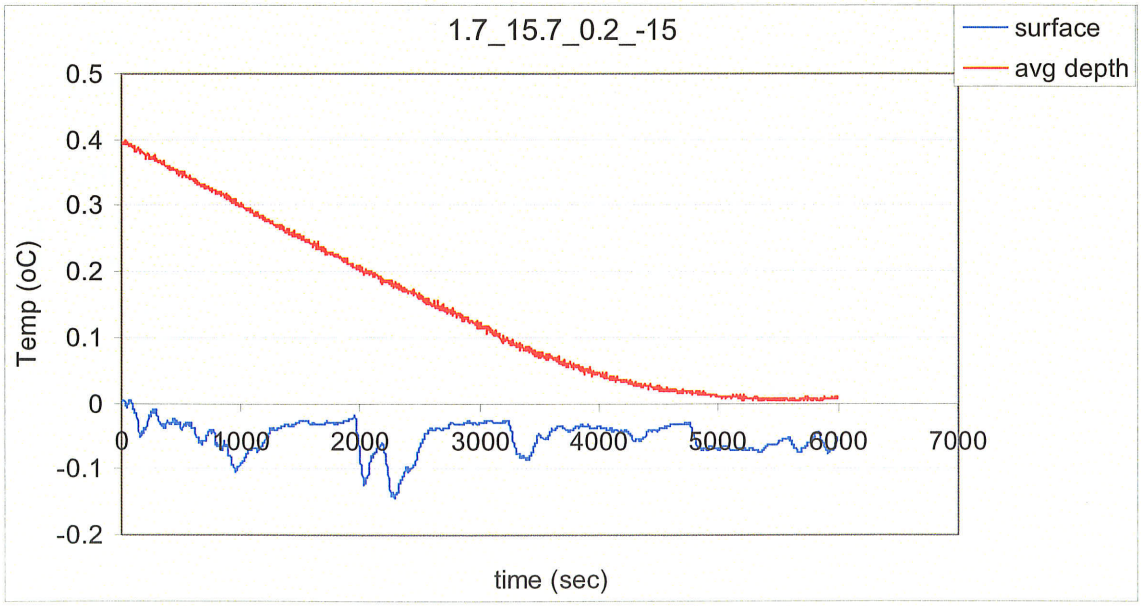

Figure A-24 Water temperature plot of bed roughness 1.7 mm, depth 15.7 cm, velocity 0.2 m/s and air temperature -15 °C.

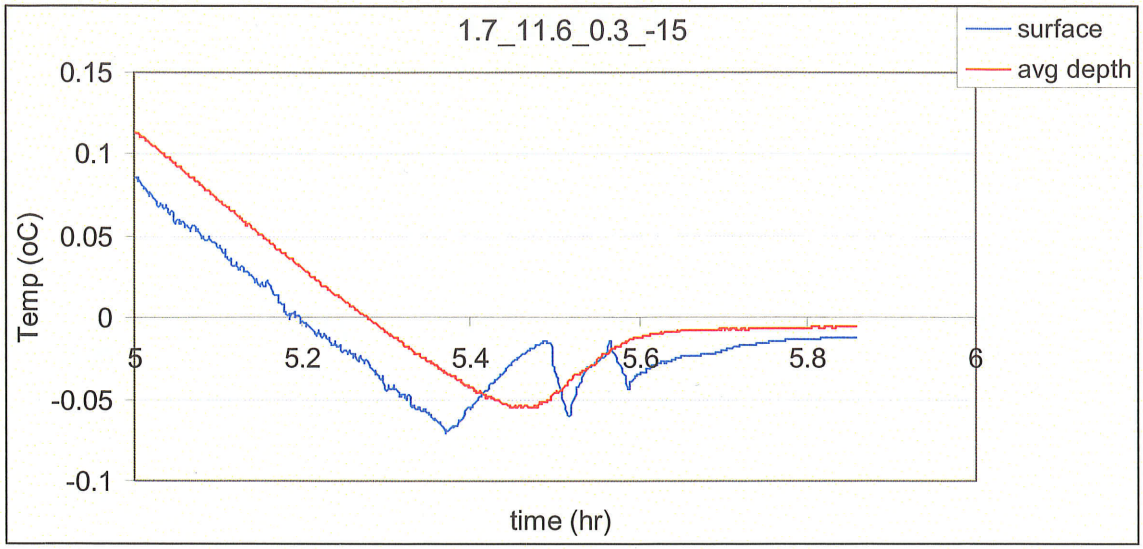

Figure A-25 Water temperature plot of bed roughness 1.7 mm, depth 11.6 cm, velocity 0.3 m/s and air temperature -15 °C.

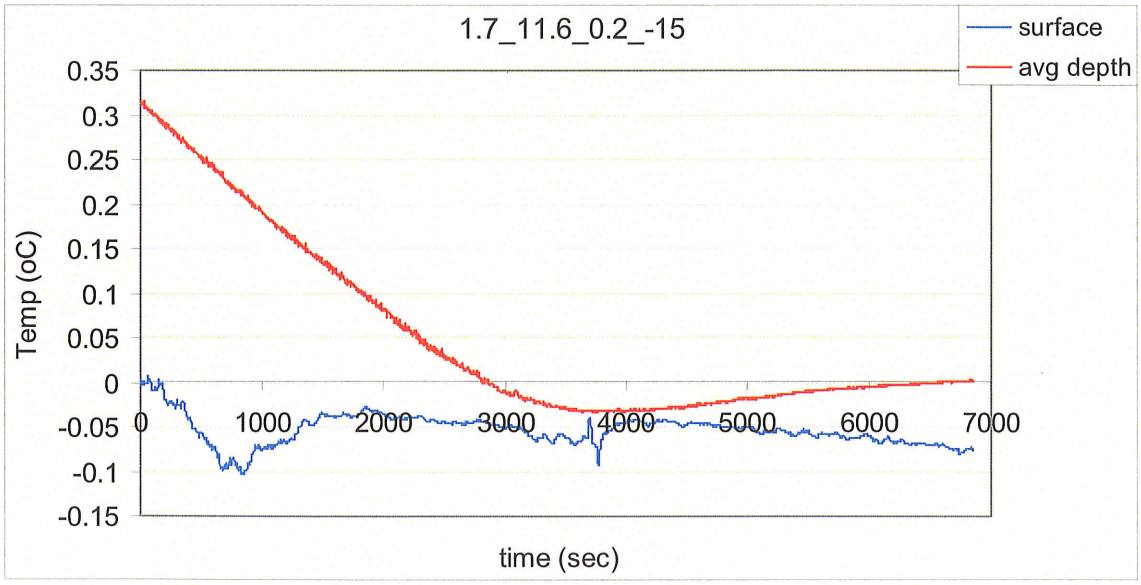

Figure A-26 Water temperature plot of bed roughness 1.7 mm, depth 11.6 cm, velocity 0.2 m/s and air temperature -15 °C.

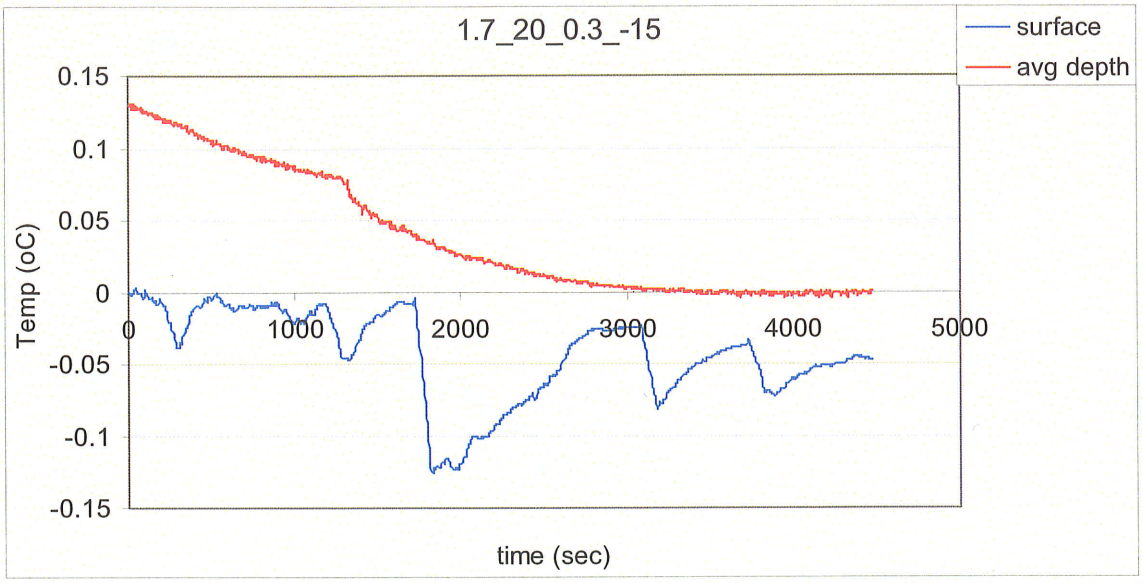

Figure A-27 Water temperature plot of bed roughness 1.7 mm, depth 20 cm, velocity 0.3 m/s and air temperature -15 °C.

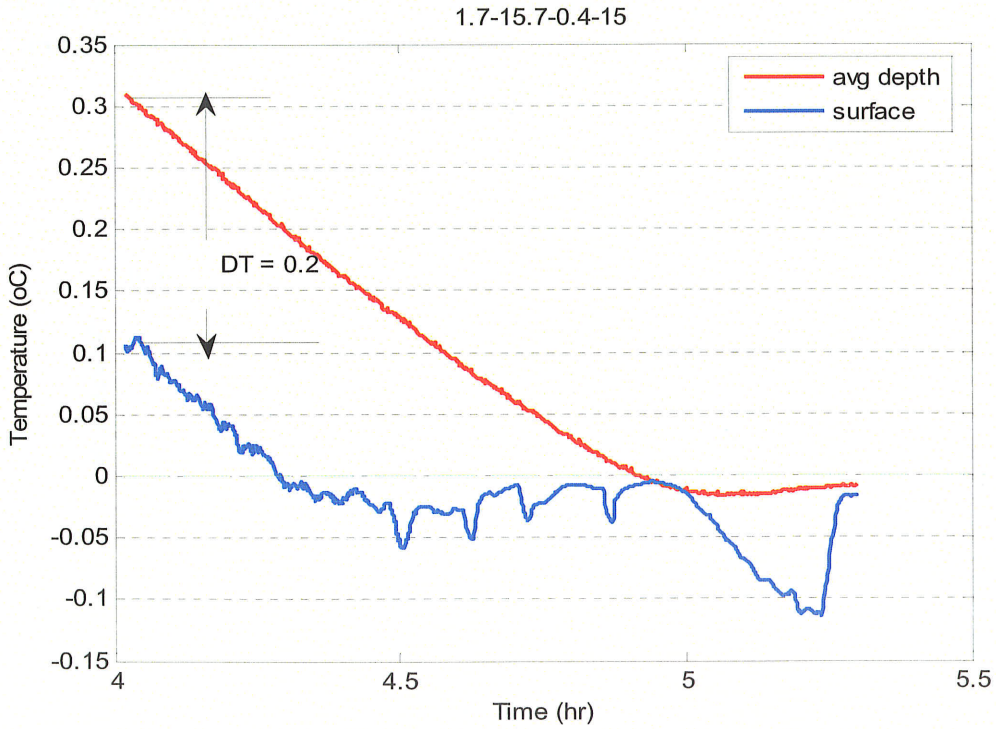

Figure A-28 Water temperature plot of bed roughness 1.7 mm, depth 15.7 cm, velocity 0.4 m/s and air temperature -15 °C.

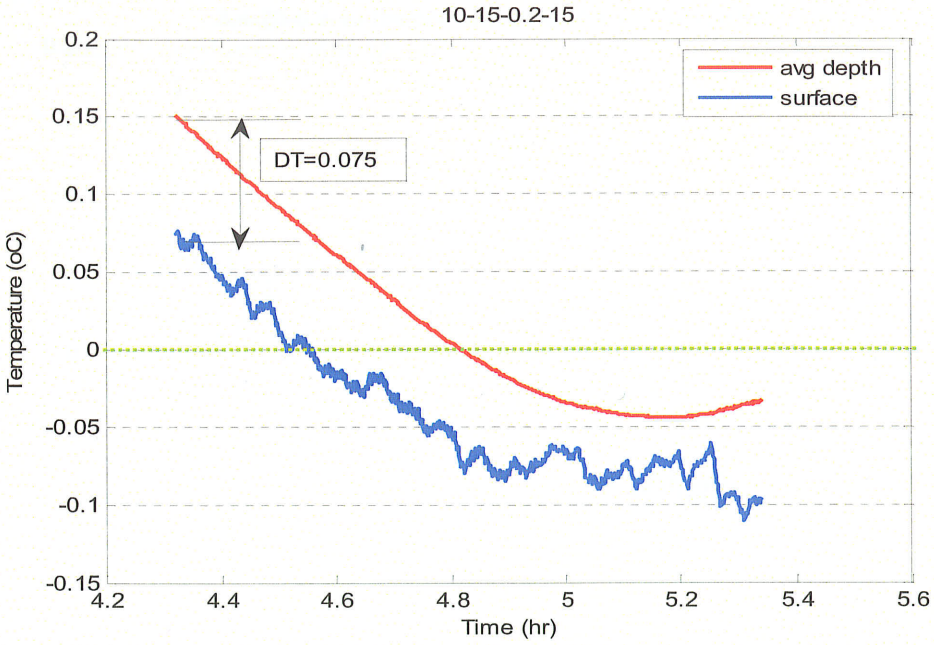

Figure A-29 Water temperature plot of bed roughness 10 mm, depth 15 cm, velocity 0.2 m/s and air temperature -15 °C.

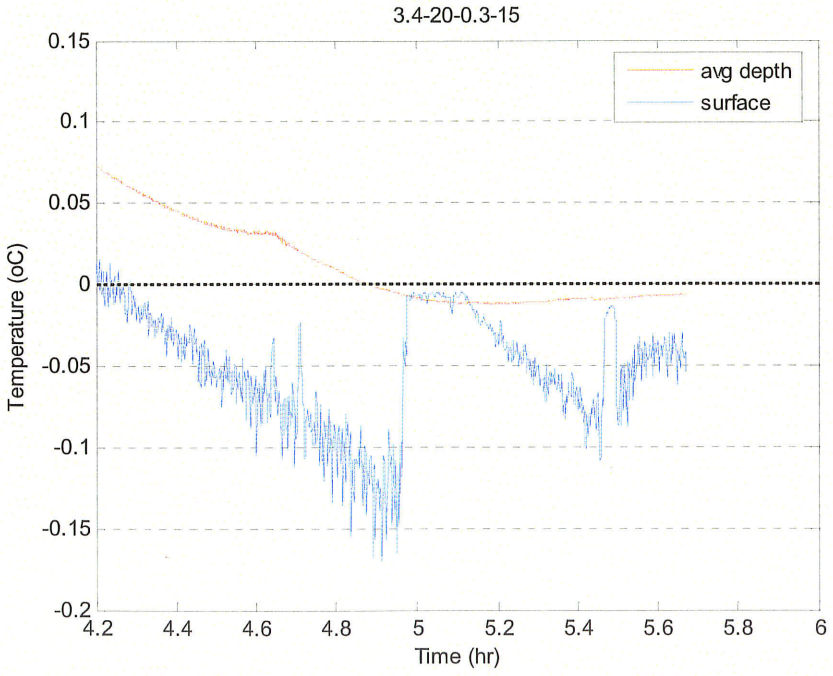

Figure A-30 Water temperature plot of bed roughness 3.4mm, depth 20 cm, velocity 0.3 m/s and air temperature -15 °C.

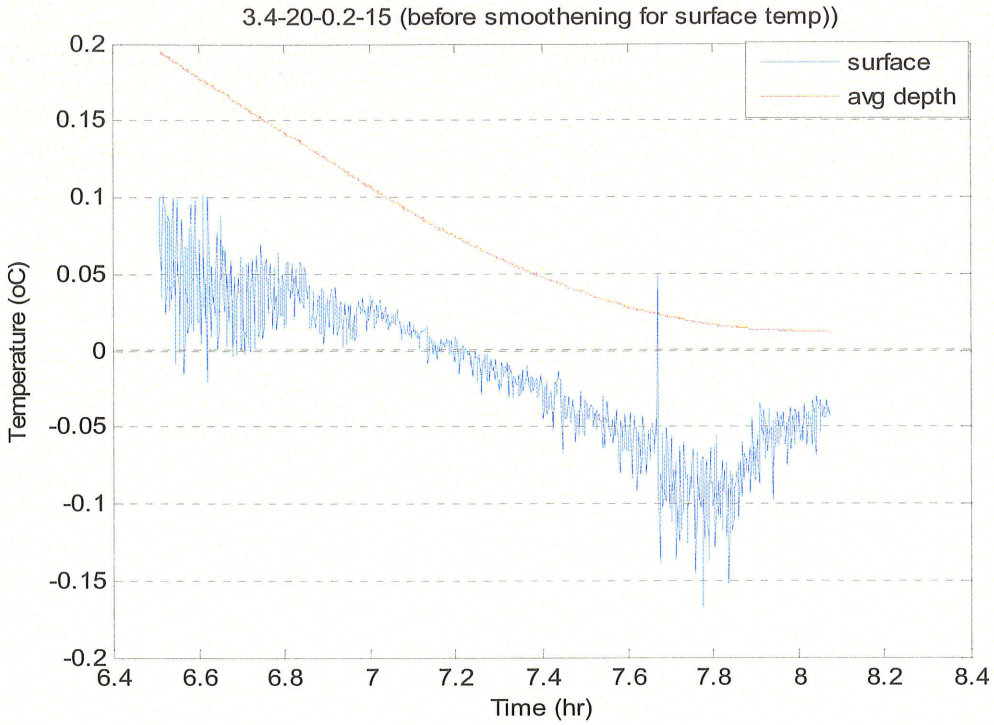

Figure A-31 Water temperature plot of bed roughness 3.4mm, depth 20 cm, velocity 0.2 m/s and air temperature -15 °C.

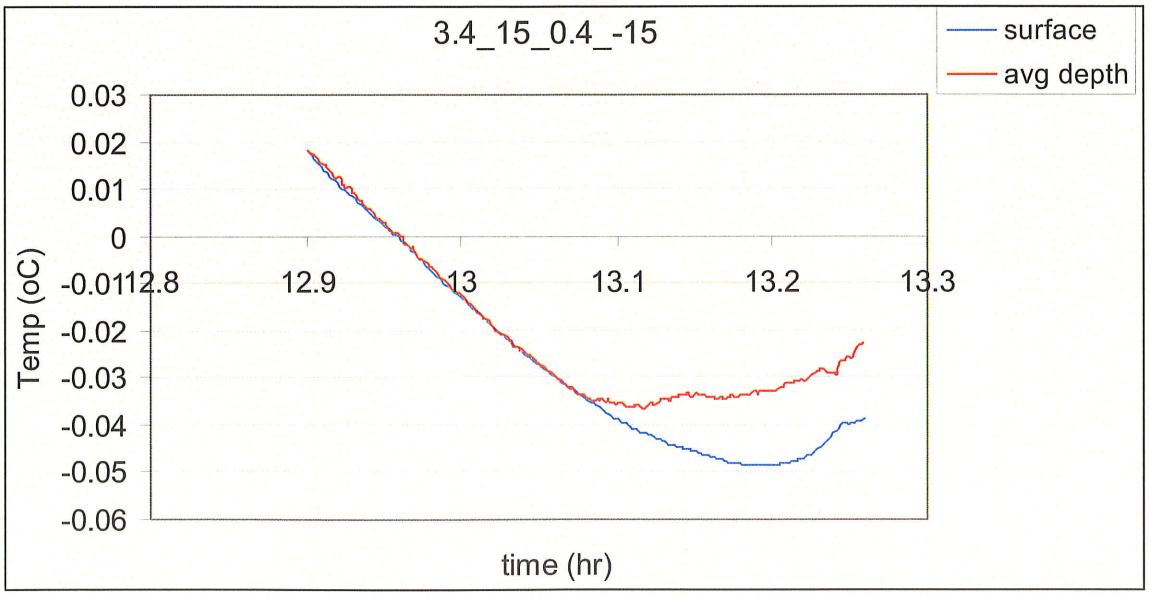

Figure A-32 Water temperature plot of bed roughness 3.4mm, depth 15 cm, velocity 0.4 m/s and air temperature -15 °C.

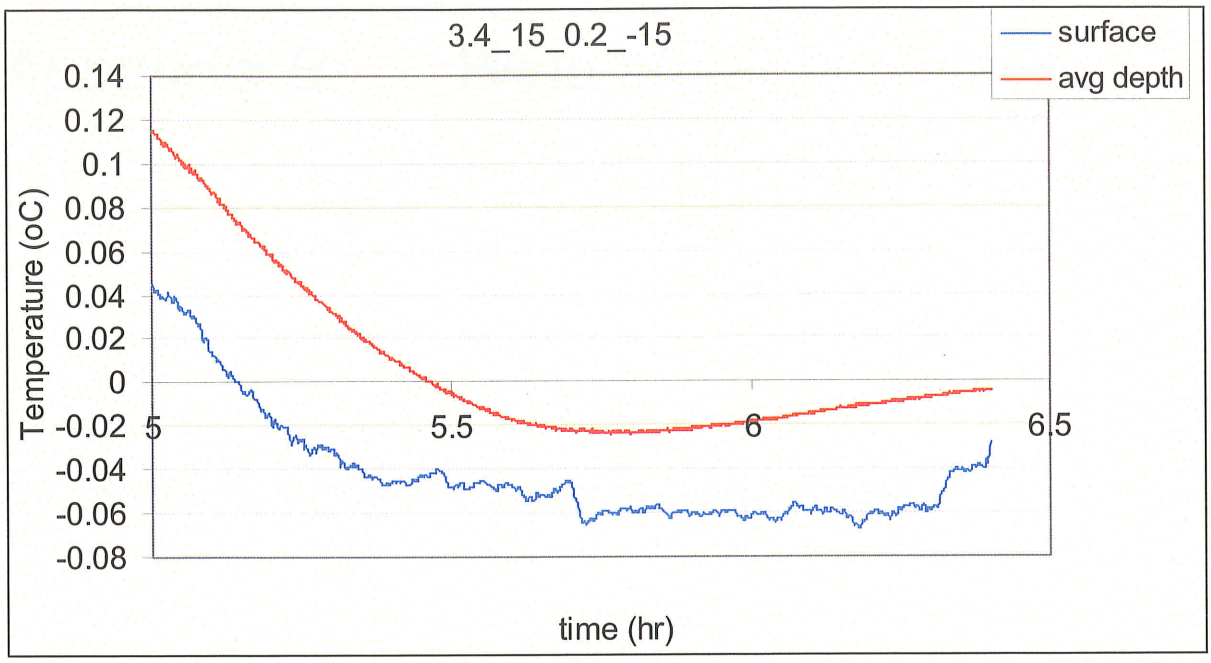

Figure A-33 Water temperature plot of bed roughness 3.4mm, depth 15 cm, velocity 0.2 m/s and air temperature -15 °C.

Appendix B: Wind shear and wave related surface turbulence

B1. Surface Turbulence due to Wind Shear

A laboratory observation of Matousek (1992) showed that waves occurred on the water surface at a wind speed of 0.30 m/s to 0.5 m/s. Recently Banerjee and MacIntyre (2005) concluded microbreaking (breaking of a wave of amplitude ~ 1 cm and length ~ 10 cm) starts to occur at wind speeds of 3 – 5 m/s. However, there is still much to be learned about the effect of the above phenomena on turbulence generation and scalar transport. To fully understand the turbulence that comes due to wind action a detailed model which incorporates wind speed, fetch, wind duration, waves, water surface stress and water surface velocities should be better developed. Due to the complexity of this process, the effect of wind on the water surface will be simplified and observed in two different ways: the effect of wind stress on turbulence characteristics at the water surface and the effect of wind generated waves on turbulence characteristics.

The stress created on the water surface due to wind action is given by (Stacey *et al.* 1995)

$$\tau_s = \rho_a C_w |W_c| (W_c - u_s), \qquad \text{(B.0.1)}$$

where ρ_a is the density of air (1.226 kg/m^3 at STP), C_w is the drag coefficient (set equal to 0.0011), W_c is the along channel component of the wind speed and u_s is the current speed at the surface in the flow direction. The current speed is included in the drag law because it was not always less than the wind speed.

The effect of surface shear generated by a gas flowing over water surface in generation of turbulence is dealt by Hunt (1984) in detail. The effect of wind over the water surface affects the mean flow condition by increasing the velocity at the surface until it approaches a value on the order of $(\tau_s/\tau_b)^{1/2}$ (where τ_b is the bed shear stress). Moreover the surface affects turbulence in the following two ways: the first being the deformation of the surface by waves and by turbulent eddies impinging on the surface. Gravity waves are formed in a channel for a gas flow Froude number of F < 1.0. For large scale turbulent eddies, the scale of a typical eddy is determined by the balance between the potential energy of the surface deflection and the kinetic energy of the eddy. But for small enough eddies the dynamic head of the impinging eddies is balanced by the surface tension. Secondly, gas motion over the liquid surface can also cause deformation of the surface by generating waves or by local pressure fluctuations in the turbulence of gas flow.

In general, when there is small surface shear stress τ_s the mean velocity gradient increases near the surface and there is a local source of small scale turbulent energy. At the time there is also large time scale turbulence diffusing into this region from the lower shear flow. The turbulence generated by the surface shear stress (without considering the effect of waves generated on the surface, where the generation of waves changes the roughness of the water surface which again

modifies the wind velocity profile) becomes of the same order as that proposed in the bottom shear stress when

$$\frac{z}{h}=\left(\frac{\tau_s}{\tau}\right)^{3/2}. \qquad \text{(B.0.2)}$$

Similar experimental results were also obtained by Rashidi and Banerjee (1990) on the effect of surface shear on turbulent intensities. The recent direct numerical simulation (DNS) of Lombardi *et al.* (1996) will be used herein when studying the turbulence intensities near the interface of liquid and gas. Lomabardie *et al.* (1996) developed a DNS analysis where the gas and liquid was coupled through continuity of velocity and stress boundary conditions at the interface. They artificially raised the surface tension to maintain a flat interface, as waves would have introduced an additional complexity. For the density ratio of 1000:1.266 (which is density of water to density of air at STP), u_{rms} (the root mean square stream wise velocity component) monotonically decreases from its maximum, reached at the interface, though there is the beginning of a plateau in the $z^+ \sim 10$ region. v_{rms} is relatively flat but has a dip in the $z^+ \sim$ 5 to 10 region. The third quantity, w_{rms}, is quite similar to that of the channel flow cases. z^+ is the non-dimensionalized length (= z^*u_τ/ν, where u_τ is the shear velocity at the interface, *i.e.*, $u_*^2=\tau_s/\rho$) measured from the interface. From the result of Lombardi *et al.* (1996) value of turbulent kinetic energy, k, shown in Figure B1.1 is extracted. As the depth increases, the turbulent kinetic energy that comes from the wind stress reduces and is dominated by the turbulent energy that is generated at the bed.

For the purpose of modeling, the above data is fitted with an exponential function given by

$$\frac{k_\tau}{u_\tau^2} = 5.29 \exp\left\{-0.0154 z^+\right\}, \qquad \text{(B.0.3)}$$

where k_τ is the turbulent energy generated due to surface wind stress. This extra amount of turbulent kinetic energy should be included in modeling wind-sheared water surfaces together with Equation 2.16.

The turbulent energy dissipation rate with the presence of surface shear stress is given by Hunt (1984) as

$$\varepsilon_w = 4\frac{u_*^3}{h} + \frac{u_\tau^3}{z}, \qquad \text{(B.0.4)}$$

on the surface and at any other depth

$$\varepsilon(y) = \frac{u_*^3}{h} E_1 . (y/h)^{-1/2} \exp(-3y/h) + \frac{u_\tau^3}{z}, \qquad \text{(B.0.5)}$$

where u_τ is the wind shear stress on the water surface and z is the water depth measured from the surface. The above result yields a decreasing dissipation rate as a function of depth from the surface (similar to the result obtained by Lombardi *et al.* (1996)), however, it gives unstable results near the surface. If we apply the same analogy as the bottom shear stress, the first grid point should be taken at a viscous sublayer depth from the surface, *i.e.*, ν/u_τ, or at $z^+ = 30$. The surface value (at $z^+ = 0$) of the dissipation rate has to be assumed from this value.

Due to the presence of surface shear stress the mean water flow velocity will also be modified. The difference in the velocity profile arises due to the change in the turbulence intensities and the Reynolds stress. It appears that the data follows a log-law profile for the region near the wall ($y^+ > 30$) and can be described in terms of Equation 2.6. The data of Rashidi and Banerjee (1990) showed that, with the presence of surface stress, the constant 'A' in Equation 2.6 varies between 4.9 to 5.8 with $\kappa = 0.4$. The variation in the value of 'A' appears to be connected with the shear rate imposed at the interface (similar results were also obtained by Lombardi *et al.* (1996)). It seems that as the interfacial shear rate increases, the value of 'A' also increases, causing a shift in the log-law profile. It appears that near the interface the velocity profile follows a logarithmic profile. The logarithmic region seems to extend from the center of the flow up to z^+ of about 20-30. For $z^+ < 20$, a deviation from the log-law profile is observed. This can be taken into account by the application of a surface damping factor.

B2. Surface Turbulence due to Wave Action

Wind blowing over a water surface exerts a stress on the water surface that causes waves to form, break and transfer momentum to the water. The wave motion, especially when waves are breaking, produces turbulence in the upper layers. The turbulence then interacts with the mean shear in the upper region to produce further turbulent kinetic energy. The net turbulent kinetic energy produced in this upper region is then transferred to the lower regions of the flow by turbulent diffusion. The total power input is dependent on the magnitude of the wind stress that creates waves on the surface. In situations where the air-interface does not break, considerable research has been done to investigate the interaction of waves with turbulence, and it was

found that turbulence intensities could be related to u_* and ν, the kinematic viscosity. However, very little is currently understood about the effect of wave breaking on turbulence generation and scalar exchange (Banerjee and MacIntyre, 2005). Wave induced-turbulence for non-breaking waves, which changes amplitude in time (in the absence of wind stress), was given by Kinsman (1984). However, for natural sinusoidal waves the amplitude may roughly be constant for a short duration of time, but still there could be turbulent generation on the water surface.

An experimental investigation of wave-turbulence interaction in free-surface channel flows was carried out by Rashidi *et al.* (1992). They concluded that wave motion has both a damping and enhancing effect on the turbulence depending on the position under the wave. The turbulence was enhanced under the crest of the waves and damped under the trough. However, the overall qualitative appearance of turbulence structures is the same as the non-wavy interfaces. They observed that the stream wise velocities increase at the interface and near the wall, whereas they decrease at the center of the flow depth. The mean flow velocity is modified in such a way that the constant 'A' in Equation 2.6 is found to be 4.9 (however, as wave amplitude increases, there is a deviation from the log-law profile which is most pronounced near the interface and near the wall). On the contrary, Thais and Magnaudet (1996) reported high levels of turbulent energy and dissipation below laboratory waves under moderate wind conditions. De Angelis and Banerjee (1999) and Fulgosi *et al.* (2003) have reported some details of DNS (direct numerical simulation) with a non-breaking deformable interface between turbulent air and the water stream. Moreover, heat loss and shear may co-

occur at the air-water interface and turbulence can be induced not only by shear or microbreaking waves, but also by heat loss.

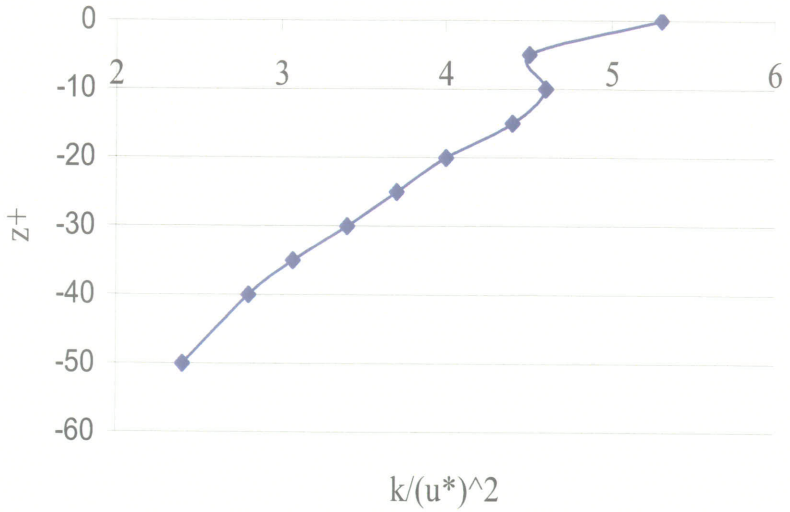

Figure B1.1 Turbulent kinetic energy due to surface wind stress.